Technische Universität München
Fakultät für Medizin

Kinetic Changes of Hematopoiesis During Aging, in Clonal Hematopoiesis of Indeterminate Potential, and in Myelodysplastic Syndromes

Michèle Constanze Buck

Vollständiger Abdruck der von der Fakultät für Medizin der Technischen Universität München zur Erlangung einer Doktorin der Naturwissenschaften (Dr. rer. nat.) genehmigten Dissertation.

Vorsitz: Prof. Dr. Marc Schmidt-Supprian

Prüfer*innen der Dissertation:

1. apl. Prof. Dr. Katharina S. Götze
2. Prof. Dr. Bernhard Küster

Die Dissertation wurde am 04.01.2023 bei der Technischen Universität München eingereicht und durch die Fakultät für Medizin am 21.03.2023 angenommen.

Table of Contents

1 Abstract 1

2 Introduction 3

2.1 Hematopoietic stem cells 3

2.2 Hematopoiesis in human and mouse 4

2.3 Aging, CHIP, and MDS 7

2.4 Additional Sex Combs Like 1 – a polycomb repressive complex protein 10

2.5 Spliceosome factor 3b - a core component of U2 small nuclear ribonucleoprotein 10

2.6 The bone marrow niche and its role in aging and malignant transformation 11

2.7 Aim of this study 12

3 Methods 14

3.1 Healthy and MDS sample collection and storage 14

3.2 Sample preparation and antibody staining for FACS 14

3.3 Serial dilution of CellTrace™ Violet stained cells 16

3.4 Cell culture 16

3.5 Index sort data analysis 17

3.6 Mutational analysis 18

3.7 Time lapse experiments 18

3.8 Multi-compartment model and parameter inference 19

3.9 Animals 19

3.10 Organ extraction 20

3.11 Mouse MSC culture 20

3.12 *In vitro* colony-forming assay of murine hematopoietic cells 20

3.13 Investigating CFU-F capacity 21

3.14 RNA isolation, cDNA transcription, and qPCR 21

3.15 Antibody staining and FACS analysis of murine cells 22

3.16 Mouse blood values 23

3.17 SDS-PAGE and Western Blot 23

3.18 Statistical analysis 24

4 Results 25

4.1 A workflow for investigating HSPC kinetics 25

4.1.1 Phenotypically defined HSPC subpopulations give rise to an expected spectrum of hematopoietic colonies 25
4.1.2 Hematopoietic stem cells differentiate in vitro 28
4.1.3 Detection limit of very rare populations by FACS is dependent on total cell counts analyzed 28
4.2 *In vitro* cultures of HSCs resemble decreased cellularity found in BM of aged individuals, which is based on reduced HSC proliferation 30
4.2.1 HSPCs are relatively increased in snapshot analysis of aged individuals 30
4.2.2 In vitro cultures of HSCs from aged individuals showed a declining blood cell production starting at the HSPC level 31
4.2.3 Computational modeling reveals a decline of HSC proliferation being responsible for declining blood cell production in aged individuals 33
4.3 Individuals with CHIP and MDS show an increasing heterogeneity in the hematopoietic tree architecture and in the number of altered kinetic rates 36
4.3.1 Characterization of our CHIP and MDS patient sample cohort 36
4.3.2 In vitro cultures of HSCs from MDS patients, individuals with CHIP, and age-matched healthy individuals without mutations showed no differences in HSPC proportions and cellular yield 40
4.3.3 The hematopoietic structure and kinetic rates are deregulated in CHIP and MDS …… 41
4.3.4 Single cell kinetics reveal higher activity of MDS HSPCs compared to the age-matched healthy controls 44
4.3.5 Sister cells in MDS354 divide more asynchronously compared to healthy samples ……. 48
4.4 A mouse model for investigating alterations in the bone marrow niche during MDS development and progression 50
4.4.1 Proofing successful deletion of ASXL1 50
4.4.2 Mice with hematopoietic knockout of ASXL1 do not show progressive peripheral cytopenia 51
4.4.3 Mice with hematopoietic deletion of ASXL1 do not show severe changes in BM cell composition 53

4.5 No observation of changes within the BM microenvironment of mice with hematopoietic deletion of *ASXL1* 56
4.5.1 Hematopoietic deletion of ASXL1 does not lead to altered numbers of BM endothelial cells, osteoblastic cells, or mesenchymal stem cells 56
4.5.2 Mesenchymal stem cells derived from mice with a hematopoietic deletion of ASXL1 do not show distinct differences in CFU-F capacity, passage-dependent cell growth, and spontaneous differentiation 57
5 Discussion 59
5.1 Depicting hematopoiesis during aging, in CHIP, and in MDS using primary *in vitro* cultures 59
5.2 A failed MDS mouse model for investigating properties of mesenchymal stem cells 62
6 Supplements 65
6.1 Supplementary Figures 65
6.2 Supplementary Tables 70
7 References 76
8 List of own Publications 88
9 Acknowledgements 90

Abbreviations

AML	Acute myeloid leukemia
ASXL1	Additional Sex Combs Like 1
BFU-E	Burst forming erythroid colonies
BIC	Bayesian information criterion
BM	Bone marrow
CAR	CXCL12-abundand reticular
cDNA	Complementary DNA
CFU	Colony forming units
CFU-E	CFU-erythrocytic
CFU-F	Fibroblast CFU
CFU-G	CFU-granulocytic
CFU-GEMM	CFU-granulocytic, erythrocytic, monocytic, megakaryocytic
CFU-GM	CFU-granulocytic, monocytic
CFU-M	CFU-monocytic
CFU-U	CFU-unclassifiable
CHIP	Clonal hematopoiesis of indeterminate potential
CI	Confidence interval
CMML	Chronic myelomonocytic leukemia
CMP	Common myelocyte progenitors
DMSO	Dimethyl sulfoxide
DNA	Deoxyribonucleic acid
EC	Endothelial cells
eGFP	Enhanced Green Fluorescent Protein
EPO	Erythropoietin
FACS	Fluorescence-activated cell sorting
FCS	Fetal calf serum
FLT3	Fms-like tyrosine kinase 3
G-CSF	Granulocyte colony-stimulating factor
GF	Growth factor
GM	Granulocyte-monocyte
GM-CSF	Granulocyte-macrophage colony-stimulating factor
GMP	Granulocyte monocyte progenitor
GTP	Guanosine triphosphate
Hb	Hemoglobin
HSC	Hematopoietic stem cell
HSPC	Hematopoietic stem and progenitor cell
HTH	Helix turn helix
IL-3	Interleukin-3

IL-6	Interleukin-6
IMDM	Iscove's Modified Dulbecco's Medium
IPSS-R	Revised International Prognostic Scoring System
LMPP	Lymphoid-primed multipotent progenitors
LOD	Limit of detection
LSC	Leukemic stem cell
LSK	$Lineage^{-}$ $Sca\text{-}1^{+}$ $c\text{-}Kit^{+}$ cells
LT-HSC	Long-term HSC
MC	Mononuclear cells
MDS	Myelodysplastic syndrome
MegE	Megakaryocyte-erythrocyte
MEP	Megakaryocyte erythrocyte progenitor
miRNA	MicroRNA
MLP	Multipotent lymphocyte progenitors
MPN	Myeloproliferative neoplasia
MPP	Multipotent progenitor
mRNA	Messenger RNA
MSC	Mesenchymal stem cells
OBC	Osteoblastic cells
ODE	Ordinary differential equation
PBS	Phosphate-buffered saline
PDMS	Polydimethylsiloxane
PDVF	Polyvinylidenefluoride
PHD	Plant homeodomain
PI	Propidium iodide
PRC2	Polycomb repressive complex 2
qPCR	Quantitative polymerase chain reaction
Rpm	Rounds per minute
SF3B1	Splicing Factor 3b Subunit 1
SFM	Serum free medium
ST-HSC	Short-term HSC
TPO	Thrombopoietin
UV	Ultra violet
VAF	Variant allele frequency
vWF	Von Willebrand factor
WBC	White blood cells
WHO	World Health Organization

1 Abstract

Myelodysplastic syndromes (MDS) are clonal disorders of hematopoietic stem and progenitor cells (HSPCs) characterized by ineffective hematopoiesis with dysplastic features and peripheral cytopenia. The disease can evolve from low risk to high risk MDS followed by transition into secondary acute leukemia (sAML). Even before MDS is evident, a considerable number of aged individuals show clonal expansion of blood cells but without features of hematologic malignancy. This phenomenon is termed clonal hematopoiesis of indeterminate potential (CHIP) and predisposes to blood cancer. The mutational spectrum found in individuals with CHIP, MDS, and sAML is overlapping, whereas the impact on hematopoiesis provoked by identical mutations differs depending on the underlying entity. The first part of this study focused on kinetic changes occurring within the hematopoietic hierarchy during aging and in individuals with CHIP and MDS. These characteristics may provide fundamental knowledge about achieving clonal dominance and the reorganization of the HSPC compartment in the process of leukemic transformation. We therefore established a data driven systems medicine approach. First, we sorted hematopoietic stem cells (HSCs), cultured them in differentiation medium, and immunophenotyped arising cell types for 7 days. Specific labeling enabled to track cell type and cell division status simultaneously. Generated data was then provided for mathematical modeling to assess plausible hematopoietic hierarchies and to investigate parameters for proliferation, differentiation, and cell death for each HSPC subcompartment.

Starting with the analysis of age-related changes, we found increased HSPC proportions in bone marrow (BM) of aged individuals (n=15) compared to young (n=10). In our HSC culture approach, we also saw a trend for increased HSPC proportions but more important, we found an overall reduced cell production in aged individuals, which was remarkably visible on the more mature cell level. This effect could be further traced to a decreasing HSC proliferation, providing a simplified model of aging hematopoiesis in which age-related decline of blood cell production has its origin on the HSC level.

Analysis of the mutational spectrum revealed that nearly 50 % of individuals in our healthy aged cohort carry a CHIP mutation. To further characterize these individuals, we compared them to healthy age-matched individuals without mutations (n=8) and to MDS patients (n=10). Applying the workflow described above, a systematic comparison of competing hematopoietic

hierarchies was performed on generated *in vitro* data. Almost all healthy non-mutated samples were best described by the classical model of hematopoiesis. However, the classical model of hematopoiesis was not sufficient to discribe hematopoiesis for some CHIP and the majority of MDS samples. Properties of models best describing hematopoiesis in CHIP and MDS were summarized in a union model to define proliferation, differentiation, and cell death of HSPC subcompartments. Deregulated rates were found at various level of the HSPC compartment with a high inter-individual heterogeneity in both CHIP and MDS. Our results depict increasing kinetic heterogeneity in CHIP and MDS and show that remodeling of the HSPC compartment is already present in a premalignant state.

Our HSC culture approach using human primary material is focused on hematopoietic cells, however, the non-hematopoietic microenvironment is playing an important role in malignant transformation of hematopoietic neoplasms. The microenvironment consists of different cell types and structures, providing a complex signaling network regulating the physiological function of HSPCs but also influencing the development of de novo AML and MDS. Vice versa, the function and genetic profile of niche cells was shown to be altered in patients with MDS and AML. In the second part of this study, we aimed to investigate alterations occurring in the bone marrow microenvironment in the course of MDS development and in fully developed MDS. Therefore, we utilized a previously published mouse model, in which the epigenetic regulator *ASXL1* is specifically deleted in the hematopoietic compartment. Unlike described in the publications, our *Vav-cre+ ASXL1*$^{fl/fl}$ mice showed only a very mild hematopoietic phenotype not sufficient to match criteria for an MDS-like phenotype. As expected from this, investigations on the BM niche including its composition and properties of mesenchymal stem cells could not reveal differences in *ASXL1* deleted mice compared to control mice.

2 Introduction

2.1 Hematopoietic stem cells

The production of blood cells is maintained by a hierarchy of progenitors originating from hematopoietic stem cells (HSCs). Unique properties of stem cells include the ability of dividing and renewing themselves for a long period of time, and while stem cells remain unspecialized, they can give rise to specialized cell types (Zakrzewski et al., 2019). HSCs accomplish these requirements within the red bone marrow (BM) where they are localized with a frequency of 1:10 0000 to 1:100 000 (Bonnet, 2002; Haas et al., 2018). Here, they are surrounded and influenced by a special microenvironment, the BM niche supporting HSC homeostasis.

Maintaining hematopoiesis throughout our entire life, HSCs have an extensive proliferative capacity. During cell expansion, a fine balance between lineage commitment and HSC self-renewal must be sustained. In mammalian adult hematopoiesis, asymmetric cell divisions have been suggested to regulate this balance (Takano et al., 2004). Alterations in the equilibrium of asymmetric versus symmetric cell divisions can affect tissue homeostasis and can lead to stem cell exhaustion or expansion (Ito and Suda, 2014). To preserve long-term proliferation capacity and genomic stability over the whole lifetime of an individual, 90 % of HSCs remain in a quiescent state in G0 phase (Passegué et al., 2005; Walter et al., 2015). Stem cell homeostasis, as well as quiescence, regeneration, and aging are affected by metabolic pathways, including hypoxia, glycolysis, and reduction-oxidation reactions (Ito and Suda, 2014).

The identification of HSCs can be realized using different methods: Transplantation studies are based on functional properties of HSCs, which are able reconstitute the entire hematopoietic system *in vivo* and to maintain blood production throughout the life span of the transplanted individual (Bonnet, 2002). The identification of HSCs via surface markers is based on phenotypical properties, allowing identification of functional human HSCs with a frequency of about 1:10 and allowing identification of functional mouse HSCs with a frequency of about 1:2. Surface markers used for this identification are lineage- CD34+ CD38- CD90+ CD45RA- for human and lineage- CD48- Sca-1+ c-Kit+ CD150+ CD244- for mouse HSCs (Kiel et al., 2005; Majeti et al., 2007). On the transcriptional level, HSCs can be identified by expression of the *HOXA3/PRDM16/HOXB6* module, as well as the expression of the *HLF/ZFP36L2* module, comprising *MECOM/EVI1*, *HFL*, and *GATA3* transcription factors (Fischbach et al., 2005; Frelin

et al., 2013; Kataoka et al., 2011; Shojaei et al., 2005; Velten et al., 2017). HSCs also express genes from the earliest priming modules, including the *FLT3*/*SATB1* module present in the early lymphoid and myeloid[1] progenitors and the *GATA2/NFE2* module present in early megakaryocyte/erythrocyte progenitors (Velten *et al.*, 2017).

2.2 Hematopoiesis in human and mouse

Hematopoiesis describes the continuous formation and turnover of all blood lineages, which is based on a hierarchy of progenitors. The well-known classical model of hematopoiesis suggests that HSCs give rise to multipotent progenitors (MPPs), which dichotomously form common myelocyte progenitors (CMPs) and multipotent lymphocyte progenitors (MLPs). CMPs can further differentiate to megakaryocyte erythrocyte progenitors (MEPs) or granulocyte monocyte progenitors (GMP, Doulatov et al. (2012); Nimmo et al. (2015)). Altogether, these cells correspond to the hematopoietic stem and progenitor cell (HSPC) compartment, identifiable by the expression of CD34 and accounting for 2.15 ± 1.01 % of all BM cells (Povsic et al., 2010). The vast majority of hematopoietic cells within the BM are further downstream of the HSPC compartment. These late progenitors differentiate from unipotent blasts through various steps to mature blood cells (**Figure 1**).

Further investigations of the hematopoietic hierarchy in mouse and human have led to revised models of the classical HSPC hierarchy, showing that hematopoiesis is less hierarchical and less strict than initially thought: Adolfsson et al. (2005) identified a new hematopoietic cell type in mouse, the lymphoid-primed multipotent progenitors (LMPPs), which are FLT3+ lineage− Sca-1+ c-Kit+ cells (LSK FLT3+ cells). This cell type possesses B-cell, T-cell and granulocyte-monocyte (GM) potential but lack megakaryocyte-erythrocyte (MegE) potential. Mouse LSK cells were known to include long-term HSCs, short-term HSCs, and MPPs. The discovery of a distinct LSK subtype that does not have MegE potential lead to the emergence of an alternate model of hematopoiesis where MEPs can directly arise from HSCs. Furthermore, loss of MegE potential in the newly defined LMPP compartment indicates a direct LMPP to GMP transition, without differentiation into CMPs first. Adolfsson *et al.* (2005) also suggested a hematopoietic model combining data supporting the classical model of

[1] In general, „myeloid" means related to or derived from the BM. In addition, it is often used for specific blood lineages, including granulocyte, monocyte, and sometimes erythrocyte and platelet lineages but excluding lymphocytes.

hematopoiesis and their findings. In this model, HSCs can generate LMPPs with lymphocyte and GM potential, and CMPs with MegE and GM potential. The direct differentiation path from HSCs to MEPs was also supported by *in vitro* studies of Takano et al, who investigated colony forming units of LSK daughter and granddaughter cells. However, a separate study from Forsberg et al. (2006) also investigated the lineage potential of FLT3+ LMPPs but found conflicting results, which instead support the classical model of hematopoiesis.

In another mouse study, a fraction of phenotypically defined HSCs was shown to express von Willebrand factor (vWF), a protein mainly expressed by platelets and endothelium (Månsson et al., 2007). The existence of a megakaryocyte-primed HSC subset was also experimentally investigated by Sanjuan-Pla et al. (2013) generating vWF-eGFP transgenic mice, isolating LSK $CD150^{+}CD48^{-}CD34^{-}$ HSCs with a high eGFP expression and transplanting them into irradiated mice. They found that vWF-eGFP+ HSCs were platelet biased, additionally contributing to other myeloid lineages whereas their lymphoid contribution was very marginal.

A direct transition from the MPP compartment to MEPs is supported by studies from Notta et al. (2016). They identified BAH1 and CD71 as erythroid and megakaryocytic differentiation markers within the human CD34+ CD38- MPP compartment.

The basis of all these studies were defined cell compartments, presumed as homogenous cell populations, phenotypically characterized by different sets of surface markers and differentially expressed transcription factors (Akashi et al., 2000). Combined index-FACS and single-cell transcriptomic analysis recently revealed that lineage commitment is a continuous process, in which stem and progenitor cells do not represent stable and discrete states (Pellin et al., 2019; Velten *et al.*, 2017). In this gradual differentiation, maturing cells pass through progenitor compartments defined by fluorescence-activated cell sorting (FACS), which can be therefore considered as transitory states (Haas *et al.*, 2018; Laurenti and Göttgens, 2018).

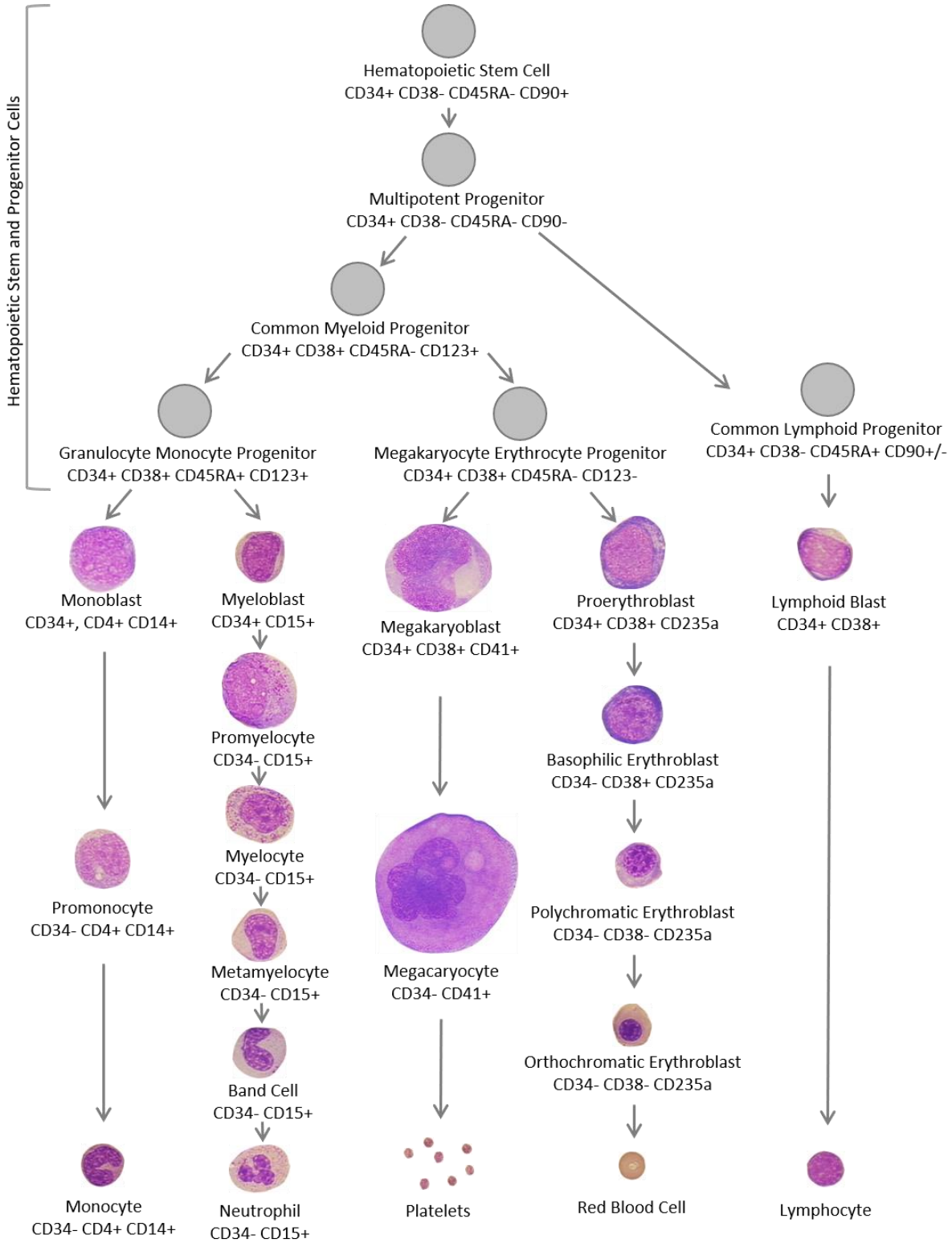

Figure 1: Human hematopoietic hierarchy according to the classical model of hematopoiesis. Early hematopoiesis takes place within the hematopoietic stem and progenitor cell (HSPC) compartment comprising hematopoietic stem cells, multipotent progenitors, common lymphoid progenitors (also referred to as multipotent lymphocyte progenitor), common myeloid progenitors, granulocyte monocyte progenitors, and megakaryocyte erythrocyte progenitors. Later hematopoietic cells comprise morphologically distinguishable cell types, as indicated. Surface markers important for this study are shown below cell type names.

2.3 Aging, CHIP, and MDS

With increasing age, the hematopoietic system undergoes dramatic changes, predominantly characterized by an increasing contribution toward myeloid cell types to the expense of lymphoid differentiation, loss of regenerative potential, and an increased number of phenotypically defined, long-term repopulating HSCs (Beerman et al., 2010; de Haan and Van Zant, 1999; Dykstra et al., 2011; Rossi et al., 2005). These observations are mainly based on murine data whereas human studies are rare and contradictory: Kuranda et al. (2011) did not observe a myeloid bias of aged human HSCs in xenograft experiments, whereas Pang et al. (2011) saw a myeloid lineage dominance along with decreased repopulating capacity in their xenograft experiments. Studies are consistent when analyzing the proportion of myeloid progenitors during aging, which were found not to be increased in humans (Kuranda *et al.*, 2011; Pang *et al.*, 2011; Rundberg Nilsson et al., 2016). In line with the mouse studies, the frequency of HSCs is significantly increased with age in human BM (Pang *et al.*, 2011; Rundberg Nilsson *et al.*, 2016), though the study by Kuranda *et al.* (2011) could not show statistically significance for a comparable HSC population.

Lymphoid to myeloid lineage skewing at the HSPC level might be caused by shifted differentiation at the branching point of MPP towards CMPs or MLPs or by altered proliferation and cell death rates at the CMP and MLP level. Furthermore, already the HSC pool was shown to be heterogeneous with HSCs biased towards the lymphoid or myeloid lineage (Beerman *et al.*, 2010; Challen et al., 2010; Morita et al., 2010; Muller-Sieburg and Sieburg, 2006). Thus, alterations in the HSC pool composition with more myeloid biased HSCs than lymphoid biased HSCs might be a reason for early lineage skewing in aged individuals (Geiger et al., 2013), resembling more the concept of a gradual hematopoietic differentiation (Pellin *et al.*, 2019; Velten *et al.*, 2017).

The size of the HSC pool is regulated by different control instances, including the niche and the cell division mode (Giebel and Bruns, 2008). Whether HSCs divide symmetric or asymmetric is strongly linked to the polarity status before mitosis, which is in turn determined by cell-intrinsic level of the activity of CDC42. During aging, CDC42 activity is elevated leading to a loss of polarity in HSCs and to more symmetric cell divisions (Florian et al., 2012; Florian et al., 2018).

Aged HSCs can accumulate genetic lesions and DNA damage, favoring the event of clonal hematopoiesis and the selection of a pre-leukemic HSC clone. Individuals with such genetic alterations but without evidence of hematologic malignancies were classified as clonal hematopoiesis of indeterminate potential (CHIP, Steensma et al. (2015)). They have a small but significantly increased risk for coronary heart disease, ischemic stroke, and show increased all-cause mortality. Most important for this study, individuals with CHIP have an increased risk of acquiring hematological neoplasia such as myelodysplastic syndrome (MDS, Jaiswal et al. (2014); Silver and Jaiswal (2019)). The most common mutated genes in CHIP are *DNMT3A*, *TET2, ASXL1*, and *PPM1D* and 80% of detected mutations overlap with mutations found in leukemia or lymphoma (Steensma *et al.*, 2015).

MDS is a heterogeneous group of clonal stem cell disorders, characterized by BM failure, and frequently progressing into acute myeloid leukemia (AML). MDS is more common in older individuals, with a median disease onset of 70 years and a median survival of only 30 months (Germing et al., 2013; Greenberg et al., 2012). In this study, MDS were classified according to the 2016 revision to the World Health Organization (WHO) classification of myeloid neoplasms and acute leukemia (Arber et al., 2016). Important criteria for diagnosing MDS are peripheral cytopenia(s), morphologic dysplasia(s), blast count, cytogenetic abnormalities, and occurrence of ring sideroblasts, which are iron laden mitochondria accumulating around the nucleus of erythroid precursors (Arber *et al.*, 2016). An important standard for assessing the prognosis of primary untreated adult MDS patients is the meanwhile revised International Prognostic Scoring System (IPSS-R). Considering cytogenetics, BM blast count, hemoglobin level, platelet counts, and the absolute neutrophil count, the IPSS-R score groups MDS patients into five risk categories with a median survival ranging from 0.8 to 8.8 years (Greenberg *et al.*, 2012).

With a share of 80% to 90%, the majority of MDS patients show recurring mutations. Mutated genes are predominantly involved in mRNA splicing, epigenetic regulation, receptor and kinase signaling, transcription regulation, tumor suppression, and adhesion. Most common mutated genes are *SF3B1*, *TET2*, *SRSF2*, *ASXL1*, *DNMT3A*, *RUNX1*, *U2AF1*, *TP53*, and *EZH2* (**Table 1**, Haferlach et al. (2014); Ogawa (2019); Papaemmanuil et al. (2013)). Furthermore, the genetic lesions affect the patients' clinical outcome: Whereas mutations in *TP53*, *EZH2*, *ETV6*, *RUNX1*, and *ASXL1* are predictive for a poor outcome, *SF3B1* when present as a single mutation shows a decreased hazard ratio (Bejar et al., 2011; Haferlach *et al.*, 2014). Mutations

are also associated with phenotypical characteristics, as shown for *RUNX1*, *TP53*, and *NRAS* being associated with severe thrombocytopenia and increased BM blasts (Bejar *et al.*, 2011), or for *SF3B1* being associated with the appearance of ring sideroblasts (Papaemmanuil et al., 2011).

Table 1: Major driver genes involved in the pathogenesis of MDS. * Mutant IDH1 and IDH2, but not unmutated forms, affect DNA methylation. **†** Germline variants are implicated in the predisposition to AML/MDS. Table copied from Ogawa (2019).

Pathway/functions	**Driver genes**
DNA methylation	*DNMT3A*, *TET2*, *IDH1*,**IDH2*,* and *WT1*
Chromatin modification	*EZH2*, *SUZ12*, *EED*, *JARID2*, *ASXL1*, *KMT2*, *KDM6A*, *ARID2*, *PHF6*, and *ATRX*
RNA splicing	*SF3B1*, *SRSF2*, *U2AF1*, *U2AF2*, *ZRSR2*, *SF1*, *PRPF8*, *LUC7L2*
Cohesin complex	*STAG2*, *RAD21*, *SMC3*, and *SMC1A* (*PDS5B*, *CTCF*, *NIPBL*, and *ESCO2*)
Transcription	*RUNX1*,†*ETV6*,†*GATA2*,†*IRF1*, *CEBPA*, *BCOR*, *BCORL1*, *NCOR2*, and *CUX1*
Cytokine receptor/tyrosine kinase	*FLT3*, *KIT*, *JAK2*, and *MPL*, *CALR*, and *CSF3R*
RAS signaling†	*PTPN11*, *NF1*, *NRAS*, *KRAS*, and *CBL* (*RIT1* and *BRAF*)
Other signaling	*GNAS*, *GNB1*, *FBWX7*, and *PTEN*
Checkpoint/cell cycle	*TP53* and *CDKN2A*
DNA repair	*ATM*, *BRCC3*, and *FANCL*
Others	*NPM1*, *SETBP1*, and *DDX41*†

The accumulation of genetic lesions (mutations and chromosomal aberrations) within HSCs are thought to be responsible for disease evolution. Proposed models for disease development suggest a linear evolution, in which mutations serially accumulate in HSCs, versus a non-linear model in which MDS stem cells have a significantly higher complexity of subclonal mutations compared to MDS blast cells suggesting a parallel clonal evolution with distinct subclones (Chen et al., 2019). During disease progression over years, the blast count, as well as number of mutations and other genetic alterations increases (Ogawa, 2019; Walter et al., 2012). In our study, we particularly focused on mutations in *ASXL1* and *SF3B1*, as they are very common in MDS, they are both founder mutations, and they represent both sides of the prognostic spectrum, with a poor and a favorable patient outcome, respectively (Mossner et al., 2016; Ogawa, 2019).

2.4 Additional Sex Combs Like 1 – a polycomb repressive complex protein

Additional Sex Combs Like 1 (*ASXL1)* codes for a nuclear protein with 1084 amino acids, characterized by an N-terminal HARE-helix turn-helix domain (HARE-HTH), an ASXH globular domain, and a C-terminal plant homeodomain (PHD). One physiological mechanism of ASXL1 is its recruitment of the Polycomb repressive complex 2 (PRC2) to leukemogenic loci, which are repressed by PRC2-mediated histone H3 lysine 27 (H3K27) tri-methylation. In contrary, deleted ASXL1 does not associate with PRC2 and subsequently leukemogenic loci were not repressed (Abdel-Wahab et al., 2012). Furthermore, the ASXH globular domain of ASXL1 is able to associate with BAP1, an ortholog of the ubiquitin carboxy-terminal hydrolase calypso in drosophila. The effect of both proteins was mutually reinforced by association of a C-terminally mutated ASXL1 protein with BAP1, leading to myeloid leukemogenesis through impairing multilineage differentiation of hematopoietic progenitors and accelerated RUNX1-ETO induced leukemogenesis (Asada et al., 2018).

These two examples are showing that mutations in *ASXL1* can promote leukemogenesis through multiple effects and that mechanisms leading to leukemogenesis might not be sufficiently investigated. On the one hand, the effect of *ASXL1* mutations on disease development and progression is mediated through a gain-of-function mutation due to expression of a truncated protein, on the other hand it is mediated through loss-of-function due to deletion of ASXL1. Mutations found in *ASXL1* are predominantly localized in exon 12, prior to the highly conserved PHD domain but after HARE-HTH and ASXH globular domain, they appear to be heterozygous, and they are frameshift or base exchange mutations leading to a premature stop of translation (Carbuccia et al., 2009; Schnittger et al., 2013).

2.5 Spliceosome factor 3b - a core component of U2 small nuclear ribonucleoprotein

The splicing factor SF3B is a multiprotein complex and an integral component of the U2 small nuclear ribonucleoprotein (snRNP). Within the spliceosome, SF3B has an essential role in pre-mRNA splicing as it recognizes the pre-messenger RNA's 3' branch site (Golas et al., 2003). Mutations in the largest subunit *SF3B1* are mostly missense substitutions in the HEAT domain. The C-terminally located HEAT-domain forms a helical structure within the protein, providing a scaffold for the U2 snRNP to support interactions with other SF3B subunits and defining an RNA binding platform for branch site recognition (Zhou et al., 2020).

2.6 The bone marrow niche and its role in aging and malignant transformation

The BM niche provides a multicellular microenvironment, regulating the hematopoietic function, including HSC quiescence, proliferation, mobilization, and lineage differentiation. The niche consists of a variety of different cells, including mesenchymal stem cells (MSC) that can differentiate into osteoblasts and adipocytes, endothelial cells, neuronal cells, and pericytes. Pericytes derive from mesenchymal origin and include a variety of stroma cells, such as pericytic MSC, Nestin-expressing cells, and CXCL12-abundant reticular (CAR) cells (Asada et al., 2017; Birbrair and Frenette, 2016; Cordeiro-Spinetti et al., 2015; Pleyer et al., 2016). HSCs can be localized in different subniches, near the inner bone surface (endosteal niche) where HSCs are predominantly quiescent, or close to blood vessels (arteriolar and sinusoidal perivascular niche). Whereas in the arteriolar niche HSCs are also shown to be quiescent, the sinusoidal perivascular niche comprises activated HSCs (Arber *et al.*, 2016; Birbrair and Frenette, 2016; Cordeiro-Spinetti *et al.*, 2015; Ikonomi et al., 2020).

HSC aging and leukemogenesis are accompanied by changes in the BM niche. Aged stroma secreting higher levels of the pro-inflammatory CC-chemokine ligand 5 (CCL5) was shown to promote myeloid lineage skewing (Ergen et al., 2012). Aged stroma is also associated with reduced levels of secreted matrix protein osteopontin (OPN), leading to loss of HSC polarity and impaired engraftment potential (Guidi et al., 2017). Furthermore, aging is associated with the loss of niche-associated adrenergic nerves, which promotes HSC aging (Maryanovich et al., 2018).

In MDS and AML patients, MSC were shown to be altered on the molecular and functional level, including chromosomal aberrations, transcriptomic and epigenetic alterations, as well as changes in cytokine secretion, support of HSC, and differentiation potential. MSCs are potent to modulate the immune system, they interact with other niche cells, as well as with normal and leukemic stem and progenitor cells. The molecular and functional alterations of MSCs during disease progression lead to remodeling of the niche, promoting disease development by abnormal stem cell niche interactions, alterations in the immune system and impaired growth control (Pleyer *et al.*, 2016).

Several studies in mice showed that alterations of specific components of the BM niche are sufficient to initiate or promote leukemia. Deletion of the miRNA processing endonuclease *Dicer1* in osteogenic progenitors leads to impaired osteoblast differentiation and mice

developed an MDS-like phenotype with peripheral cytopenia, dysgranulopoiesis, dysplastic megakaryocytes and occasionally AML (Raaijmakers et al., 2010). A mouse model with constitutive activation of *β-catenin* in osteoblasts leads to altered differentiation of myeloid and lymphoid progenitors and the development of AML (Kode et al., 2014). A mixed form of MDS and myeloproliferative neoplasia (MPN) was found in mice with loss of *Sipa1*, a RAP1 GTPase-activating protein, which is mainly expressed by mesenchymal stem and progenitor cells (Xiao et al., 2018). In humans, the concept of niche-induced leukemogenesis is supported by the occurrence of rare cases of donor-derived leukemia upon BM transplantation, where preexisting niche changes in the host are thought to support malignant transformation (Wiseman, 2011). In contrary, several studies report donor-derived leukemia arising from CHIP providing another hypothesis for leukemic transformation after transplantation (Gondek et al., 2016; Rojek et al., 2016).

2.7 Aim of this study

The HSPC compartment, including HSCs, MPPs, MLPs, CMPs, GMPs, and MEPs is shown to be altered during aging, in CHIP, and in myeloid malignancies. Data particularly describing the structure of the hematopoietic hierarchy and kinetic rates in the HSPC compartment are rare and often based on mouse studies. However, this kind of data is very important to understand how clonal dominance is achieved and to understand characteristics of a leukemic stem cell compartment. To address this, we aimed to establish a cell culture approach providing appropriate data for computational modeling to analyze the hematopoietic hierarchy as well as proliferation, differentiation, and cell death rates of each HSPC subcompartment. Human primary samples were used to purify HSC according to their surface marker profile and cells were cultured in medium allowing differentiation towards mature blood cells. Cell numbers, cell types, and cell divisions were analyzed at various time points to follow the process over time. Data was then provided for computational modeling revealing differences occurring in hematopoiesis during aging, in CHIP, and in MDS (**Figure 2**).

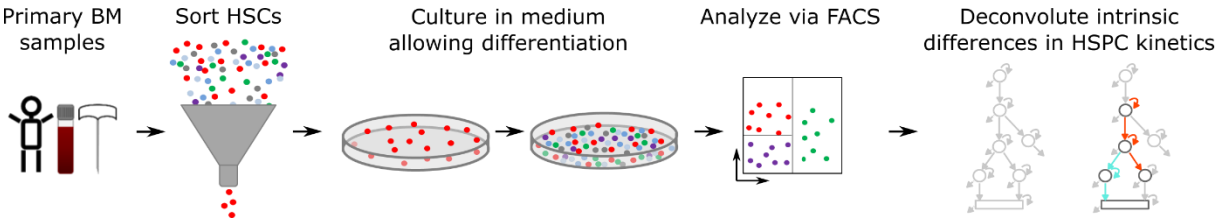

Figure 2: Workflow for investigating HSPC kinetics using human primary material. BM from healthy individuals and individuals with CHIP and MDS will be sorted for HSCs. HSCs will be cultured in medium allowing cell growth and differentiation, followed by time-resolved FACS analysis of these cultures to investigate different cell type numbers. Generated data will be provided for mathematical modeling unveiling alterations in HSPC kinetics, such as proliferation, differentiation, and cell death of HSPC subpopulations.

Our HSC culture approach is focused on cell-intrinsic driven alterations, whereas *in vivo* the normal and diseased hematopoietic system is influenced by the microenvironment and vice versa. In the second part of this study, we want to investigate alterations occurring in the BM niche during the course of MDS development and in fully developed MDS. We therefore utilize a previously described mouse model with hematopoietic deletion of *ASXL1* (genotype *Vav-cre+ ASXL1$^{fl/fl}$, Abdel-Wahab et al. (2013)*). We planned to analyze general alterations that may occur within the BM niche composition, followed by evaluation of alterations in MSC properties and function (MSC growth, osteogenic and adipogenic differentiation).

3 Methods

3.1 Healthy and MDS sample collection and storage

BM samples were obtained from MDS patients undergoing routine clinical evaluation. Healthy BM samples were collected from donor BM filters courtesy of the Stiftung Aktion Knochenmarkspende Bayern or obtained from femoral heads of patients undergoing hip replacement surgery courtesy of Dr. Martin Nolde and Dr. Dominikus Hausmann. Written informed consent in accordance with the Declaration of Helsinki was obtained from all patients according to protocols approved by the ethics committee of the Technische Universität München.

For cell extraction, BM filters were washed with PBS in a reverse direction, starting with the smallest filter. Received cell suspension was pooled to a volume of 50 ml. Femurs were chopped, placed into PBS and BM cells were mechanically extracted by shaking. Remaining bone pieces were removed by a 70 µm cell strainer. Cells were centrifuged (450xg, 10 min) and pellets were resuspended in 50 ml PBS. BM from MDS patients was diluted in IMDM to a total volume of 50 ml.

For healthy and MDS samples, mononuclear cells (MC) were isolated by gradient separation. Therefore, 2 parts of diluted sample were layered over 1 part of ficoll (Merck, Cat: L0115). Samples were centrifuged for 15 min, 2100 rpm, without break and MC were collected from the interphase. The MC suspensions were again centrifuged (10 min, 1500 rpm), cell pellets were mixed with freeze medium (10 % DMSO (Serva, Cat: 20385), 90 % heat inactivated FCS (Merck, Cat: S0115 or Biochrom, Cat: S0115), $5x10^7$ cells/ml), and frozen at -80°C using a freezing chamber maintaining a controlled freezing rate of approximately 1°C per minute. Healthy and MDS samples were stored in an N2 biobank.

3.2 Sample preparation and antibody staining for FACS

For sorting HSCs, frozen patient and donor BM samples were quickly thawed in a 37 °C water bath and immediately placed into IMDM (1x) + GlutaMAX (Gibco, Cat: 31980-022). Dead cells were reduced by density gradient centrifugation as described in the previous section. Cells were then washed with 2 ml PBS, centrifuged (450xg, 10 min) and pellets were mixed with 2 ml of 1 µM CellTrace™ Violet stain (ThermoFisher Scientific, Cat: C34557) in PBS (37°C) and incubated for 20 min at 37°C. The reaction was stopped by adding 10 ml ice-cold HF2 medium

containing 1xHBSS (Gibco, Cat:14185-045), 2% heat-inactivated FCS (Biochrom, Cat: S0115), 0.01 M HEPES (Gibco, Cat: 15630-056), and 100 U/ml Pen/Strep (Gibco, Cat: 15140-122). After incubating 5 min on ice, the suspension was centrifuged and antibody staining was performed.

First, cells were incubated with 100 µl biotin-coupled lineage mix (**Table 2**) for 20 min on ice and in the dark. Samples were then centrifuged (1500 rpm, 5 min) and pellets resuspended with 100 µl of fluorescence-coupled antibody mix (**Table 2**). After incubating 40 min on ice and in the dark, 2 ml of HF2 was added and the cell suspension was centrifuged (1500 rpm, 5 min). Pellets were resuspended in 500 µl HF2 with 0.2 µg/ml propidium iodide and filtered using a 40 µm cell strainer.

The sorting procedure was performed on a BD FACSAriaTM III equipped with 488 nm, 405 nm, 561 nm, and 633 nm lasers either in purity, single cell, or index mode. Purity of bulk-sorted HSC at day 1 in culture ranged from 77.9 - 95.4% (median purity 91.2%).

Table 2: Antibody panel mix used for identifying HSPC subpopulations, including HSCs, MPPs, MLPs, CMPs, GMPs, and MEPs in human BM cells.

Antibody target	Conjugate	Clone	Dilution	Company	Order No
Biotin-coupled lineage mix					
CD4	Biotin	RPA-T4	1:100	BioLegend	300504
CD8a	Biotin	RPA-T8	1:100	BioLegend	301004
CD15	Biotin	H198	1:100	BioLegend	323016
CD19	Biotin	H1BT9	1:100	BioLegend	302204
CD235a	Biotin	HIR2	1:100	eBioscience	13-9987-82
Fluorescence-coupled antibody mix					
CD34	FITC	581	1:20	BD	555821
CD90	PE	5E10	1:20	eBioscience	12-0909-42
CD123	BV510	6H6	1:20	BioLegend	306021
CD38	APC	HB7	1:40	BD	345807
CD45RA	PE-Cy7	HI100	1:40	BD	560675
CD45	PeCy5.5	HI30	1:100	BioLegend	304028
Streptavidin	APC/Cy7		1:100	BioLegend	405208

For analysis of cell compartments on day 1-7, cultured cells were harvested, centrifuged and antibody staining was performed as described for the sorting procedure, but without

CellTrace™ Violet staining. Additionally, 50 µl of Flow-Count Fluorospheres (Beckman Coulter, Cat: 7547053) were added right before sample acquisition. FACS analysis was performed on a BeckmanCoulter CyAn, equipped with 405nm, 488nm, and 633 nm lasers. Compensation and gating were performed using the FlowJo V10 software. In every FACS analysis and prior to applying the cell type specific gating strategy, cell debris, doublets, and dead cells were excluded using the gating software. Since CD38+ cells have been shown to lose CD38 expression during *in vitro* short-term culture (von Laer et al., 2000), the correct separation of CD38- and CD38+ compartments were based on backgating on CD90+ HSC. Gates were adjusted for each day of measurement and for each sample acquisition.

3.3 Serial dilution of CellTrace™ Violet stained cells

For determining FACS detection limit (LOD), a serial dilution of CellTrace™ Violet stained cells was performed. BM of a healthy individual was thawed and parted. One part was stained with CellTrace™ Violet stain as described in Sample preparation and antibody staining for FACS . Both, stained and unstained cell suspensions were counted and mixed in a serial dilution. Cells were measured on a BeckmanCoulter CyAn, and CellTrace™ Violet positive and negative cells were assessed for 100 or 1000 counts using the FlowJo V10 software. LOD for both cell numbers was estimated based on the standard deviation of the response and the slope (European Medicines Agency (1995)):

$$LOD_X = \frac{3.3\ \sigma}{S}$$

σ standard deviation
S slope

Notably, it is recommended that the upper concentration level for calculating the LOD should not exceed 10 times the expected LOD (Thomas et al., 2016). Therefore, prior to the LOD calculation, measured values were plotted against the used concentration and the expected LOD was manually estimated. Values not exceeding 10 times the expected LOD were then used for calculating the LOD.

3.4 Cell culture

For HSC-culture, either serum-free medium supplemented with 5 growth factors (SFM + 5GF) or serum-free medium supplemented with 8 growth factors (SFM + 8GF) was used (**Table 3**). Bulk-sorted HSCs were cultured at a concentration of $2.5x10^3$ cells/ml. Single-HSCs were

sorted into the inner wells of a 96-well plate and cultured in 100 µl medium. Outer wells were filled with H_2O.

Table 3: List of ingredients for serum-free medium supplemented with 5 growth factors (SFM + 5GF) or serum-free medium supplemented with 8 growth factors (SFM + 8GF). Since usage of SFM + 8GF lead to a higher cell yield than SFM + 5GF as shown in **Figure 4**, SFM + 8GF was used for all following experiments.

Reagent	Company, order number	SFM + 5GF	SFM + 8GF
IMDM(1x)+GlutaMAX	Gibco, 31980-022	80%	80%
BIT9500	StemCell Technologies, 09500	20%	20%
2-mercaptoethanol	Gibco, 31350-010	10 µM	10 µM
Ciprofloxacin	CiproHEXAL, 200mg/100ml	8 µg/ml	8 µg/ml
LDL	StemCell Technologies, 02698	4 µg/ml	4 µg/ml
SCF	R&D Systems, 255-SC	100 ng/ml	100 ng/ml
FLT3-Ligand	R&D Systems, 308-FK	100 ng/ml	100 ng/ml
TPO	R&D Systems, 288-TP	25 ng/ml	25 ng/ml
IL3	R&D Systems, 203-IL	10 ng/ml	10 ng/ml
IL6	R&D Systems, 206-IL	10 ng/ml	10 ng/ml
GM-CSF	R&D Systems, 215-GM		50 ng/ml
G-CSF	Filgrastim, Hexal		50 ng/ml
Erythropoietin	Janssen, PZN: 00878122		2 U/ml

Clonogenic capacity determined by colony forming unit (CFU) assay was either assessed for index-sorted or purity-sorted human HSCs. For index-sored HSCs, 100 µl of human StemMACS™ HSC-CFU Media with EPO (Miltenyi, Cat: 130-091-280) was prepared in each well of a 96-well plate. After sorting single-HSCs into these wells, plates were cultured for 21 days in a humidity chamber at 37°C with 5% CO_2. For purity sorted HSCs, 1000 cells were mixed with 3 ml human StemMACS™ HSC-CFU Media with EPO and split into two 30 mm culture dishes. Cells were cultured at 37°C with 5% CO_2 for 14 to 21 days. Colonies were scored with an inverted microscope using standard criteria.

If there was a sufficient number of HSCs after sorting, or if there was enough frozen BM material for repeated sorting, samples were analyzed in replicates.

3.5 Index sort data analysis

Index sort files were analyzed using the FlowJo V10 software and following instructions described in The Daily Dongle (2016). Briefly, single CD34+ HSPCs cells from a healthy

individual were index-sorted into three 96-well plates. This results in three sort files, each containing 96 cells. By applying the index sort script, each of the 96 cells appears as a new population. Each population was exported into single files, which can be manually assigned to a specific well number (A1 to H12) and mapped to results from the colony forming unit assays by adding keywords. All files (3x96) were concentrated into one file considering all necessary parameters (fluorescence channels) and keywords (well number and colony status). After concentrating all files (3x96) into one file, gating can be performed as usual, but including information about the colony forming unit status.

3.6 Mutational analysis

MDS patient samples were sequenced for diagnostic purposes for the most common mutations (Haferlach *et al.*, 2014). Healthy control samples were tested for clonal hematopoiesis-associated mutations using a previously described NGS assay covering 68 genes recurrently altered in myeloid neoplasms (Rothenberg-Thurley et al., 2017) by the Laboratory for Leukemia Diagnostics, Department of Medicine III, University Hospital, Ludwig-Maximilians-Universität, Munich, Germany. For assessing variant allele frequencies (VAF) in HSCs, DNA from a minimum of 200 sorted HSCs was subjected to whole-genome amplification (GenomiPhi V2, GE Healthcare), and subsequently analyzed using the same 68-gene panel by Laboratory for Leukemia Diagnostics, Department of Medicine III, University Hospital, Ludwig-Maximilians-Universität, Munich, Germany.

3.7 Time lapse experiments

Polydimethylsiloxane (PDMS) microwells were designed and fabricated by Alexandra Murschhauser from the Faculty of Physics and Center for NanoScience (CeNS), Ludwig-Maximilians-Universität, Munich, Germany. Each PDMS insert is consistent of 30 custom made microwells, each with a diameter and a depth of 300 µm. Inserts were placed onto a glass bottom dish and sterilized by 10 min UV exposure. Before seeding, PDMS microwells were incubated with 3 ml SFM + 8GF at 37°C. Then, bulk-sorted HSCs were directly pipetted into the microwells and incubated for 10 min. Density was checked and if necessary, another seeding step followed to achieve optimal microwell occupation (i.e. 2-3 cells per well). Time-lapse measurements were performed with a Nikon Ti Eclipse microscope (Nikon, Japan) and an incubation box (Okolab, Italy) at 37°C and 5% CO_2. A 20 min time interval for image acquisition was sufficient for accurate manual tracking. Manual single cell tracking was carried out using

the software tTt by Moritz Thomas from the Helmholtz Zentrum München–German Research Center for Environmental Health, Institute of Computational Biology, Neuherberg, Germany. Each cell was manually assigned to a cell fate: (i) division, (ii) cell death, or (iii) termination of tracking due to loss of cell identity, either because the cell could no longer be reliably tracked or because acquisition ended at 165 h. The single cell analysis was performed with PyCharm 2018.3.2 by Lea Schuh from the Helmholtz Zentrum München–German Research Center for Environmental Health, Institute of Computational Biology, Neuherberg, Germany.

3.8 Multi-compartment model and parameter inference

Mathematical modeling was performed by Lisa Bast from the Helmholtz Zentrum München–German Research Center for Environmental Health, Institute of Computational Biology, Neuherberg, Germany. Hematopoiesis was modeled as a biochemical reaction network of seven species S = {HSC, MPP, MLP, CMP, GMP, MEP, CD34-}, as published for models A – J in Bast et al. (2021). For the A, B, D, G, I union model (**Figure 13B**) the ordinary differential equation (ODE) system of the multi-compartment model includes reactions $R_1 - R_7$ for proliferation, $R_{22} - R_{27}$ for cell death, and R_8, $R_{10} - R13$, $R_{16} - R_{21}$ for differentiation between cell compartments according to Table 1-2 in Bast *et al.* (2021). Parameter inference was conducted by maximum likelihood estimation for every individual separately (see Transparent Methods in Bast *et al.* (2021)).

3.9 Animals

To generate mice with a homozygous, heterozygous, or without deletion of *ASXL1* in the hematopoietic system, *Vav-cre* (Tg(Vav1-icre)A2Kio) mice were crossed to *ASXL1* (STOCK Asxl1$^{tm1.1Iaai}$/J) mice. Genotypes of littermates were analyzed by PCR using the KAPA Mouse Genotyping Hot Start Kit (peqlab, Cat: 07-KK7352-01) according to the manufactures protocol. Temperatures for primer annealing were adjusted. Primer sequences, as well as annealing temperatures are described in **Table 4**. Mice of either genotype had libitum access to food and water and were housed and fed according to federal guidelines.

Table 4: Primers used for mouse genotyping. *Vav-cre* transgene was detected by *Vav-cre* forward (FW) and reverse (RW) primer, resulting in a 236 bp product. Wild type and floxed *ASXL1* was detected by *ASXL1* FW and RW primer, resulting in a 251 bp and 450 bp product, respectively. Excision of *ASXL1* after Cre recombination was confirmed by primers detecting a floxed portion of the construct (*ASXL1* Del FW and RW primer).

Primer	Sequence	Annealing temperature
Vav-cre	FW AGATGCCAGGACATCAGGAACCTG RW ATCAGCCACACCAGACACAGAGATC	58 °C
ASXL1	FW ACACCAACCAGCCGTTTTAC RW TCCTTGGATTTTTCTCAGCA	58 °C
ASXL1 Del	FW ACGCCGGCTTAACTGTACACG RW GACTAAGTTGCCGTGGGTGCT	64 °C

3.10 Organ extraction

For organ extraction, mice were sacrificed by cervical dislocation after anesthetizing with Isofluorane. Peripheral blood was directly extracted by puncture of the heard. Femur and tibia of mice were dissected, BM flushed, and cells resuspended in HF2 buffer. Femur and tibia were then smashed, adherent cells were extracted after collagenase treatment for 1.5 h at 37°C, and cells were resuspended in HF2 buffer. Remaining bone pieces were used for direct MSC culture. Peripheral blood, BM, and cells extracted after collagenase treatment were viable frozen at -80°C by mixing cell pellets with freeze medium (10% DMSO (Serva, Cat: 20385), 90% heat inactivated FCS (Merck, Cat: S0115 or Biochrom, Cat:S0115), $5x10^7$ cells/ml) and a controlled freezing rate of approximately 1°C per minute. For long-term storage, samples were transferred into an N_2 biobank.

3.11 Mouse MSC culture

MSCs were either obtained from smashed bone pieces, or from cells extracted after collagenase treatment (see Organ extraction). Bone pieces or cells were plated in mouse MSC medium (MEM α, GlutaMAX™ (Gibco, Cat: 32561037), supplemented with 10% FCS, 100 U/ml Pen/Strep (Gibco, Cat: 15140-122), and 0.05 mM 2-mercaptoethanol) and cultured at 37°C, 5% CO_2 until passage 3, obtaining an enriched MSC population. MSCs were splitted at a confluency of 60 to 70%.

3.12 *In vitro* colony-forming assay of murine hematopoietic cells

BM of *Vav-cre+ ASXL1*$^{fl/fl}$, *Vav-cre+ ASXL1*$^{fl/wt}$, and *Vav-cre- ASXL1*$^{fl/fl}$ mice was quickly thawed, washed with IMDM and mixed with cytokine-supplemented methylcellulose medium

(Methocult, STEMCELL Technologies, Cat: M3434) at a density of $4x10^4$ cells/replicate. Colonies were counted and classified after 10 days of culturing at 37°C and 5% CO_2.

3.13 Investigating CFU-F capacity

For assessing fibroblast colony-forming units (CFU-F), 100 mouse MSCs from passage 3 were plated onto one well of a 6 well plate. Cells were cultured at 37°C and 5% CO_2 in MSC medium for 3 days until small colonies were formed. Cells were visualized by crystal violet staining: Adherent MSCs were washed with PBS and fixed with 70% ethanol for 10 min at room temperature. Cells were stained for 1 h with 0,1% crystal violet stain. Staining solution was removed and wells were washed with deionized water. Colonies were counted with an inverted microscope.

3.14 RNA isolation, cDNA transcription, and qPCR

RNA isolation was performed using the RNeasy Mini Kit (QIAGEN) from frozen cell pellets containing approximately 10^7 cells. Cell pellets were resuspended in 350 µl RLT buffer containing 1% β-mercaptoethanol and were then centrifuged for 3 min at 10000 rpm. After adding 350 µl ethanol to the separated supernatant, lysates were transferred onto RNeasy Mini spin columns and centrifuged for 15 sec at 10000 rpm. The flow through was discarded and 700µl RW1 buffer was added to the column, followed by centrifugation (15 sec at 10000 rpm). The flow-through was discarded and 500 µl RPE buffer was added to the column and again centrifuged (15 sec at 10000 rpm). After discarding the flow-through, 500 µl of RPE buffer was added to the column and centrifuged at maximum speed for 2 min. The column was placed onto a new 1.5 ml collection tube and RNA was eluted by adding 16 µl RNase free water onto the column membrane and centrifugation for 1 min at maximum speed. RNA concentration and purity were measured using the NanoDrop™.

Reverse transcription of RNA was carried out using the QuantiTectRev. Transcription Kit (QIAGEN, Cat: 205311) according to the manufacturer's protocol. Briefly: Up to 1µg of isolated RNA was mixed with 2 µl gDNA Wipeout Buffer (7x) and RNase-free water to a total volume of 14 µl. The mixture was incubated for 2 min at 42°C and then immediately placed on ice. To each mixture, 6 µl of RT master mix containing 1 µl Quantiscript Reverse Transcriptase, 4 µl Quantiscript RT Buffer (4x), and 1 µl RT Primer Mix, was added. Samples were incubated for 15 min at 42°C followed by incubation for 3 min at 95°C. cDNA was stored at -20°C.

Real time quantitative PCR was performed using the Brilliant III Ultra-Fast SYBR® Green QPCR Maser Mix (Agilent Technologies, Cat: 600882) and specific primer for *RUNX1*, *PPARG*, and *RPL13A*. Each reaction contained 10 µl Reference dye with Master mix (1:50), 8 µl H_2O, 0.5 µl of each Primer (diluted 1:10 with H_2O), and 1µl cDNA, resulting in a total volume of 20 µl. Samples were analyzed in triplicates and non-template controls were performed to detect contaminations. Real time PCR was performed with the StepOnePlus™ System (Applied Biosystems™). *RUNX1* and *PPARG* were relatively quantified using the comparative delta CT calculation method and after normalization to *RPL13A*.

3.15 Antibody staining and FACS analysis of murine cells

For analyzing mature hematopoietic cells, stem cells, and stroma cells in mice, viable frozen cells were thawed, resuspended in IMDM(1x)+GlutaMAX (Gibco, Cat: 31980-022), and counted. Then, 1 to 10 $x10^6$ cells were mixed with respective antibody panel mixes summarized in **Table 5**. Single stains of each fluorophore serve for compensation. Antibodies were incubated for 1 h. Cells were then washed with HF2 medium, centrifuged, and pellets were resuspended in 500 µl HF2 with 0.2 µg propidium iodide. FACS analysis was performed on a BeckmanCoulter CyAn, equipped with 405nm, 488nm, and 633 nm lasers. Compensation and gating were performed using the FlowJo V10 software. Prior to applying the cell type specific gating strategy, cell debris, doublets, and dead cells were excluded using the gating software.

Table 5: Antibody panel mixes used for identifying mature hematopoietic cells, stromal cells, and stem cells in mice. Each antibody was used at a concentration of 1:500.

Antibody target	Conjugate	Company	Order No
Mature panel			
CD3e	PE Cy5.5	Invitrogen	35-0031-82
Gr1	eFluor 450	Invitrogen	48-5931-82
B220	PE Cy7	Invitrogen	25-0452-82
CD11b	APC	Invitrogen	17-0112-82
TER119	PE	Invitrogen	12-5921-83
MSC panel			
Alcam	PE	R&D	FAB1172P
CD31	APC	Invitrogen	17-0311-82
CD144	eFluor 450	Invitrogen	48-1441-82
Sca1	PE Cy7	Invitrogen	25-5981-82
TER119	PE Cy5.5	Invitrogen	35-5921-82
CD51	Biotin	Invitrogen	13-0512-82
Streptavidin	APC/Cy7	BioLegend	405208
Stem cell panel			
TER119	Biotin	Invitrogen	13-0112-85
CD11b	Biotin	eBioscience	13-0112-85
B220	Biotin	eBioscience	13-0452-85
CD48	Biotin	Invitrogen	13-0481-85
Gr1	Biotin	eBioscience	13-5931-85
CD3e	Biotin	eBioscience	13-0031-85
Streptavidin	PerCP Cy5.5	eBioscience	45-4317-82
CD150	PE	Invitrogen	12-1501-82
Sca1	PE Cy7	eBioscience	25-5981-82
c-Kit	APC	eBioscience	17-1171-83
CD34	FITC	eBioscience	11-0341-85
Single stains for compensation			
CD45	FITC	Invitrogen	11-0451-82
CD45	PE	Invitrogen	12-0451-82
CD45	PE Cy7	Invitrogen	25-0451-82
CD45	Per CP Cy5.5	eBioscience	45-0451-82
CD45	eFluor 450	eBioscience	48-0451-82
CD45	APC	eBioscience	17-0451-82
CD45	APC Cy7	Invitrogen	47-0451-82

3.16 Mouse blood values

Peripheral blood of mice was analyzed after blood sampling with the scil Vet ABC ™Hematology Analyzer.

3.17 SDS-PAGE and Western Blot

Mouse BM or spleen cell suspensions obtained after organ extraction were centrifuged and pellets were lysed by adding 30 – 50 µl lysis buffer. Samples were pipetted up and down for

re-suspension, incubated 30 min on ice, and sonicated (10 sec, 4 cycles, 30% power). The lysates were centrifuged at 6000 xg for 10 min at 4°C and supernatants were collected and diluted in PBS supplemented with protease inhibitor. Protein concentrations were analyzed using the DC Protein Assay (Bio-Rad). For each sample, 50 µg protein was mixes with PBS (supplemented with protease inhibitor) to a total volume of 15 µl. The suspension was then mixed with 15 µl 2x loading dye and heated for 5 min at 95°C. Prepared samples were loaded ono Mini-PROTEAN TGX Stain-Free Gels (Bio-Rad). As a molecular weight marker, 3 µl PageRulerPlusPrestained Protein Ladder (Thermo Fisher Scientific) was used. Proteins were separated in SDS running buffer at 120 V for 1.5 h. Afterwards, gels were immediately placed into transfer buffer. For Western blot, the BioRad Criterion Blotter, a wet blotting system was used. The polyvinylidenefluoride (PDVF) membrane was activated in methanol for 30 sec. Then, sponge, filters and PDVF membrane were incubated in transfer buffer. The blotting sandwich was arranged as follows: Sponge, 2 filter papers, gel, PDVF membrane, filter paper, and sponge. Proteins were blotted in cooled transfer buffer at 100 V for 30 min.

After the blotting procedure, membranes were blocked in 5% milk/TBS-T for 1 h at room temperature at gentle shaking. After three times of washing with TBS-T for 5 min, the primary antibody for ASXL1 (Santa Cruz, Cat: sc-293204, clone 6E2, diluted 1:500) was added and incubated overnight at 4°C in TBS-T containing 1% BSA and 0.1% sodium azide. Prepared antibody solutions were stored at 4°C and reused several times.

On the next day, primary antibody was removed and the membrane was washed three times in TBS-T each for 10 min at room temperature with gentle shaking. Then, the anti-mouse HRP-linked secondary antibody (1:10000) was added and incubated for 1.5 h. After removing secondary antibodies, membranes were washed three times with TBS-T at room temperature. Antibody binding was visualized on light-sensitive screens (Kodak) using ECL substrate.

3.18 Statistical analysis

Statistical analysis was performed using the GraphPad Prism software, if not stated otherwise. Statistical tests and corresponding p-values are summarized in **Table S3**. Dot plots are showing individual values and median line.

4 Results

4.1 A workflow for investigating HSPC kinetics

For analyzing HSPC kinetics as proposed in **Figure 2**, it is essential to have a robust FACS gating scheme for sorting HSCs and analyzing HSPC subpopulations, optimal culture conditions and knowing methodological limitations. For establishing these essential steps, we tested our gating scheme on the functional level, compared culture media, and tested the detection of rare populations via FACS.

4.1.1 Phenotypically defined HSPC subpopulations give rise to an expected spectrum of hematopoietic colonies

For identifying HSPC compartments by flow cytometry, a high-resolution 10-parameter gating strategy adapted from Doulatov et al. (2010); Majeti *et al.* (2007); and Manz et al. (2002) was applied. The gating strategy was based on the expression of lineage markers, CD45, CD34, CD38, CD45RA, CD123, and CD90 for identifying HSC, MPP, MLP, CMP, GMP, and MEP compartments. Lineage marker were chosen for a negative selection of cells not being HSPCs but expressing CD45 and CD34 (**Table 6**).

Table 6: Cells of the hematopoietic hierarchy and their expression of surface markers used in this study. Marker not expressed on the cell surface are indicated with -, marker with a dim expression are indicated with (+), and marker with a higher expression are indicated with +.

	Lineage										
	CD4	CD8a	CD15	CD19	CD235a	CD45	CD34	CD38	CD45RA	CD90	CD123
HSC	-	-	-	-	-	(+)	+	-	-	+	
MPP	-	-	-	-	-	(+)	+	-	-	-	
MLP	-	-	-	-	-	(+)	+	-	+	-/+	
CMP	-	-	-	-	-	(+)	+	+	-		+
GMP	-	-	-	-	-	(+)	+	+	+		+
MEP	-	-	-	-	-	(+)	+	+	-		-
Myeloblast			+			+	+				
Monoblast	(+)					+	+				
Proerythroblast					+	+	+				
T-cell	+	+				+	-				
B-cell				+		+	-				

To test if phenotypically defined HSPC subpopulations give rise to the expected type of colonies, we sorted lineage- CD45dim CD34+ HSPCs in single-cell index mode into three 96-well plates, performed single-cell based colony forming unit assays, and linked grown colonies to the index sort data file (**Figure 3A**). **Figure 3B** depicts the index sort data file comprising 288 (3x96) counts, which were classified as CMP, GMP, MEP, HSC, MLP, and MPP, according to their marker expression. Counts displayed in red gave rise to indicated colonies. Out of 288 sorted HSPCs, 79 cells gave rise to a colony. Except for MLPs and MPPs, every HSPC subpopulation gave rise to various types of colony forming units (CFU), including CFU-granulocytic, erythrocytic, monocytic, megakaryocytic (CFU-GEMM), CFU-granulocytic, monocytic (CFU-GM), CFU-granulocytic (CFU-G), CFU-monocytic (CFU-M), burst forming erythroid colonies (BFU-E), and some white unclassifiable colonies (CFU-U). For a better overview, we displayed the total amount of index-sorted HSCs, MPPs, MLPs, CMPs, GMPs, and MEPs and linked them to different colony subtypes (**Figure 3C**). Cells phenotypically classified as HSCs gave rise to red (BFU-E), white (CFU-M, CFU-G, and CFU-GM), and mixed (CFU-GEMM) colonies. CMPs gave rise to red (BFU-E) and white colonies (CFU-M, CFU-G, CFU-GM, and CFU-U), whereas further differentiated GMPs only gave rise to white colonies (CFU-M, CFU-GM, and CFU-U). Cells classified as MEPs predominantly gave rise to red colonies. Only a few MPPs and MLPs were sorted. Summarizing these data, HSPC compartments gave rise to the expected spectrum of colonies.

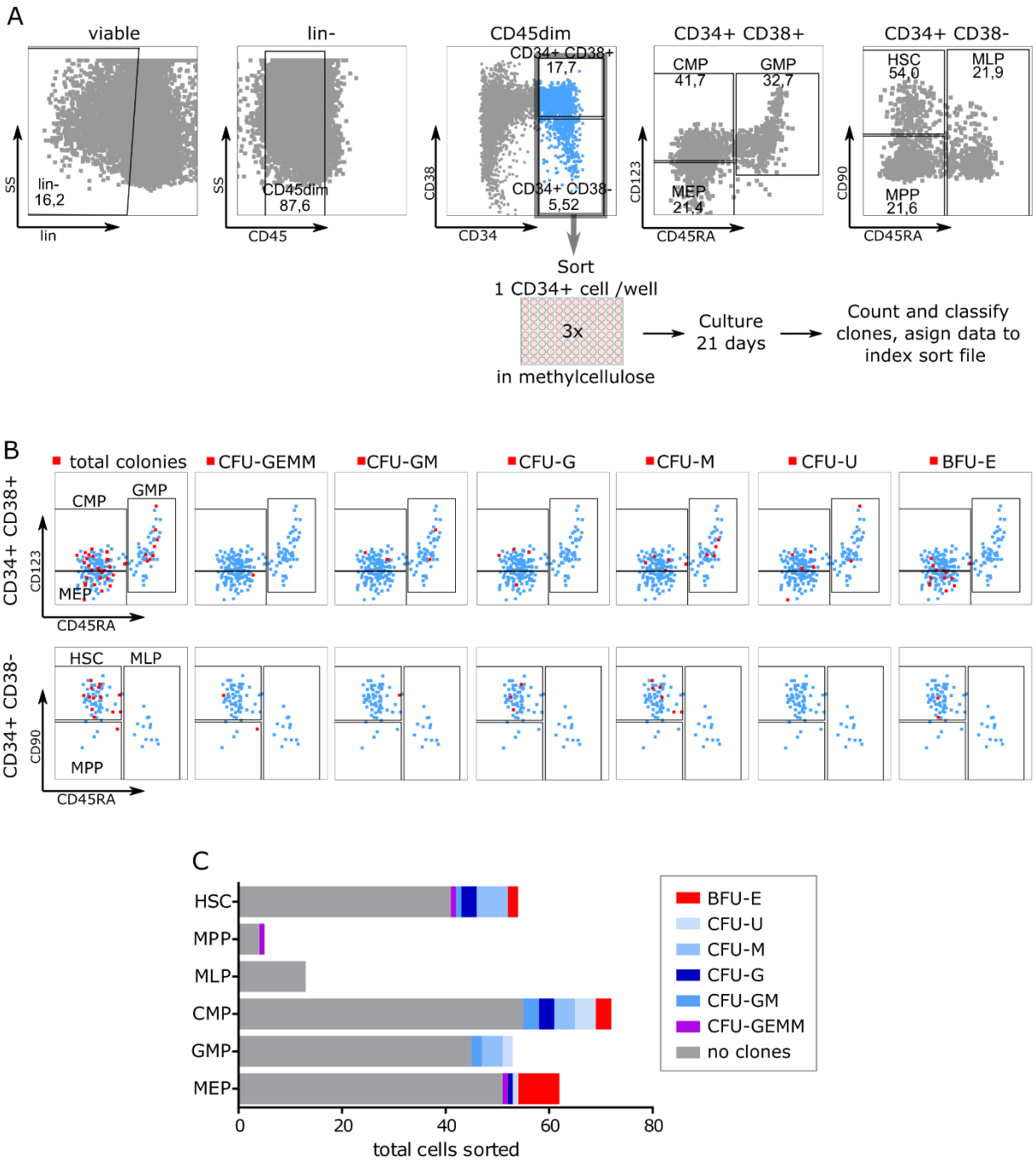

Figure 3: Index sort of human HSPCs and subsequent colony forming unit capacity. (**A)** Gating scheme for identifying lineage- CD45dim CD34+ HSPCs, including HSCs, MPPs, MLPs, CMPs, GMPs, and MEPs. As indicated, CD34+ HSPCs were index-sorted into 3 x 96-well-plates with methylcellulose. Cells were subsequently cultured for 21 days, colonies counted and classified, and linked to index sort file. **(B)** Illustration of index sort file, gated on CD34+ CD38+ cells to depict CMPs, GMPs, and MEPs or gated on CD34+ CD38- cells to depict HSCs, MPPs, and MLPs. Sort file was linked to information generated after single-cell colony forming unit assays: Red dots indicate either total colonies, CFU-GEMM, CFU-GM, CFU-G, CFU-M, white colonies which could not be classified (CFU-U), or BFU-E. **(C)** Total amount of index-sorted HSCs, MPPs, MLPs, CMPs, GMPs, and MEPs were linked to different colony subtypes.

4.1.2 Hematopoietic stem cells differentiate in vitro

For investigating HSPC-intrinsic proliferation, differentiation, and apoptosis in an *in vitro* approach it is essential to have a medium supporting HSC maturation into all lineages. We compared HSCs cultured for 6 days in serum free medium (SFM) either supplemented with 5 growth factors (GF) or 8 GF (see Methods). At day 1 of the HSC-culture, cells are undifferentiated, showing a high percentage of lineage- CD45dim CD34+ CD38- cells. At day 6, cells differentiated into lineage- CD45dim CD34+ CD38+ cells and CD34- cells using both media (**Figure 4A**).

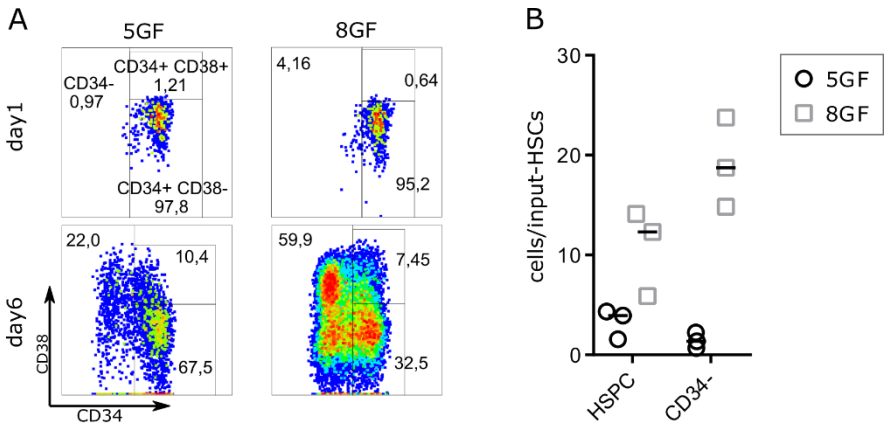

Figure 4: Comparison of growth and differentiation capacity of sorted HSCs cultured in serum free medium (SFM) supplemented either with 5 or 8 growth factors (GF). SFM+5 GF is supplemented with SCF, FLT3, IL-3, IL-6, and TPO, whereas SFM + 8GF is supplemented with SCF, FLT3, IL-3, IL-6, TPO, EPO, G-CSF, and GM-CSF. **(A)** Representative gating scheme of two healthy samples at day 1 and at day 6 after sorting HSCs. Plots are gated on lineage- CD45dim populations. **(B)** Investigation of HSPC and CD34- cell yield at day 6, normalized to total input HSCs on day 1.

To quantify *in vitro* cell production of both media, we normalized absolute cell counts from day 6 to absolute HSC number on day 1. Cells cultured in SFM + 8GF showed a higher yield of lineage- CD45dim CD34+ HSPCs and lineage- CD45dim CD34- cells compared to SFM + 5GF (**Figure 4B**), suggesting SFM + 8GF to be the preferred medium to investigate HSPC differentiation.

4.1.3 Detection limit of very rare populations by FACS is dependent on total cell counts analyzed

Analyzing human HSC-cultures meets two challenges: A very low number of total cells and very rare subpopulations arising during the differentiation process. To test if FACS meets the requirements for analyzing HSC-culture, we determined the limit of detection (LOD). Therefore, serial dilution was prepared using a mixture of unstained BM cells and cells stained

with CellTrace™ Violet stain. The dilution series was then measured by FACS and the frequency of CellTrace™ Violet positive cells was determined (**Figure 5A**). To mimic the low total cell number, either 1000 or 100 total cell counts were analyzed. LOD for both cell numbers was estimated based on the standard deviation of the response and the slope (European Medicines Agency (1995)). The LOD for 1000 and 100 analyzed cells was 0.49% and 8,26%, respectively (**Figure 5B**). These data suggest that FACS analysis is sufficient to identify rare populations of >0.49% by only measuring 1000 cells. For future experiments, this suggests to start with at least 1000 HSCs to detect rare populations. Considering that HSC expand about thirty times when culturing for 6 days (**Figure 4B**), a sufficient number of cells can be achieved over time when starting with a couple of hundred HSCs.

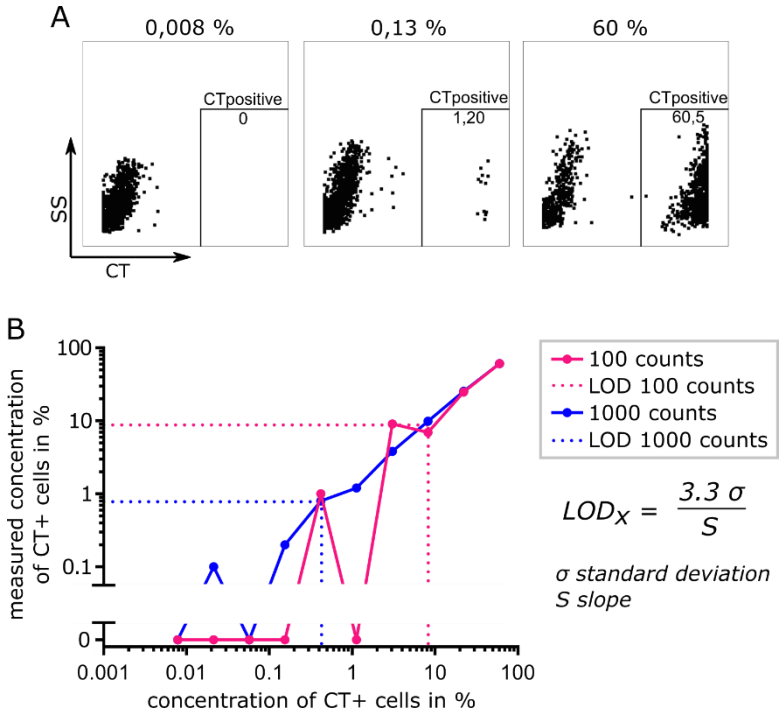

Figure 5: Detection limit of FACS analysis was investigated by serial dilution of CellTrace™ Violet stained cells in unstained cells. (A) FACS plots showing CellTrace™ Violet stain positive (CTpositive) counts for samples with an applied concentration of 0.008%, 0.13%, or 60% of CellTrace™ Violet stain positive cells. Plots were gated on viable cells. In total 1000 counts are shown in each plot. **(B)** Illustration of serial dilution showing measured and applied concentrations of CellTrace™ Violet positive cells. The blue line indicates the analysis of 1000 total counts, the pink line indicates the analysis of 100 total counts. Doted lines show the limit of detection (LOD) when measuring 1000 or 100 cells. LOD was estimated based on the standard deviation of the response and the slope.

4.2 *In vitro* cultures of HSCs resemble decreased cellularity found in BM of aged individuals, which is based on reduced HSC proliferation

Changes occurring in the hematopoietic system during aging are supposed to be caused by selection pressures from cell-intrinsic and cell-extrinsic factors. In this section, we are aiming to exclusively analyze HSPC-intrinsic alterations in aged individuals occurring in the hematopoietic architecture and in HSPC kinetics.

4.2.1 HSPCs are relatively increased in snapshot analysis of aged individuals

For identifying age-related changes in BM HSPC composition, we compared a group of 10 young individuals (median age 40, age range 20 to 52) with a group of 15 aged individuals (median age 68, age range 57 to 79, **Table S1**). BM of these individuals was analyzed by applying the HSPC gating strategy described in **Figure 3A**. With this gating strategy, HSCs, MPPs, MLPs, CMPs, GMPs, and MEPs were identified as shown for a representative young individual in **Figure 6A**. We find a significantly higher proportion of HSPCs (normalized to lineage- cells) in BM of aged individuals compared to the younger group (p=0,0176, Mann-Whitney test), as similarly described by Kuranda *et al.* (2011) and Taraldsrud et al. (2009) (**Figure 6B**, left panel). This increase could not be traced to one specific HSPC subpopulation, but rather every subpopulation shows a tendency to be increased during aging (**Figure 6B**, right panel). Cell proportions can only reflect the total number of cells, when there is no difference in cellularity, but during aging, the BM cellularity is clearly decreasing (Hartsock et al., 1965). Since data on cellularity is not available for our cohort, we consulted the study from Hartsock *et al.* (1965), investigating the BM cellularity during aging. They analyzed the percentage of hematopoietic tissue in the iliac crest from individuals younger than 10 years to individuals at the age of 79. These values were used to normalize HSPC and HSC proportions of our snapshot analysis from total BM according to their age group. Indeed, the relative increase found in aged total BM was repealed: Young and aged HSPCs and HSCs were present at a similar level after adjustment for cellularity (**Figure 6C**).

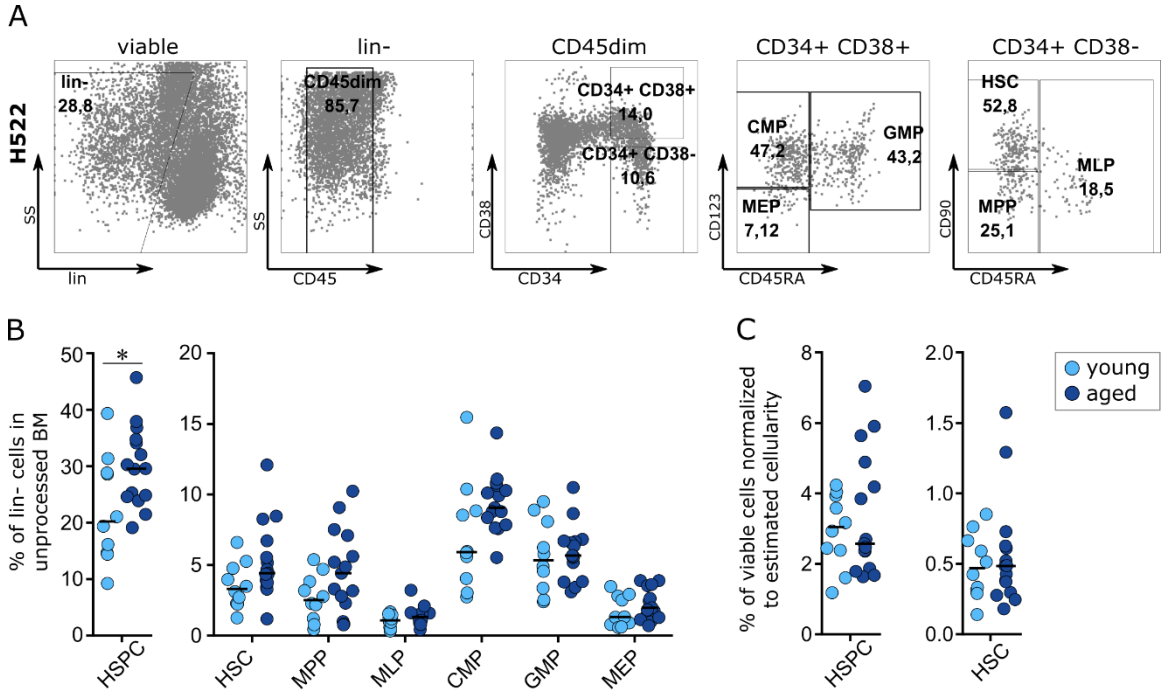

Figure 6: The percentage of HSPCs is increased in aged BM, but the effect is repealed after correction for assumed BM cellularity. (A) Representative FACS plots for identifying HSPCs and HSPC subpopulations, including HSC, MPP, MLP, CMP, GMP, and MEP. (**B)** Relative proportions of HSPCs and HSPC subpopulations in unprocessed BM samples from 10 young (median age 40) and 15 aged (median age 68) healthy individuals. Aged HSCPCs show a significantly higher proportion than young HSPCs (p=0,0176, Mann-Whitney test). Populations were normalized to lineage- (lin-) cells. **(C)** Combination of our study, investigating HSPC and HSC proportions in unprocessed BM with a study from Hartsock *et al.* (1965) investigating age-dependent BM cellularity. Proportions of HSPCs and HSCs within all viable cells estimated in unprocessed BM were further normalized to the age-dependent percentage of hematopoietic tissue in the iliac crest estimated from Hartsock *et al.* (1965).

4.2.2 In vitro *cultures of HSCs from aged individuals showed a declining blood cell production starting at the HSPC level*

For analyzing HSPC kinetics in young and aged individuals in greater depth, we set up a 7-day *in vitro* cell culture approach. First, we are aiming to recapitulate changes found in BM composition and then to assess absolute cell numbers and track cell divisions which is now possible using an *in vitro* cell culture system. Therefore, lineage- CD45dim CD34+ CD38- CD90+ CD45RA- HSC were sorted and cultured in SFM + 8GF for 7 days and repeatedly analyzed by FACS. Sorted HSCs differentiated during culturing into MPP, MLP, CMP, GMP, MEPs, and CD34- cells[2] (**Figure 7A**, **Figure S1**, and **Figure S2**). Reflecting the status in total BM, we could find a tendency for higher HSPC proportions (normalized to lineage- cells) in in aged individuals after 7-days culturing HSCs (**Figure 7B**).

[2] CD34- cells refer to hematopoietic cells more mature than HSPCs.

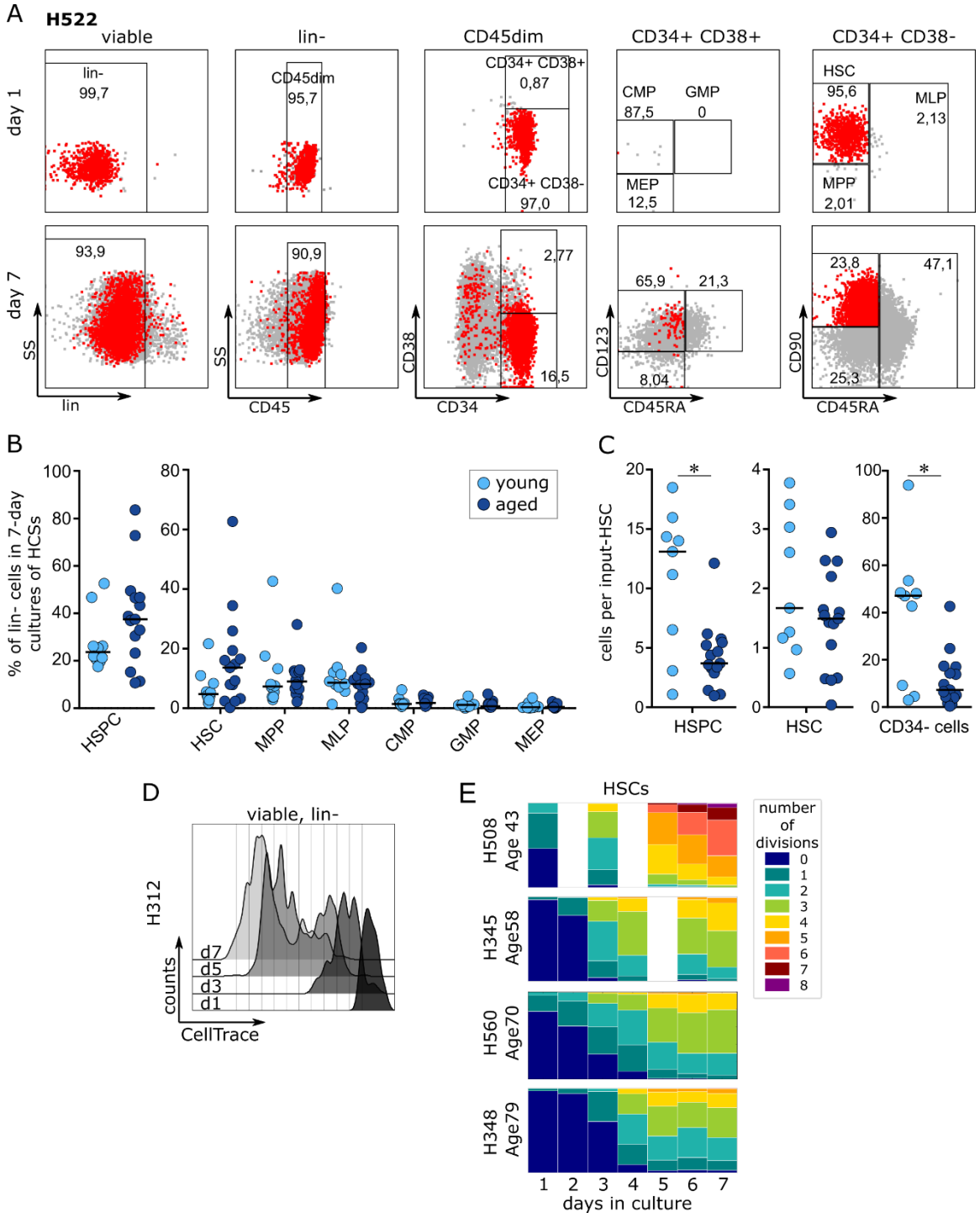

Figure 7: HSC cultures reveals slower or less HSPC expansion in aged individuals with further effects on the CD34- compartment. (A) Representative FACS plots for identifying HSPC subpopulations at day 1 and at day 7 after sorting HSCs and culturing in SFM +8 GF. To better identify the HSC population, all cells being CD90+, CD45RA- were highlighted in red. **(B)** Relative proportions of HSPCs and HSPC subpopulations 7 days after sorting HSCs from 10 young and 15 aged healthy individuals. Populations were normalized to lineage- (lin-) cells. **(C)** HSCs from aged individuals yield significantly less HSPCs and CD34- cells (p= 0,0074 and p= 0,0106, Mann-Whitney test), whereas the number of HSCs stays constant. Yield is defined as the absolute number of a respective cell type at day 7 normalized to the absolute number of HSCs at day 1. **(D)** Overlay of representative FACS plots illustrating cell divisions from day 1 (d1) to day 7 (d7) after sorting and culturing HSCs. Prior to sorting, cells were stained with CellTrace™ Violet stain, which fluorescence intensity halve at each cell division. FACS plots were gated on lineage- cells. **(E)** Percentage of HSCs (y-axis) passing up to 8 cell divisions during 7-day culture. Cell divisions and cell types were tracked simultaneously enabling to assign every count to both characteristics at each measured time point.

To quantify *in vitro* cell production, we normalized absolute cell counts from day 7 to absolute HSC number on day 1. Both, HSPC yield and CD34- cell yield was reduced in aged individuals compared to young (p= 0,0074 and p= 0,0106, Mann-Whitney test). However, the median HSC yield in young and aged individuals is similar (**Figure 7C**).

We additionally introduced a cell division tracer enabling to estimate number of cell divisions by the decreasing intensity of a fluorescence dye (**Figure 7D**). Using this approach, we can track HSCs, MPPs, MLPs, CMPs, GMPs, MEPs, and CD34- cells over 7 days and simultaneously link every cell to the cell division state. When focusing on the HSC compartment, aged HSCs seem to divide less or slower than younger HSCs (**Figure 7E**), indicating that mechanisms leading to reduced HSPC yield and probably reduced BM cellularity already start at the HSC level.

4.2.3 Computational modeling reveals a decline of HSC proliferation being responsible for declining blood cell production in aged individuals

Hematopoiesis starting at the HSC level and ending with mature blood cells is characterized by its structural hierarchy and by an interplay between proliferation, differentiation, and cell death. Reduced blood cell production in aged individuals can originate from changes in each of these properties and at any step of the hematopoietic hierarchy. To deconvolute and localize these changes, we applied data generated from our 7-day *in vitro* culture approach to a computational analysis. For computational analysis of the FACS data, we worked in close collaboration with Lisa Bast and Carsten Marr from the Helmholtz Zentrum München–German Research Center for Environmental Health, Institute of Computational Biology, Neuherberg, Germany. Programming, implementation of mathematical models, and data plotting was performed by Lisa Bast.

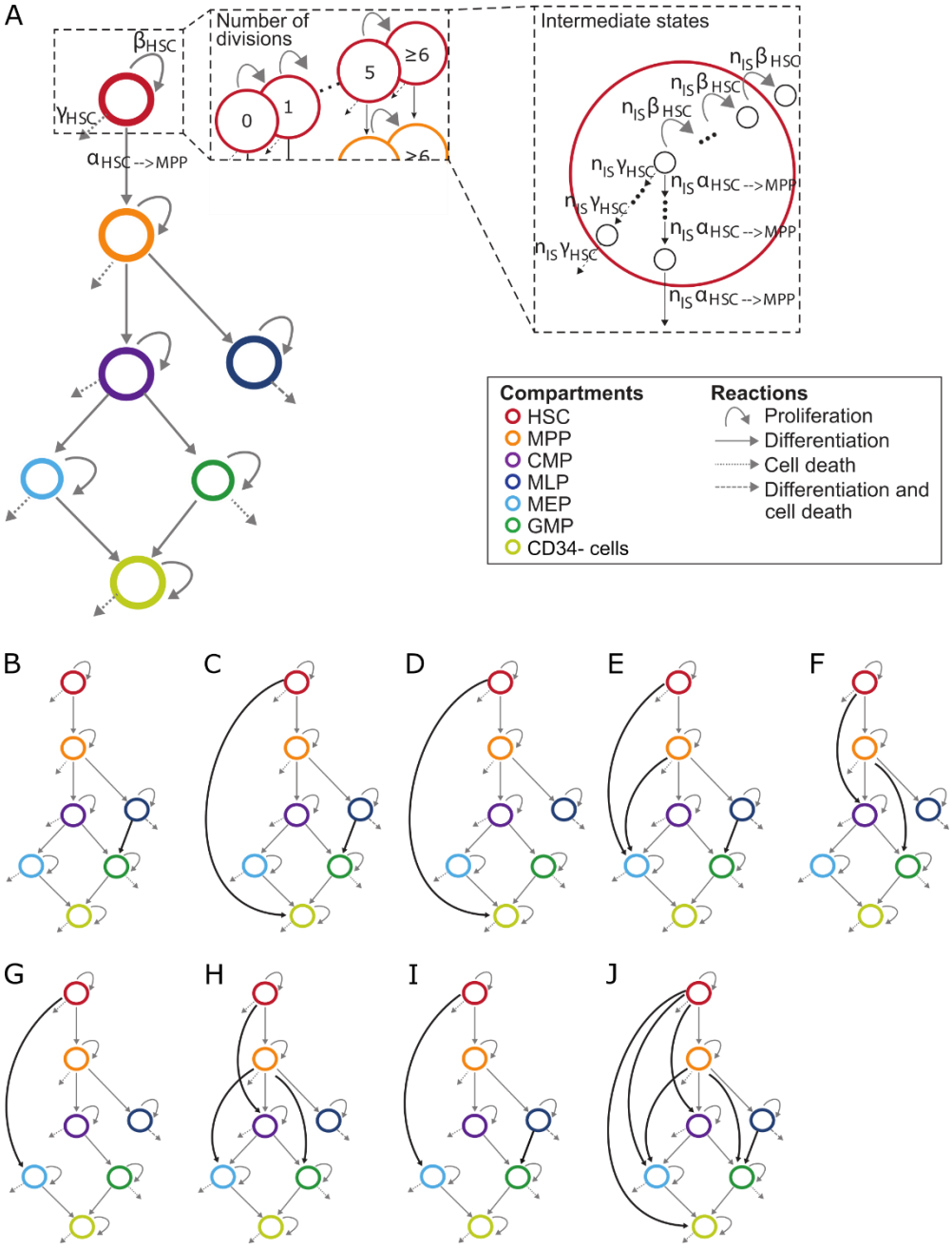

Figure 8: Competing lineage hierarchies used for computational modeling were derived and suggested from literature of human and mouse hematopoiesis (figure modified from Bast *et al.* (2021)). Every cell type in each hierarchy accounts for the number of cells proliferating (β), differentiating (α) or dying (γ), as representatively shown for the HSC compartment in A. We included the cell division state of each cell and introduced intermediate states (n_{IS}) to model realistic non-exponentially distributed waiting times. **(A)** The classical model of hematopoiesis. **(B)** Model A plus a transition between the MLP and GMP compartment. **(C)** Model A plus a transition between the HSC and mature compartment and a transition between the MLP and GMP compartment. **(D)** Model A plus a transition between the HSC and mature compartment. **(E)** Model A plus a transition between the HSC and MEP compartment and the MPP and MEP compartment and the MLP and GMP compartment. **(F)** Model A plus a transition between the HSC and CMP compartment and the MPP and GMP compartment. **(G)** Model A pus a transition between the HSC and MEP compartment and lacking the transition between CMP and MEP compartment. **(H)** Model A plus a transition between the HSC and CMP, the MPP and MEP, and the MPP and GMP compartment. **(I)** Model A plus a transition between the HSC and MEP compartment and the MLP and GMP compartment, but lacking the transition between the CMP and MEP compartment. **(J)** Model A plus every additional transition found in literature.

In recent years, the classical model of hematopoiesis has been challenged by several studies mainly performed in mice (Doulatov *et al.*, 2012; Haas *et al.*, 2018; Laurenti and Göttgens, 2018). To test if the classical model of hematopoiesis as shown in **Figure 1** is also applicable to our data, we computationally tested the plausibility of 10 competing hierarchies (**Figure 8**, published in Bast *et al.* (2021)). For each lineage hierarchy, cell state kinetics, including proliferation (β), differentiation (α), and cell death (γ) was modeled with ordinary differential equations (ODEs). Additionally, we accounted for the cell division state and implemented realistic, non-exponential waiting times via intermediate states ($n_{IS,}$ representatively shown for HSCs in **Figure 8A**). All lineage hierarchies were fitted to data from 10 healthy individuals which were processed as described in the previous section. For each individual, the *in vitro* cell culture approach provides up to 343 data points, including HSC, MPP, MLP, CMP, GMP, MEP, and CD34- cell numbers, all of them linked to the cell division status and measured repeatedly for up to 7 days. To identify best performing, plausible, and rejected hierarchies, the model's performance on the data was ranked according to their Bayesian information criterion (BIC) values. The classical model of hematopoiesis (model A) was plausible for all 10 individuals and performed best in 9 individuals (**Figure 9A**, data published in Bast *et al.* (2021)). This suggests the classical model of hematopoiesis as basis to assess proliferation, differentiation, and cell death of HSCs, MPPs, MLPs, CMPs, GMPs, MEPs, and CD34- cells. The 21 parameters (3 rates for each of the 7 cell types) of the model were fitted to the data points measured and differences between young and aged individuals were tested. Using this approach, we identify a decreasing HSC proliferation in aged individuals compared to young (p= 0,0462, Bonferroni corrected Mann-Whitney test, **Figure 9B** and **Figure S4**).

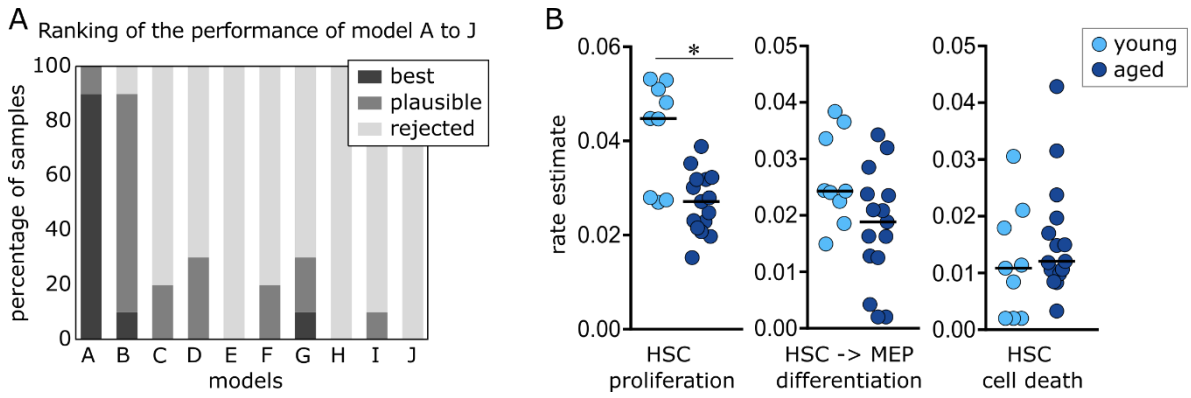

Figure 9: Healthy hematopoiesis is best described by the classical model of hematopoiesis and shows reduced HSC proliferation during aging. (A) The classical model of hematopoiesis (Model A) is plausible in all measured healthy individuals (n=10) and even performs best in 90% of individuals. Ranking of the model's performance (Model A to J shown in **Figure 8**) on data of 10 healthy individuals was performed according to their Bayesian information criterion (BIC) values. The BIC value identifies best performing, plausible, and rejected hierarchies for each individual. **(B)** Rate estimates identify HSC proliferation as significantly reduced in aged individuals (p= 0,0462, Bonferroni corrected Mann-Whitney test). Shown are all three HSC rate estimates for young and aged individuals. For a detailed view including HSC, MPP, MLP, GMP, GMP, MEP, and CD34- cell rate estimates of each sample see **Figure S4**.

4.3 Individuals with CHIP and MDS show an increasing heterogeneity in the hematopoietic tree architecture and in the number of altered kinetic rates

Both, CHIP and MDS arise from mutations in HSPCs. Although, changes within the HSPC compartment are described by several studies, the precise position and quality (e.g., proliferation, differentiation, and cell death) of changes has not yet been investigated sufficiently.

4.3.1 Characterization of our CHIP and MDS patient sample cohort

A recent study from our group showed an unusually high frequency of CHIP among hip arthroplasty patients (Hecker et al., 2021), suggesting also a high frequency of CHIP in our aged cohort. We therefore sent our healthy samples for sequencing which revealed nearly 50% of individuals with CHIP in our healthy aged cohort. Mutations occurred in genes including *DNMT3A*, *SF3B1*, *NFE2*, *KRAS*, and *TP53* and variant allele frequencies (VAF) ranging between 1% and 27% (**Table 7** and **Table S2**). In healthy individuals without CHIP, the median age was 63 years and 50% were female. In individuals with CHIP the median age was 70 years and 86% of individuals were female.

Table 7: Sample characteristics including age, gender, disease/entity, IPSS-R score, karyotype, and mutations. Healthy age-matched samples can be divided in two groups, one group without mutations and the other with mutations, now corresponding to CHIP.

ID	Age	Gender	Disease/Entity	IPSS-R score	Karyotype	Mutations
H353	57	m	Healthy			**-**
H657	62	f	Healthy			**-**
H311	63	m	Healthy			**-**
H380	63	m	Healthy			**-**
H791	63	f	Healthy			**-**
H607	68	f	Healthy			**-**
H312	70	m	Healthy			**-**
H559	76	f	Healthy			**-**
C345	58	f	CHIP			**DNMT3A**
C391	65	f	CHIP			**DNMT3A**
C552	68	f	CHIP			**SF3B1**
C560	70	f	CHIP			**DNMT3A**
C775	72	f	CHIP			**KRAS**
C561	76	m	CHIP			**TP53** **DNMT3A**
C348	79	f	CHIP			**DNMT3A** **NFE2**
MDS360	54	m	MDS-RS-MLD	low risk (3)	46,XY	**SF3B1** **SRSF2**
MDS373	60	m	MDS-RS-MLD	low risk (2)	46,XY	**SF3B1** **DNMT3A** **TET2** **TET2**
MDS377	64	f	MDS-EB1	high risk (5)	45,XX,-7	**ASXL1** **DNMT3A** **SETBP1**
MDS227	68	f	MDS/MPN-RS-T	low risk (3)	46,XX	**SF3B1** **TET2**
MDS279	70	f	MDS-EB1	int risk (4.5)	46,XX	**ASXL1** **KRAS**
MDS620	75	f	MDS-EB2	very high (7)	complex	**ASXL1**
MDS140	76	m	CMML-2	high risk (6)	46,XY	**ASXL1** **RUNX1** **SRSF2** **TET2**
MDS326	77	m	MDS-RS-MLD	low risk (2)	46,XY	**TET2**
MDS135	77	m	MDS-RS-MLD	low risk (3)	46,XY	**ASXL1** **SF3B1** **TET2** **WT1**
MDS354	78	m	MDS-RS-MLD	int risk (3.5)	46,XY	**ASXL1** **SF3B1** **TET2** **WT1**

For analyzing MDS patient samples, we focused on samples harboring mutations in *ASXL1* (associated with a poor prognosis), *SF3B1* (associated with a favorable prognosis), and/or *TET2* (no effect on patient survival, see **Table 7** for summarized patient characteristics). Patients mostly showed more than one mutated gene and sometimes had additional chromosomal aberrations (**Table 7** and **Table S2**). For classifying MDS patients according to WHO criteria (Arber *et al.*, 2016), peripheral cytopenia as well as BM blast counts and dysplasia were

assessed (**Figure 10A** and **B**, **Table 7**). Half of the cohort was diagnosed as MDS-RS-MLD, a subtype with multi-lineage dysplasia (MLD) and ring sideroblasts (RS). These patients show a low to intermediate risk profile according to the IPSS-R. An excess blast (EB) count was found in 40% of the patient cohort. These patients show 5 – 9% blasts in the BM (MDS-EB-1) or 10 – 19% blasts in the BM (MDS-EB-2 and CMML-2). Chronic myelomonocytic leukemia (CMML) is an entity associated to MDS, but with a strong monocytic component. Patients with increased blasts are associated with an intermediate to very high risk according to the IPSS-R. Furthermore, one patient of the cohort was diagnosed as MDS/MPN-RS-T. This entity is characterized by MDS-specific properties including ring sideroblasts and excess platelets (synonym thrombocytes, T), a key criterium for essential thrombocythemia corresponding to MPN.

We further profiled our BM samples for HSPC proportions to investigate MDS- and CHIP-associated changes. Therefore, the gating strategy initially described in **Figure 3A** was used. The proportion of HSPCs (normalized to lineage- cells) is significantly reduced in BM of MDS patients comparted to aged-matched healthy samples without mutations (Kruskal Wallis test, p=0,0441, followed by Dunn's multiple comparison test, p=0,0382). This was mainly based on decreased proportions of CMPs and GMPs (Bonferroni corrected Kruskal Wallis test, p=0,0025 and p=0,0027, followed by Dunn's multiple comparison test, p=0,0031 and p=0,0074, respectively, **Figure 10C**). HSPC proportions of CHIP samples lie mostly in between healthy and MDS samples. However, it has to be noted that BM of our MDS patients is in most cases hypercellular as it is characteristic in MDS. Therefore, changes in HSPC proportions might not reflect absolute cell numbers.

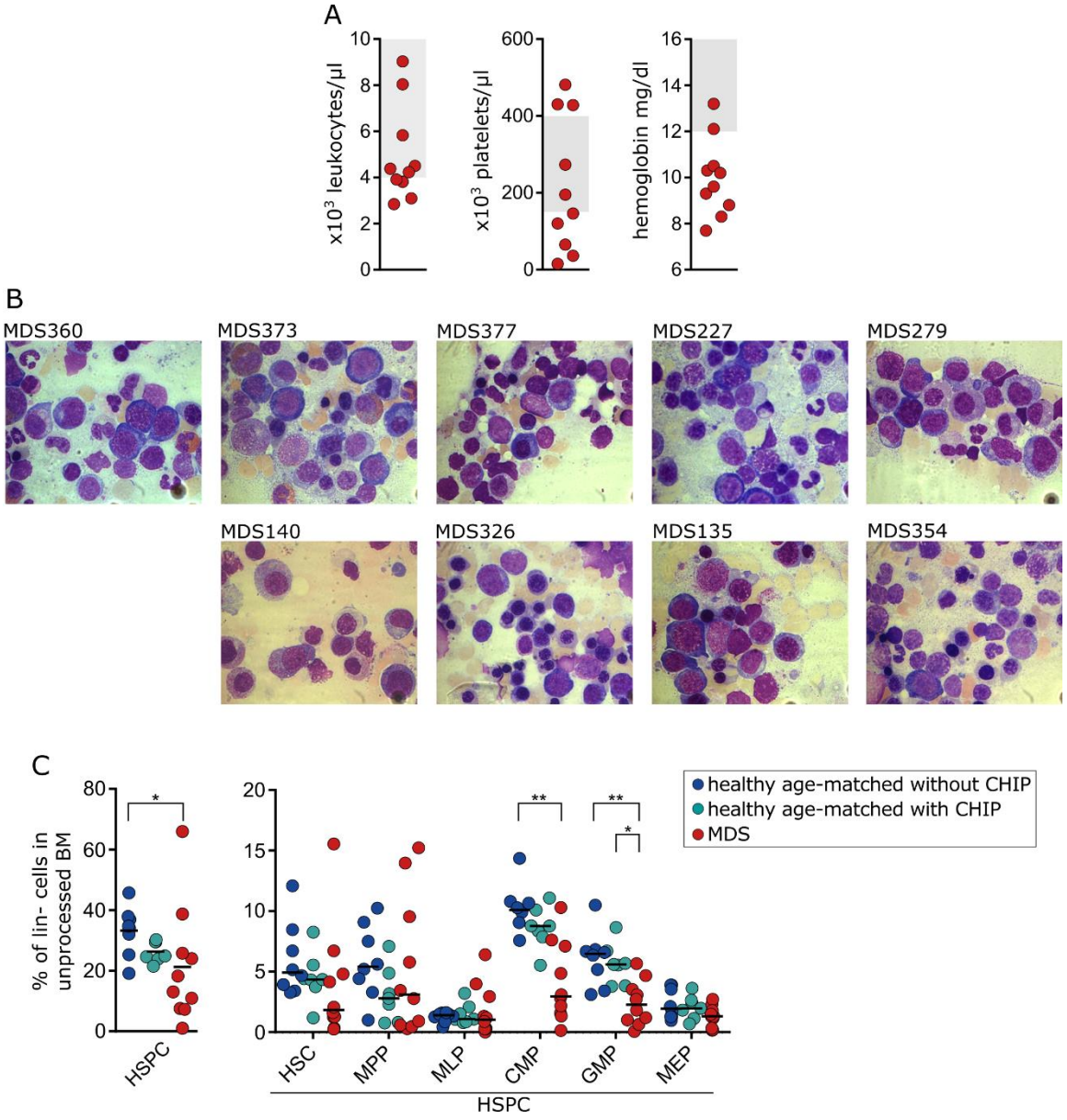

Figure 10: Patient sample characteristics. (A) Blood values, including leucocyte count, platelet count, and hemoglobin level of 10 MDS samples. **(B)** Cytomorphology of BM from 9 MDS patients, visualized by Pappenheim staining. **(C)** Relative proportions of HSPCs and HSPC subpopulations in unprocessed BM samples from healthy individuals, individuals with CHIP, and MDS patients. MDS patients show significantly less HSPCs in MDS BM compared to healthy controls (Kruskal Wallis test, p=0,0441, followed by Dunn's multiple comparison test, p=0,0382). This was based on decreased CMP and GMP proportions (Bonferroni corrected Kruskal Wallis test, p=0,0025 and p=0,0027, followed by Dunn's multiple comparison test, p=0,0031 and p=0,0074, respectively). Populations were normalized to lineage- (lin-) cells.

4.3.2 In vitro *cultures of HSCs from MDS patients, individuals with CHIP, and age-matched healthy individuals without mutations showed no differences in HSPC proportions and cellular yield*

MDS is characterized by ineffective hematopoiesis: While the BM is often hypercellular, filled with dysplastic early and predominantly late progenitors, the peripheral blood shows cytopenia. On the contrary, individuals with CHIP have per definition normal blood counts, but changes on the HSPC level within the BM has not been sufficiently detailed. In a first step, we wanted to investigate the clonogenic capacity of MDS, CHIP, and healthy HSCs to investigate the whole range of hematopoiesis, starting with the HSC and ending with colonies of predominantly mature cells. Therefore, lineage- CD45dim CD34+ CD38- CD90+ CD45RA- HSC were sorted, cultured in methylcellulose for 14 to 21 days, and resulting colonies were counted and classified. Healthy individuals with or without CHIP showed similar clonogenic capacity, reflecting the normal blood counts found in individuals with CHIP. MDS HSCs showed significantly reduced colony forming units and a significant reduction of BFU-E formation (Kruskal Wallis test, p=0,0002 and p<0,0001, followed by Dunn's multiple comparison test, p=0,0055 and p=0,0011, respectively, **Figure 11**).

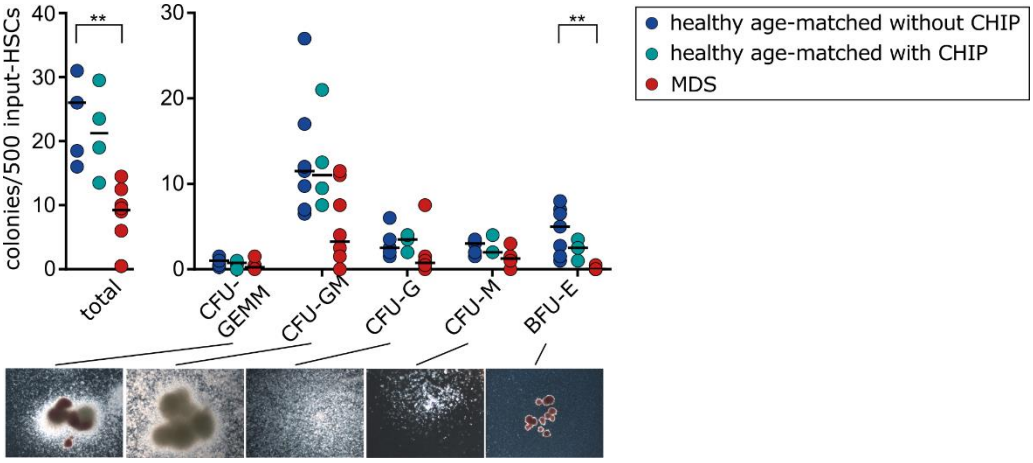

Figure 11: HSCs form MDS patients have a significantly lower total clonogenic capacity and a significantly lower erythroid clonogenic capacity than healthy controls (Kruskal Wallis test, p=0,0002 and p<0,0001 , followed by Dunn's multiple comparison test, p=0,0055 and p=0,0011, respectively). Assessment of total number of colonies per 500 sorted input-HSCs, as well as subdivision of colonies into CFU-GEMM, CFU-GM, CFU-G, CFU-M, and BFU-E. Representative images of CFU-GEMM, CFU-GM, CFU-G, CFU-M, and BFU-E are shown at the bottom.

In the next step, we wanted to assess changes in HSPC subpopulations in our 7-day *in vitro* cell culture approach. Therefore, lineage- CD45dim CD34+ CD38- CD90+ CD45RA- HSC were

sorted, cultured in SFM + 8GF, and repeatedly analyzed by FACS (representative FACS plots are shown in **Figure S2** and **Figure S3**). HSC-cultures from MDS, CHIP, and aged-matched healthy individuals showed no differences in proportions of HSPCs and their subpopulations at day 7 (normalized to lineage- cells). However, MDS samples showed a higher heterogeneity (**Figure 12A**). To quantify *in vitro* cell production, we normalized absolute cell counts from day 7 to absolute HSC numbers on day 1. Comparison of MDS, CHIP, and age-matched healthy samples without mutations showed no difference in HSPC, CD34- cell, and HSC yield after 7 days in culture (**Figure 12B**).

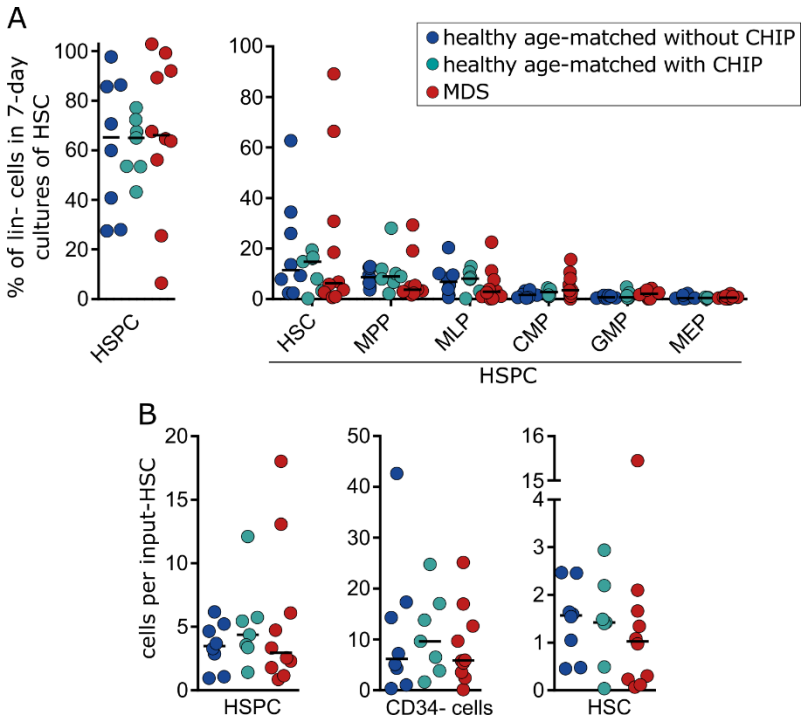

Figure 12: Similar *in-vitro* expansion of HSPCs in age-matched healthy individuals without mutations, individuals with CHIP, and MDS patients. (A) Relative proportions of HSPCs and HSPC subpopulations after sorting and culturing HSCs for 7 days from 8 age-matched healthy individuals without mutations, 7 individuals with CHIP, and 10 MDS patients. Populations were normalized to lineage- cells. **(B)** Cellular yield of HSPCs, CD34- cells, and HSCs analyzed after sorting and culturing HSCs for 7 days. Yield is defined as the absolute number of a respective cell type at day 7 normalized to the absolute number of HSCs at day 1.

4.3.3 The hematopoietic structure and kinetic rates are deregulated in CHIP and MDS

In vitro cell expansion of HSPC subpopulations in MDS, CHIP, and age-matched healthy individuals was similar. However, cell expansion is an interplay between proliferation, differentiation, and cell death. To account for these properties in detail, we used our 7-day *in vitro* cell culture system and computationally tested competing hematopoietic hierarchies and

then investigated proliferation, differentiation, and cell death rates of HSCs, MPPs, MLPs, CMPs, GMPs, MEPs, and CD34- cells.

First, we computationally tested the plausibility of the 10 competing hierarchies shown in **Figure 8** (programming and implementation of mathematical models was performed by Lisa Bast from the Helmholtz Zentrum München–German Research Center for Environmental Health, Institute of Computational Biology, Neuherberg, Germany). Similar to healthy samples without mutations, the classical model of hematopoiesis (model A) is plausible for all CHIP samples. However, the classical model performs best in only 4 out of 7 CHIP samples according to the BIC (**Figure 13A**). Other best performing models were model B and E, with additional transitions between the MLP and GMP, the HSC and MEP, and the MPP and MEP compartment. Heterogeneity is even more prevalent in MDS patient samples: The classical model of hematopoiesis (model A) is plausible in only 4 of 10 samples and performs best in 3 of these samples. Other best performing models were model B (3 samples), model D (2 samples), and model G (2 samples, **Figure 13A**). These models show additional transitions between the MLP and GMP compartment, the HSC and mature compartment, and the HSC and MEP compartment. Taken together, the classical model of hematopoiesis is not sufficient to describe hematopoiesis for the majority of MDS samples. To make it possible to compare proliferation, differentiation, and cell death rates of HSCs, MPPs, MLPs, CMPs, GMPs, MEPs, and CD34- cells, we defined a union model. The union model includes all additional transitions from models performing best in healthy, CHIP, or MDS samples (model A, B, D, G, I, **Figure 13B**). The parameters of the 7 cell types of the union model were fitted to the data points measured and deregulated rates were identified by applying a 95% confidence interval (CI) based on healthy age-matched controls without mutations (**Figure S5**). Deregulated rates were then summarized for each individual in **Figure 13C**, **D**, and **E**. Samples with altered rates, showed a very heterogeneous picture: Up- and down-regulated rates are present at different positions of the hematopoietic hierarchy and involve proliferation, differentiation, and cell death rates. In CHIP samples, 6 out of 7 samples showed deregulated rates and up to 4 deregulated rates could be detected in a single individuum (**Figure 13D**). In MDS samples, 9 out of 10 samples showed deregulated rates and we could detect up to 8 deregulated rates in a single individual (**Figure 13E**).

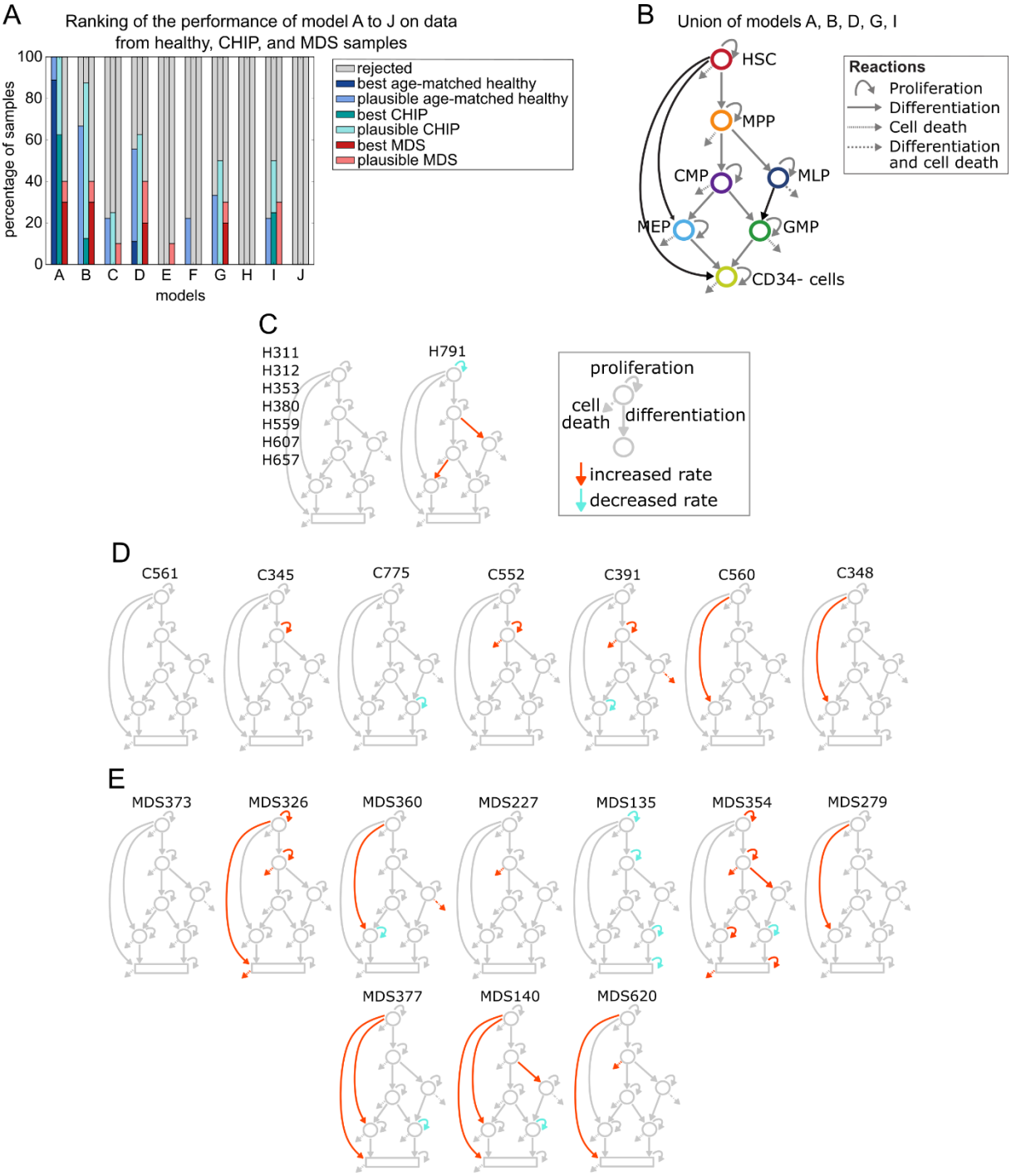

Figure 13: Computational modeling reveals increasing heterogeneity in CHIP and MDS regarding the choosen hematopoietic hierarchy and the number of altered rates per individual. (A) The classical model of hematopoiesis (model A in **Figure 8**) is not sufficient to discribe hematopoiesis for some CHIP and the majority of MDS samples. Systematic comparison of 10 competing hierarchies (see **Figure 8**) was performed according to BIC values and best performig, plausible, and rejected models were identified for 8 age-matched healthy individuals without mutations, 7 individuals with CHIP, and 10 MDS patients. **(B)** Union of models wich performed best according to BIC values in at least one healthy, CHIP, or MDS sample. **(C)** Up- and down-regulated rates for each age-matched healthy individual without mutations. Rates were asessed by fitting *in vitro* generated data to the union model shown in B. A 95% confidence interval based on healthy age-matched individuals without mutations is then used to identify the deregulated rates (**Figure S5**) **(D)** Up- and down-regulated rates for each individual with CHIP. Rates were determined as discribed in C. **(E)** Up- and down-regulated rates for each MDS patient. Rates were determined as discribed in C.

4.3.4 Single cell kinetics reveal higher activity of MDS HSPCs compared to the age-matched healthy controls

Unlike cell lines, human primary material shows higher heterogeneity even in the same cell type from the same donor. To analyze inter-cellular heterogeneity in the very rare HSC population from MDS patients and age-matched healthy individuals, cell growth and death was assessed on the single-cell level. Therefore, HSCs were sorted in single-cell mode into 96-well plates and cultured in SFM + 8GF to allow cell expansion and differentiation. Cell number of each well was counted repeatedly (**Figure 14A**).

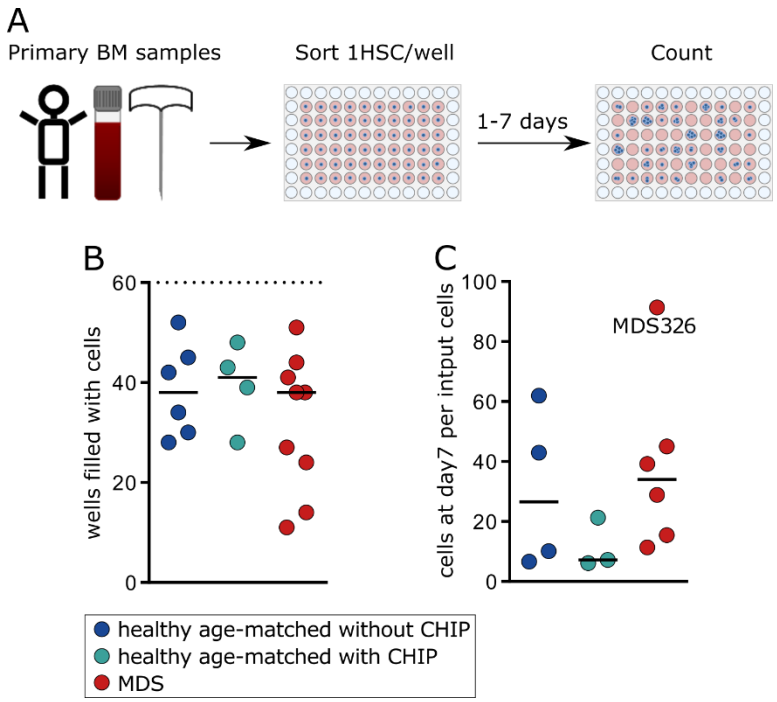

Figure 14: Cell growth of sorted single-HSCs from healthy individuals without CHIP, individuals with CHIP, and MDS patients. (A) Workflow for investigating HSC expansion. Primary BM cells were used to sort 1 HSC in 1 well of a 96-well plate. Outer wells were filled with water, resulting in 60 wells to be filled with cells. Cells were cultured in SFM + 8 GF for up to 7 days and counted regularly. **(B)** Number of wells occupied with at least one cell after sorting. Dashed line indicates the maximum of 60 wells which can be occupied in each experiment. **(C)** Cell yield investigated after 7 days of culturing HSCs. The total amount of cells across all wells at day 7 was normalized to the total amount of cells at day 1 (input cells).

After sorting single-HSCs per well, not all wells were found to be occupied with cells. A median of 38 wells, 41 wells, and 38 wells were filled with cells in MDS, CHIP, and healthy age-matched samples, respectively, with no significant differences between these groups (Kruskal-Wallis test, **Figure 14B**). To analyze the cellular yield in single-cell experiments, we normalized the absolute cell number counted throughout each plate on day 7 to the number of occupied wells on day 1. Similar to bulk-analysis (**Figure 12C**), there were no differences in cell yield between

MDS, healthy age-matched samples without CHIP, and healthy age-matched samples with CHIP (**Figure 14C**).

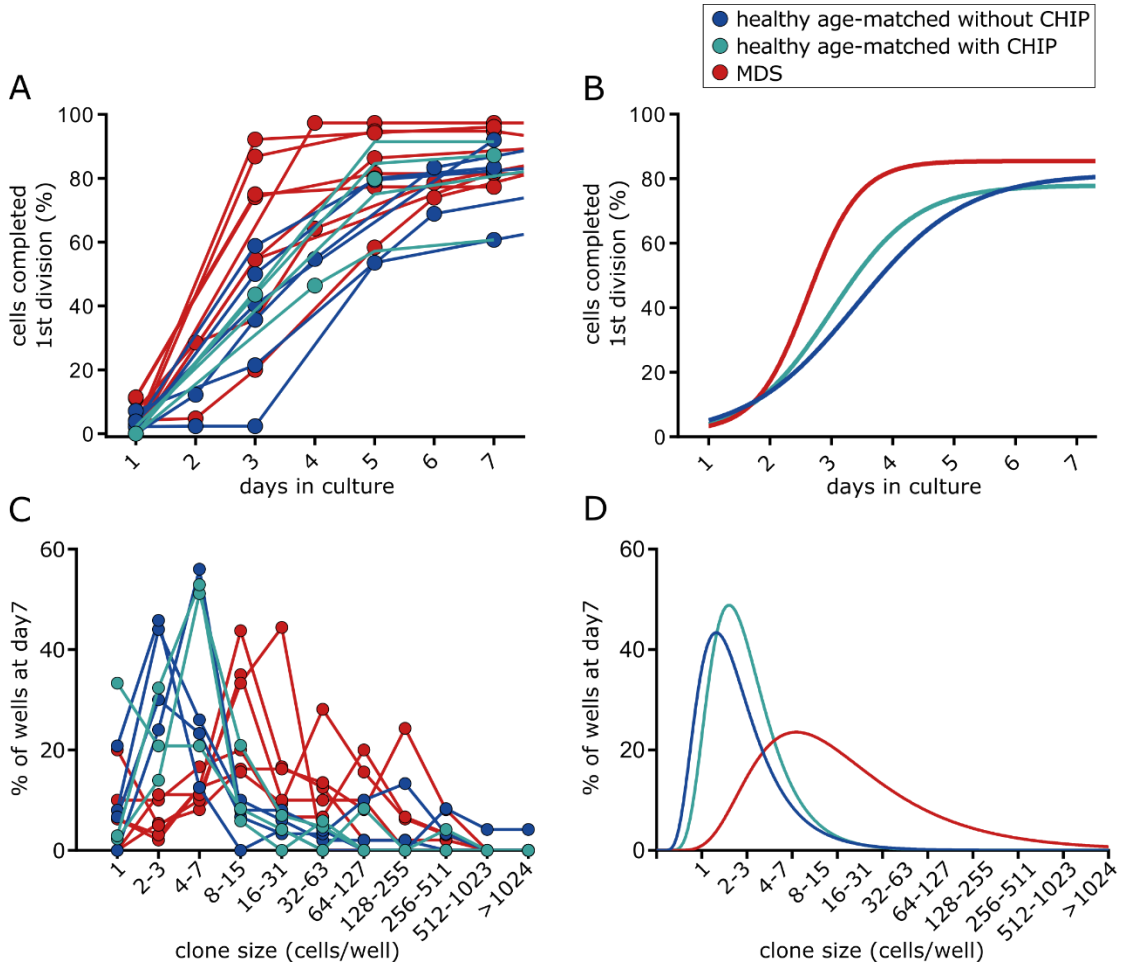

Figure 15: Dynamic cell growth of sorted single-HSCs from healthy individuals without CHIP, individuals with CHIP, and MDS patients. (A) Percentage of cells which divided at least one time at a specific time point throughout the 7 days of culturing. Empty wells were excluded from the analyis. **(B)** Sigmoidal fitting of A using the graph pad software. **(C)** Porportion of wells with a specific clone size after 7-day culture of single HSCs. Clone size was categorized into 11 classes following a logarithmic pattern. **(D)** Non-linear (Log (Gaussian)) fitting of C using the graph pad software.

To deconvolute changes in HSC cell division, we analyzed time to first division for processed samples. The percentage of cells divided at least one time was reported for each analyzed time point (**Figure 15A**). For comparing MDS, healthy age-matched individuals, and individuals with CHIP, a sigmoidal fitting with variable slope was performed for each group using the GraphPad Prism software (**Figure 15B**). The resulting curves are described by the bottom, top, EC50, and hill slope values (**Table 8**). The bottom of the curve was restrained by being greater than 0. The top of the curve describes how many cells do divide at least one time. The EC50 value is defined as the days in culture in which half of the cells between the baseline (bottom)

and the maximum (top) divided. The Hill slope describing the steepness of the curve corresponds to cell division speed. An important value for estimating the correlation between the measured Y values and Y values predicted by the model is R square. This value is always between 0 and 1, whereby 1 indicates that the model predicts each Y value perfectly with no random variability. Our models are good predictors for our group behavior, since the R square value for all three generated curves is 0.9 (**Table 8**). For comparing MDS, CHIP, and healthy fits, we used the extra-sum-of squares F test. This test assumes as null hypothesis that all group's fitting curve can be adequately fitted by a single curve considering bottom, top EC50, and hill slope value. When applying a significance level (alpha) of 0.05, the null hypothesis is rejected (p=0.0001). This means the preferred model contains different curves for each data set, indicating significantly different kinetics for HSC division in samples from MDS, CHIP, and age-matched healthy individuals. In detail, HSCs from MDS patients showed a high number of cells which divided at least one time (Top = 85.49), and a high cell division speed (HillSlope = 1.03) compared to HSC from CHIP (77.96 and 0.64 respectively) and healthy groups (81.52 and 0.49 respectively, **Table 8**).

Table 8: Curve values for the sigmoidal fitting of the time to first division curve (Figure 15A, B). Best-fit values, Std. error, and 95% confidence intervals were analyzed for bottom, top, EC50, and hill slope values. Goodness of fit is described by the degrees of freedom, R square, absolute sum of squares and an alternative way to quantify the standard deviation of the residuals (Sy x). The bottom value was constrained to be greater than 0.

	Age-matched healthy without CHIP	Age-matched healthy with CHIP	MDS
Best-fit values			
Bottom	~ 1,356e-016	~ 1,667e-016	1,593
Top	81,52	77,96	85,49
EC50	3,401	3,005	2,617
HillSlope	0,4890	0,6351	1,031
Std. Error			
Bottom			5,792
Top	3,825	5,682	2,579
EC50	0,3121	0,3641	0,1840
HillSlope	0,1637	0,4111	0,3953
95% Confidence Intervals			
Bottom			0,0 to 13,27
Top	73,70 to 89,34	65,69 to 90,23	80,29 to 90,69
EC50	2,763 to 4,039	2,218 to 3,791	2,246 to 2,988
HillSlope	0,1543 to 0,8237	-0,2530 to 1,523	0,2337 to 1,828
Goodness of Fit			
Degrees of Freedom	29	13	44
R square	0,8865	0,8886	0,8835
Absolute Sum of Squares	4195	2029	7396
Sy.x	12,03	12,49	12,97
Constraints			
Bottom	Bottom > 0,0	Bottom > 0,0	Bottom > 0,0

Although cellular yield after 7-day culturing is similar in MDS, CHIP, and age-matched healthy samples, differences in cell division dynamics can be present on the single cell level. As a direct output for single cell expansion potential, clone size for each cultured HSC was estimated after 7-day culturing (**Figure 15C**). Generated data was used for a non-linear fitting (Log (Gaussian)) for each group using the GraphPad Prism software and fitted curves were plotted (**Figure 15D**). The curves are described by the amplitude, center, and width values (**Table 9**). Considering these three characteristics, we tested whether one curve can adequately fit all three data sets (null hypothesis). According to the extra-sum-of-squares F test, the preferred model contains different curves for each data set ($p<0.0001$). We are specifically interested in differences of the center value, indicating differences in clone size. Using the extra-sum-of-squares F test, we tested whether the center is the same for all data sets. The preferred model has different center for each data set ($p<0.0001$) with a higher center value for MDS samples compared to CHIP and healthy individuals (3.1, 1.6, and 1.3 respectively), suggesting that MDS HSCs generate bigger clones. However, as a limiting factor, it has to be considered that the R square value for the fitted curves ranges from 0.4 to 0.7, indicating a modest prediction of the Y values by the chosen model (**Table 9**).

Table 9: Curve values for the non-linear fitting of the clone size curve (Figure 15C, D). Best-fit values, Std. error, and 95% confidence intervals were analyzed for amplitude, center, and width values. Goodness of fit is described by the degrees of freedom, R square, absolute sum of squares and an alternative way to quantify the standard deviation of the residuals (Sy x).

	Age-matched healthy without CHIP	Age-matched healthy with CHIP	MDS
Best-fit values			
Amplitude	43,39	48,85	23,56
Center	1,322	1,607	3,094
Width	0,4584	0,3805	0,4461
Std. Error			
Amplitude	6,466	7,488	2,500
Center	0,08988	0,07643	0,1830
Width	0,09107	0,05092	0,05609
95% Confidence Intervals			
Amplitude	30,33 to 56,46	33,56 to 64,14	18,57 to 28,56
Center	1,140 to 1,503	1,451 to 1,763	2,728 to 3,460
Width	0,2744 to 0,6424	0,2766 to 0,4845	0,3340 to 0,5582
Goodness of Fit			
Degrees of Freedom	41	30	63
R square	0,6787	0,6646	0,4419
Absolute Sum of Squares	2474	2240	3940
Sy.x	7,769	8,641	7,908
Constraints			
Width	Width > 0,0	Width > 0,0	Width > 0,0

4.3.5 Sister cells in MDS354 divide more asynchronously compared to healthy samples

By using simple single cell assays, the clonal capacity and related dynamics at a daily resolution can be assessed and linked to a single HSC, as described in the previous section. Additional high-resolution time lapse microscopy enables to track every cell, their movements and divisions. Linking the behavior of daughter cells to the cell of origin enables to correlate specific properties of these cells. We performed time lapse experiments in cooperation with Joachim Rädler and Alexandra Murschhauser from the Faculty of Physics and Center for NanoScience (CeNS), Ludwig-Maximilians-Universität, Munich, Germany and in cooperation with Carsten Marr, Lea Schuh and Moritz Thomas from the Helmholtz Zentrum München– German Research Center for Environmental Health, Institute of Computational Biology, Neuherberg, Germany.

For analyzing sister cell behavior, we sorted lineage- CD45dim, CD34+ CD38- CD90+ CD45RA- HSCs in bulk mode of one MDS sample (MDS354) and two healthy controls (H500, H522). Cells were seeded randomly at a density of 1-2 cells/well in specific PDMS microwells. Each microwell was designed to have a diameter of 300 µm and in total 30 microwells were present in one culture dish (**Figure 16A**). Each well was imaged automatically every 20 min for approximately 7 days in appropriate culture conditions. Using these images, each cell was manually tracked, assigned to a cell fate (death or division) and using these data, time-resolved cell division trees were generated (**Figure 16B**). Sister cell correlations were analyzed by plotting cell cycle time of one sister against the cell cycle time of the other sister (**Figure 16C**). Comparing MDS354 to the healthy controls, sister cell correlations appeared to be much less constrained in the MDS sample. To test for this difference, we introduced the sister cell ratio, which is defined as the cell cycle time of the shorter living sister divided by cell cycle time of the longer-lived sister. MDS354 showed a significantly lower sister cell ratio than the two healthy samples ($p=0.0089$ and $p=0.024$, Dunn's test, **Figure 16D**).

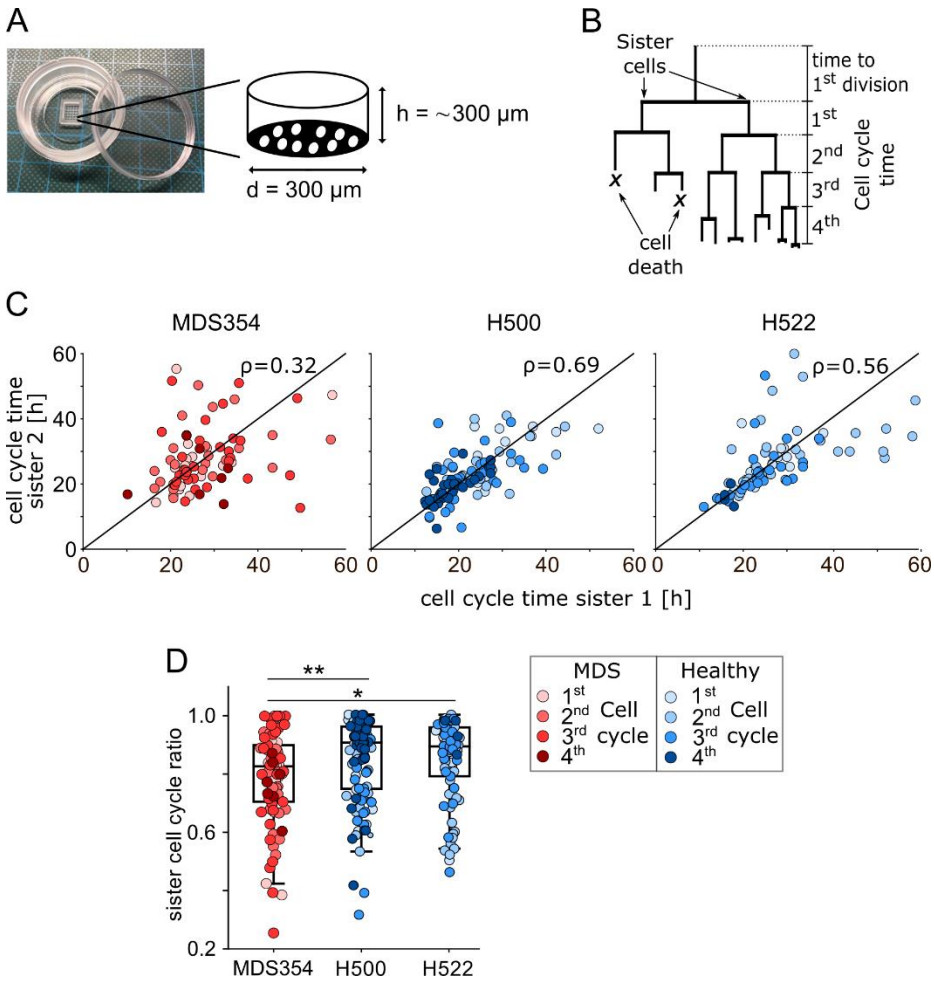

Figure 16: Investigating cell cycle time and sister cell correlation of MDS354 and two healthy age-matched samples in a time lapse experiment. **(A)** Customized culture dish used for the experiment containing 30 microwells each with a diameter of 300 µm. **(B)** Schematic illustration of a cell division tree for investigating cell cycle times (vertical axis), sister cell correlations, and cell death (X). Sister cells are defined as two cells arising from one parent cell. **(C)** Cell cycle time of each tracked pair of sisters. Linear correlation is measured by the Pearson correlation coefficient (ρ). **(D)** Abstraction of sister cell cycle time. Sister cell cycle ratio is calculated by dividing the longer-lived sister by the shorter-lived sister. Statistical analysis was performed using the Dunn's test.

4.4 A mouse model for investigating alterations in the bone marrow niche during MDS development and progression

The aim of this section was to investigate alterations in the BM microenvironment during MDS development using a mouse model with an MDS-like phenotype. To reflect human MDS, we set minimal criteria for our mice including presence of peripheral cytopenia in at least one lineage and morphologic dysplasia. These criteria were fulfilled in a mouse model with a conditional deletion of *ASXL1*, described by Abdel-Wahab *et al.* (2013).

4.4.1 Proofing successful deletion of ASXL1

ASXL1 was shown to be expressed throughout the adult hematopoietic compartment (Abdel-Wahab *et al.*, 2013). To obtain a hematopoietic specific deletion of ASXL1, *ASXL1$^{fl/fl}$* mice were crossed to *Vav-cre* transgenic mice as described by Abdel-Wahab *et al.* (2013). To prove ASXL1 knockout, ASXL1 protein expression was analyzed in spleen and BM via Western blot (**Figure 17A**). As expected, ASXL1 protein was present in mice with floxed *ASXL1*, but without *Vav-cre* (*Vav-cre- ASXL1$^{fl/fl}$*). Furthermore, ASXL1 could be also detected in mice with a heterozygous (*Vav-cre+ ASXL1$^{fl/wt}$*) and a homozygous (*Vav-cre+ ASXL1$^{fl/fl}$*) deletion of *ASXL1*, but at a lower level. However, ASXL1 protein size in our Western blot investigations were not consistent with described sizes by Abdel-Wahab *et al.* (2013). They detected a protein size of about 180 to 200 kDa.

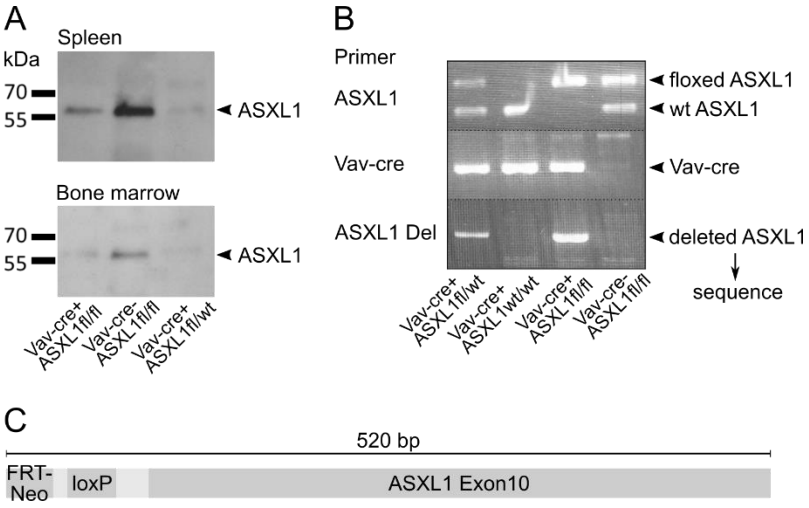

Figure 17: Investigation of *ASXL1* deletion in *Vav-cre+ ASXL1* floxed mice. (A) Western blot investigating *Vav-cre* mediated deletion of ASXL1 at the protein level of splenocytes and BM cells. **(B)** Genotyping PCR for verifying floxed *ASXL1*, wild type *ASXL1*, *Vav-cre*, and deleted *ASXL1*. The PCR product detecting deleted *ASXL1* was sent for sequencing. **(C)** Alignment of the sequenced PCR product obtained by applying the *ASXL1* Del primer.

For a reliable verification of *ASXL1* deletion, we focused on an alternative genotyping strategy described by Abdel-Wahab *et al.* (2013). The standard genotyping strategy includes primers for *ASXL1*, detecting the floxed *ASXL1* and the wild type *ASXL1* and primers detecting *Vav-cre*. The additional *ASXL1* Del primers, were supposed to detect a product only when *ASXL1* is deleted. Indeed, we could only detect a signal for deleted *ASXL1* in *Vav-cre+* mice with at least one floxed *ASXL1* allele (**Figure 17B**). However, *ASXL1* Del primer described by Abdel-Wahab *et al.* (2013), fail to align to the mouse genome using BLAST. Therefore, the *ASXL1* Del product was sequenced and aligned. Of the total 520 base pairs (bp), bp 1-32 aligned to the FRT-Neo cassette and bp 42-75 aligned the loxP sites, which were both localized in intron 4, whereas bp 97-520 aligned to exon 10 of the *ASXL1* gene (**Figure 17C**). Thus, only mice with a complete deletion of exon 5 to 9 in at least one allele result in a positive signal in the PCR using the *ASXL1* del primer.

4.4.2 Mice with hematopoietic knockout of ASXL1 *do not show progressive peripheral cytopenia*

To recapitulate findings from Abdel Wahab et al., that loss of *ASXL1* in the hematopoietic system leads to progressive leukopenia, anemia, and dysplastic signs in granulopoiesis, we measured blood values and analyzed blood smears from the different genotypes. At the age of 6 to 10 months, mice with a hematopoietic deletion of *ASXL1* in both alleles showed significantly less white blood cells (WBC) compared to control mice with floxed *ASXL1* alleles but lack of *Vav-cre* (p=0.0163, Mann-Whitney test). We could not observe changes in 6 to 10 month old mice in hemoglobin or platelet levels (**Figure 18A**).

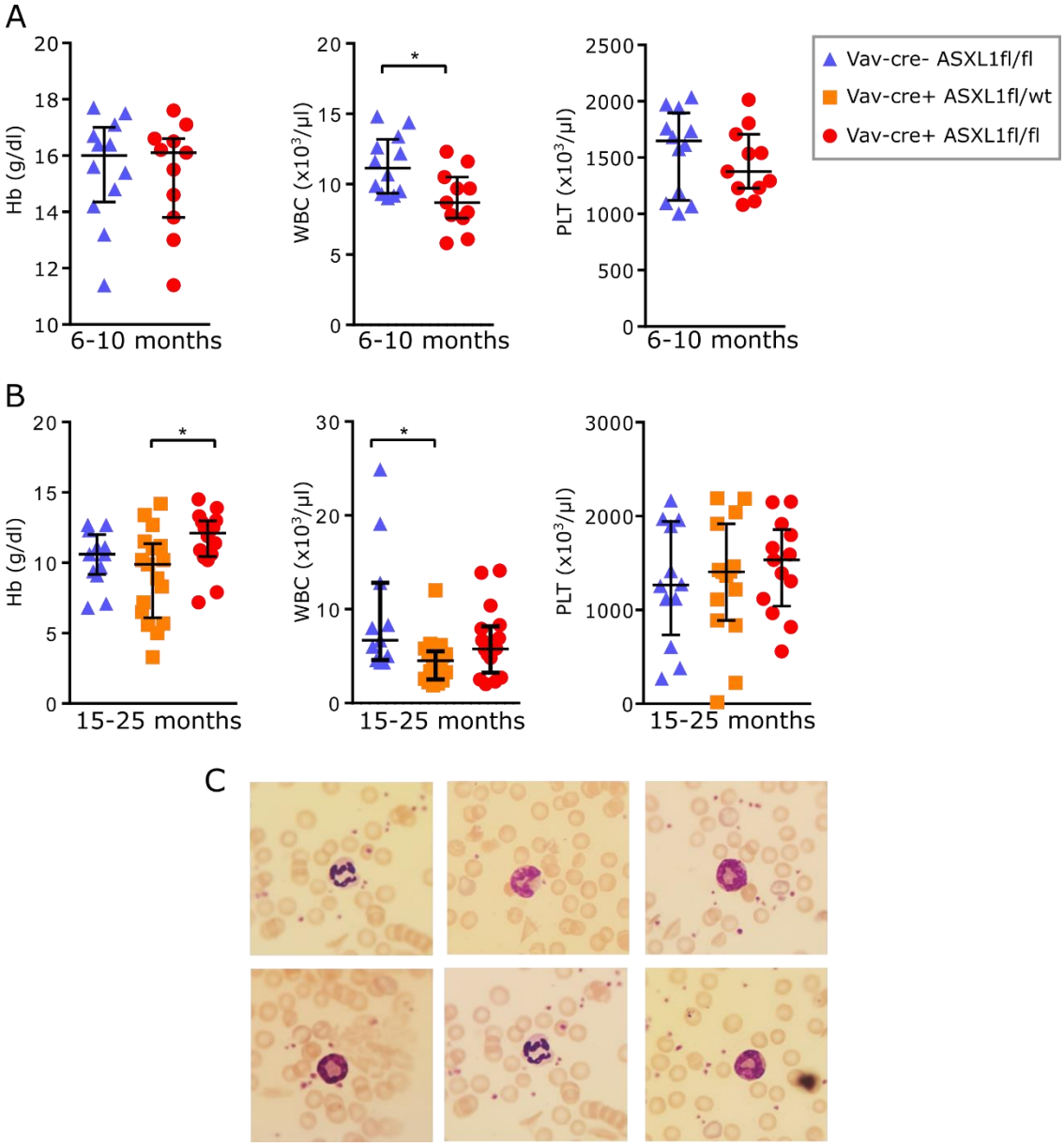

Figure 18: Peripheral blood analysis of mice with a homozygous or a heterozygous deletion of *ASXL1* within the hematopoietic system and control mice. (A) Hemoglobin (Hb) level, white blood cell (WBC) number, and platelet (PLT) number were assessed in 6-10 month old mice. WBC counts were significantly lower in *ASXL1* deleted mice comparted to the control group (p=0.0163, Mann-Whitney test) **(B)** Hb level, WBC number, and PLT number were assessed in 15-25 month old mice with all genotypes. Hb levels were significantly lower in mice with a heterozygous knockout of *ASXL1* compared to mice with a homozygous knockout of *ASXL1* (Kruskal-Wallis test p= 0,0364, followed by Dunn's multiple comparison test, p= 0,0339). WBC counts were significantly lower in mice with a heterozygous knockout of *ASXL1* compared to control mice (Kruskal-Wallis test p= 0,0225, followed by Dunn's multiple comparison test, p= 0,0262). **(C)** Representative images of granulocytes in the peripheral blood of *Vav-Cre+ ASXL1$^{fl/fl}$* mice, visualized by Pappenheim staining.

Since the MDS phenotype seen in *ASXL1* deleted mice is described as a progressive development of disease, we decided to analyze mice at the age of 15 to 25 months to obtain a more severe phenotype. We analyzed mice with homozygous and heterozygous deletion of *ASXL1* within the hematopoietic system, as well as controls.

Mice with a heterozygous knockout of *ASXL1* showed significantly lower hemoglobin levels than mice with a homozygous knockout (Kruskal-Wallis test p= 0,0364, followed by Dunn's multiple comparison test, p= 0,0339). However, when comparing both groups to the control group, no significant difference in hemoglobin levels could be observed. Furthermore, we could observe significantly lower WBC counts in mice with a heterozygous knockout of *ASXL1* compared to control mice (**Figure 18B**, Kruskal-Wallis test p= 0,0225, followed by Dunn's multiple comparison test, p= 0,0262). Cytomorphologic accession of blood smears did not reveal any dysplastic signs in granulocytes of mice with a homozygous deletion of *ASXL1* (**Figure 18C**). Taken together, mice with hematopoietic deletion of *ASXL1* do show mild changes in blood values compared to control mice, but these changes are not sufficient to match criteria for an MDS-like phenotype.

4.4.3 Mice with hematopoietic deletion of ASXL1 *do not show severe changes in BM cell composition*

In the next step, we analyzed the composition of hematopoietic cells within the BM of homozygous, heterozygous, or control mice. Using FACS analysis, we identified Ter119- CD3e+ T-lymphocytes, Ter119- B220+ B-lymphocytes, Ter119- CD3e- B220- CD11b+ Gr1- monocytes, and Ter119- CD3e- B220- CD11b+ Gr1+ granulocytes (**Figure 19A**). Assessed cell counts within these gates were normalized to total BM cells extracted from femur and tibia. Comparing our different mouse genotypes, we could not observe severe changes in BM composition of mature cells (**Figure 19B**).

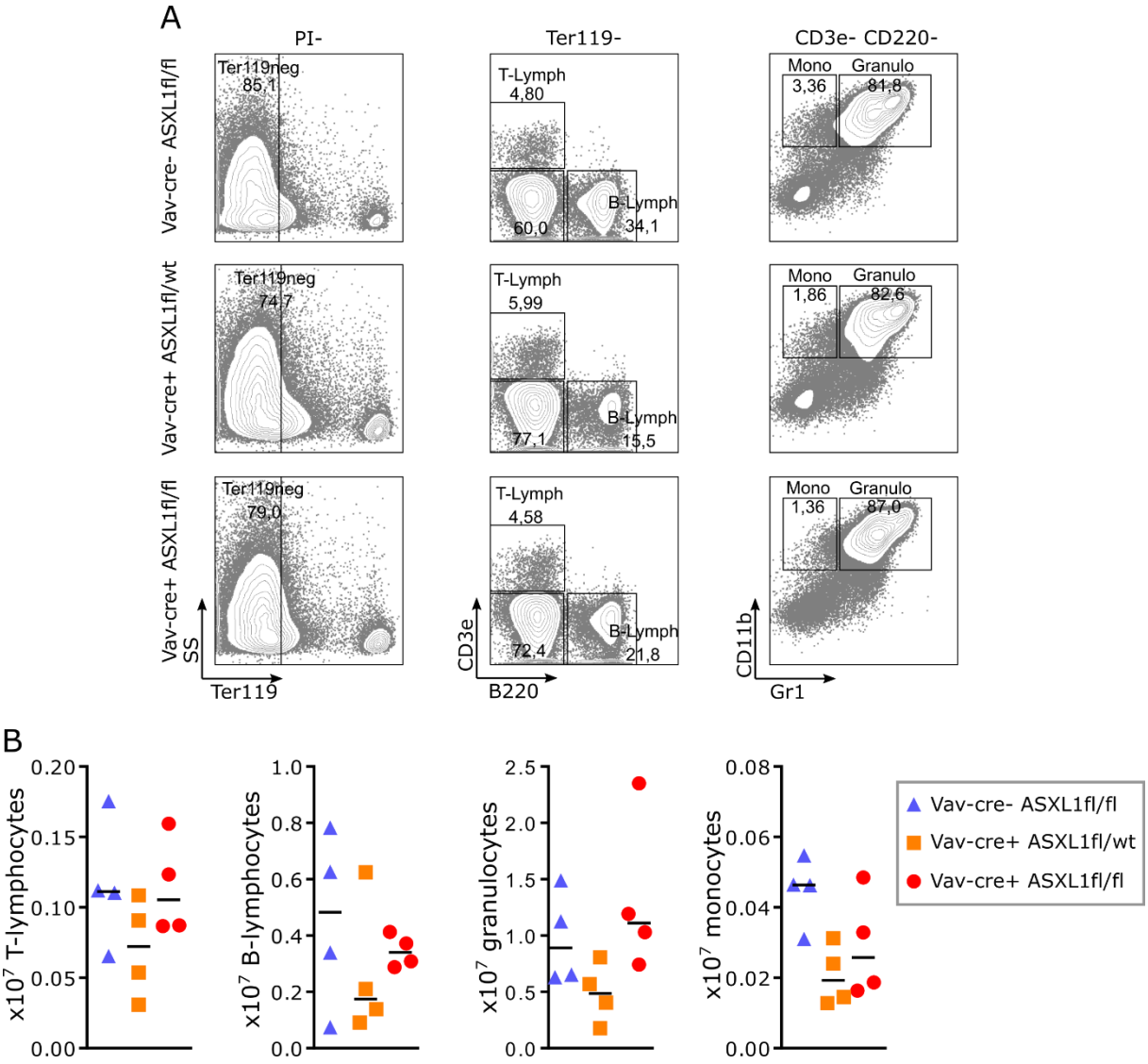

Figure 19: Analysis of mature blood cells within the BM of mice with a homozygous or a heterozygous deletion of *ASXL1* within the hematopoietic system and control mice. (A) Representative gating scheme for identifying T-lymphocytes, B-lymphocytes, monocytes (Mono), and granulocytes (Granulo) in homozygous, heterozygous, or control mice. **(B)** Absolute cell numbers of T-lymphocytes, B-lymphocytes, granulocytes, and monocytes were assessed by normalizing cell proportions to absolute cell numbers extracted from mouse femur and tibia.

We furthermore analyzed hematopoietic stem and progenitor cells in the BM of these mice. We identified lineage- Sca1- cKit+ multipotent progenitors (MPs), lineage- Sca1+ cKIT+ (LSK) cells, CD34- CD150+ CD48- LSK cells (LT-HSCs), and CD34+ CD150low CD48- LSK cells (ST-HSCs) via FACS (**Figure 20A**). Assessed cell counts within the gates were normalized to total BM cells extracted from femur and tibia. Comparing our different mouse genotypes, we could not observe significant changes in BM composition of MPs, LSK cells, ST-HSCs, or LT-HSCs (**Figure 20B**).

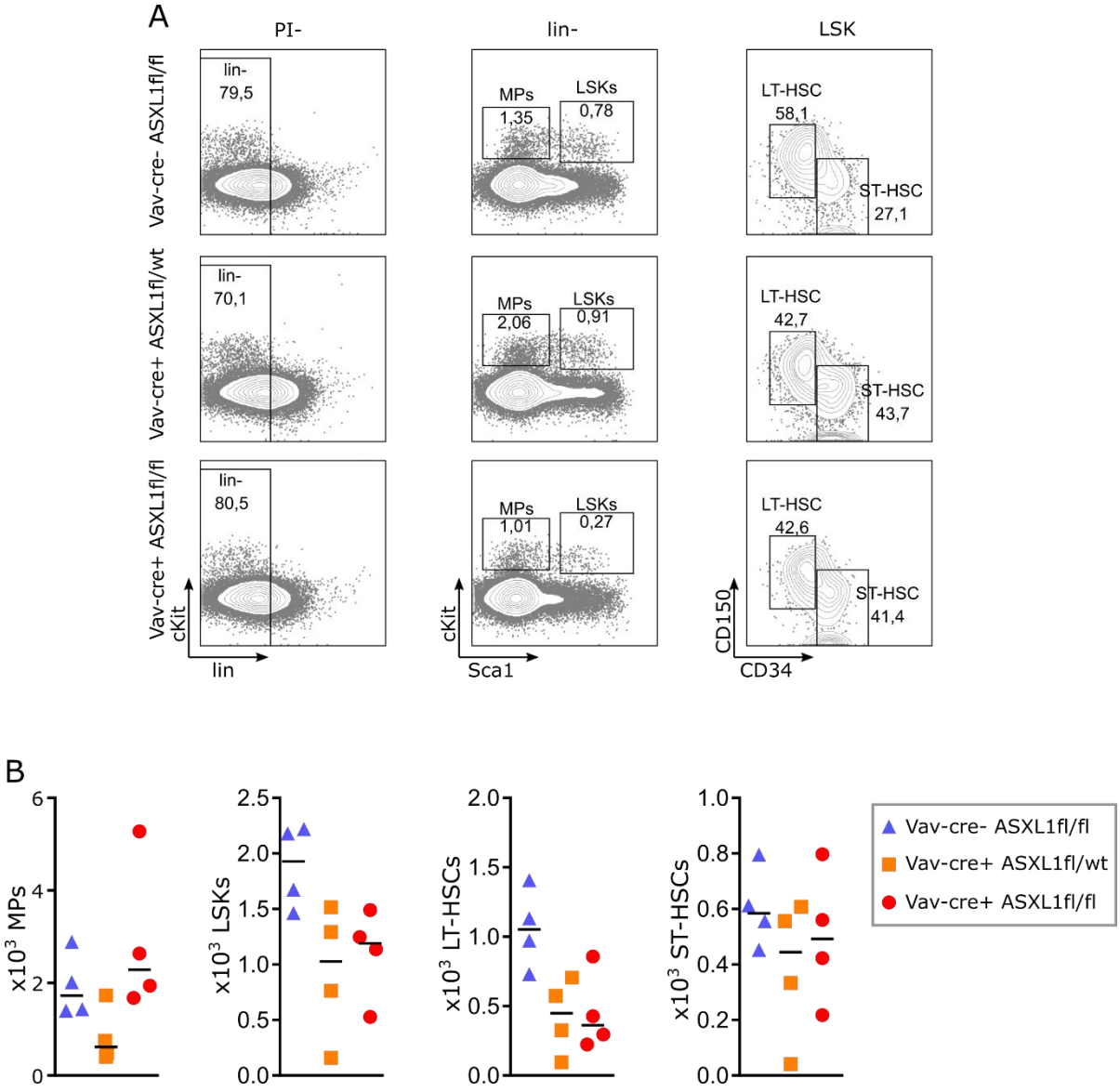

Figure 20: Analysis of stem and progenitor cells within the BM of mice with a homozygous or a heterozygous deletion of *ASXL1* in the hematopoietic system and control mice. (A) Representative gating scheme for identifying multipotent progenitors (MPs), lineage- Sca1+ Kit+ cells (LSKs), long-term HSCs (LT-HSC), and short-term HSCs (ST-HSC) in homozygous, heterozygous, and control mice. **(B)** Absolute cell numbers of MPs, LSKs, LT-HSCs, and ST-HSCs were assessed by normalizing cell proportions to absolute cell numbers extracted from mouse femur and tibia.

To assess the proportion of hematopoietic CFU within the BM, cells were plated in methylcellulose-based medium allowing growth of primitive erythroid progenitor cells, granulocyte progenitor cells, macrophage progenitor cells, and multi-potential progenitor cells. No significant difference in total colony number or colony subtypes was seen (**Figure 21**).

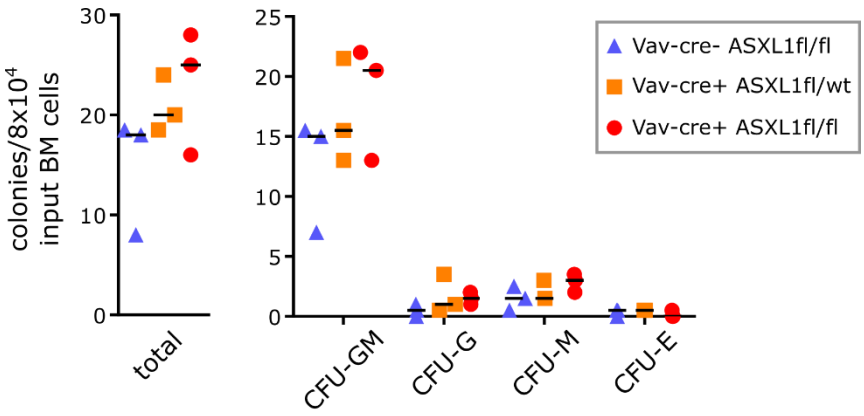

Figure 21: Analysis of CFU assessed after culturing murine BM cells in methylcellulose-based medium. Classification of multi-potential CFU-GEMM, CFU-GM, CFU-G, CFU-M, and CFU-erythrocytic (CFU-E).

4.5 No observation of changes within the BM microenvironment of mice with hematopoietic deletion of *ASXL1*

It is hypothesized that MDS development is dependent on a pathogenic reciprocal interaction between the MDS clone, healthy hematopoietic cells, and the BM microenvironment: Signals from the MDS clone disrupt normal HSC function directly as well as through induction of a dysfunctional BM microenvironment. In turn, also the altered BM environment is insufficient to support normal hematopoiesis but instead facilitated MDS clonal expansion. MSCs from MDS patients were shown to be structurally, epigenetically, and functional altered resulting in an impaired stromal support contributing to deficient hematopoiesis in MDS (Geyh et al., 2013; Weickert et al., 2021). In this study, we were aiming to depict changes in the BM microenvironment caused by a genetically altered hematopoietic clone.

4.5.1 Hematopoietic deletion of ASXL1 *does not lead to altered numbers of BM endothelial cells, osteoblastic cells, or mesenchymal stem cells*

To investigate endothelial cells (ECs), osteoblastic cells (OBCs), or MSCs within the BM, adherent cells were extracted from femurs and tibias of mice with homozygous or heterozygous hematopoietic deletion of *ASXL1* and control mice. Using FACS analysis, non-hematopoietic (CD45− TER119−) cells were further classified as ECs (CD31+), MSCs (CD31− SCA-1+ Alcam-/low) and OBCs (CD31− SCA-1- CD51+, **Figure 22A**). To assess absolute cell numbers, counts within the gates were normalized to total cell number extracted. There was no significant difference in EC, OBC, and MSC number in mice with hematopoietic deletion of *ASXL1* compared to control mice (**Figure 22B**).

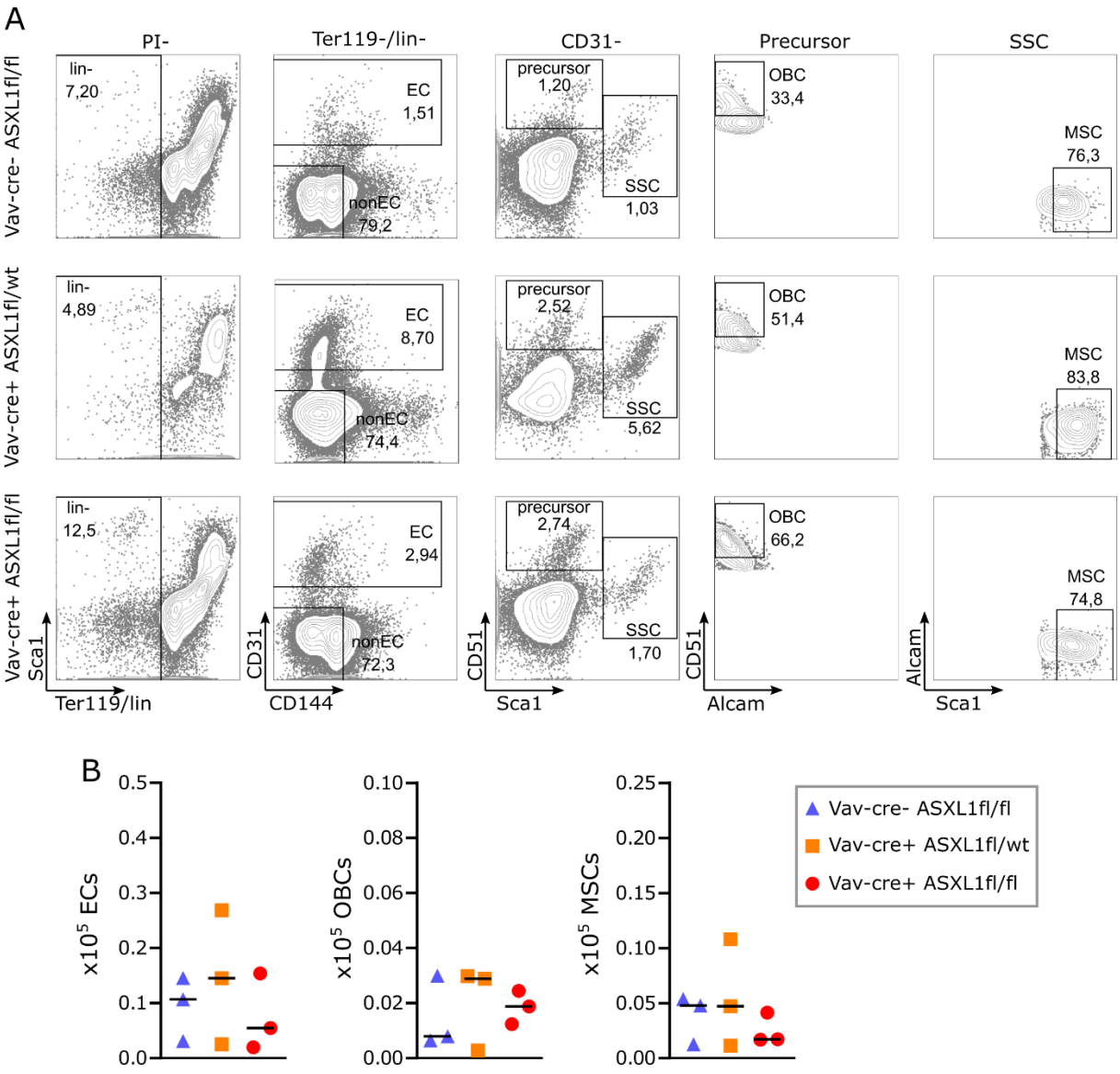

Figure 22: Analysis of niche cells extracted from the BM through collagenase treatment of mice with a homozygous or a heterozygous deletion of *ASXL1* within the hematopoietic system and control mice. (A) Representative gating scheme for identifying endothelial cells (EC), osteoblastic cells (OBC), or mesenchymal stem cells (MSC) in homozygous, heterozygous, or control mice. **(B)** Absolute cell numbers of ECs, OBCs, and MSCs were assessed by normalizing cell proportions to absolute cell numbers extracted from mouse femur and tibia after collagenase treatment.

4.5.2 Mesenchymal stem cells derived from mice with a hematopoietic deletion of ASXL1 *do not show distinct differences in CFU-F capacity, passage-dependent cell growth, and spontaneous differentiation*

To investigate whether MSCs derived from mice with a hematopoietic deletion of *ASXL1* show differences on the functional level, we investigated MSC growth and differentiation. Therefore, collagenated cells were plated in order to obtain an enriched MSC population until passage 3. To test how many MSCs at passage 3 give rise to fibroblast colonies (CFU-F), 100

MSCs were plated and colonies were counted after 3 days culturing and crystal violet staining. Mice with a homozygous, a heterozygous, or without a deletion of *ASXL1* in the hematopoietic system did not show differences in CFU-F capacity (**Figure 23A**).

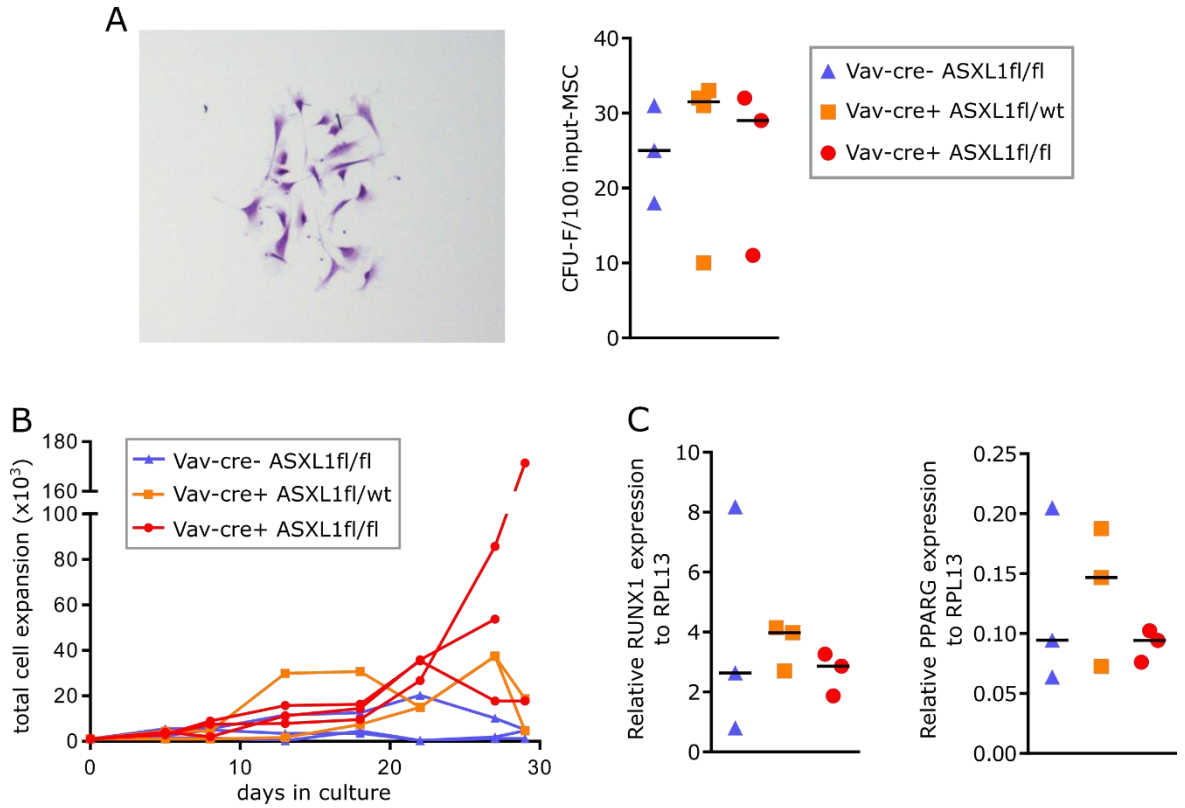

Figure 23: Functional analysis of MSCs from mice with a homozygous or a heterozygous deletion of *ASXL1* within the hematopoietic system and control mice. (A) Representative image of a fibroblast colony obtained after 3 days of culturing MSCs (left panel). Number of colonies was assessed per 100 plated MSCs from passage 3 (right panel). **(B)** Passage dependent cell growth. Symbols indicate time point of passaging, counting and re-plating of 10.000 cells. First measured time point starts with MSCs counted at passage 4, last measured time point indicates passage 11. **(C)** Spontaneous differentiation of MSCs at passage 3 with 80% confluence was investigated by qPCR of early osteogenic (RUNX1) and adipogenic (PPARG) marker. Relative expression of genes was investigated by normalization to RPL13.

To test MSC growth capacity over several passages, MSCs from mice with a heterozygous, homozygous, or without deletion of AXL1 within the hematopoietic system were re-plated over several passages. After 8 passages, there was a strong trend for a higher MSC expansion in *ASXL1* deleted mice compared to control mice (**Figure 23B**).

Furthermore, MSCs were assessed for spontaneous differentiation at passage 3 and 80% confluence via qPCR. Runx1 expression for early osteogenic and PPARG expression for early adipogenic differentiation was assessed and normalized to RPL13. No significant difference could be observed in mice with a heterozygous, homozygous, or without deletion of *ASXL1* within the hematopoietic system (**Figure 23C**).

5 Discussion

5.1 Depicting hematopoiesis during aging, in CHIP, and in MDS using primary *in vitro* cultures

Identifying alterations in the hematopoietic structure and kinetics is key for understanding aging and in disease. Most insight into human hematopoiesis so far relies on snapshot analyses from primary tissue, potentially affected by cell source differences and preprocessing biases. Snapshot analysis led to the common perception that HSCs increase with age in humans (Pang *et al.*, 2011; Rundberg Nilsson *et al.*, 2016). However, we and others (Kuranda *et al.*, 2011) could not show significant differences between young and aged HSC proportions. Similarly, studies investigating HSPC proportions in MDS show variable results. Consistent with our investigations, Pang et al. (2013) observed a decreased GMP proportion in MDS. Whereas they analyzed low-risk MDS, we utilized a mixed high-risk and low-risk MDS cohort. Both studies normalized their cell counts to the lineage- compartment and lineage markers were used to separate CD34+ leukemic blasts from the HSPC compartment. The utilization of lineage markers is the biggest difference of our study to investigations made by Ostendorf et al. (2018). Their FACS antibody panel did not include lineage markers to separate CD34+ blasts from HSPCs. While they showed increased HSPC numbers in MDS, due to increased GMP proportions, it is worth noting that their MDS cohort included exclusively patients with increased blast counts, potentially contributing to a falsely high HSPC number. Another detail to consider when comparing different studies that evaluate various HSPC compartments can be the normalization method. A study from Will et al. (2012) showed the expansion of CMP in low-risk and GMP in high-risk MDS when normalizing to the CD34+ CD38+ compartment. However, by normalizing CMP, GMP, and MEP counts to the CD34+ CD38+ compartment which includes exclusively CMPs, GMPs, and MEPs, results cannot be compared to other populations outside the CD34+ CD38+ compartment. Thus, the increase in CMP and GMP observed by Will et al might not be related to HSCs, MPPs, MLPs, or more mature cells.

When assessing the quantity of human HSPCs, BM cellularity is not considered in most cases. In contrast to mouse studies where femur and tibia are completely flushed to harvest the majority of red BM, human BM cells are extracted by aspiration from the iliac crest or by flushing cropped femoral heads from hip arthroplasty patients. Both methods do not allow to quantify absolute cell numbers. Our results showing increased HSPC proportions in aged

individuals (**Figure 6B**) have to be seen in context with a decreasing BM cellularity during aging (Hartsock *et al.*, 1965). To account for this shift, we normalized our HSPC frequencies to their assumed cellularity based on the individual's age resulting in a repealing of the initially determined effect (**Figure 6C**). A similar effect could be present in MDS, which is often accompanied by an increased BM cellularity (Schemenau et al., 2015). Decreased HSPC proportions based on decreased CMP and GMP proportions (**Figure 10C**) may not reflect absolute cell numbers present the human body of these patients.

Our standardized *in vitro* culturing approach makes BM samples from different sources comparable in terms of numbers and kinetics, and computational profiling reveals the preferred hematopoietic hierarchy for each sample and rate differences in cell type resolution. Mirroring decreasing blood production and decreasing BM cellularity during aging, we find a lower HSPC and mature cell production in the aged cohort of our HSC cultures (**Figure 7C**). This effect could be traced back to the very top of the hematopoietic hierarchy: HSC proliferation is significantly decreased in aged individuals comparted to young (**Figure 9B**), providing a simplified model of aging human hematopoiesis.

Understanding kinetic properties within the HSPC compartment in CHIP and in MDS can provide fundamental knowledge about achieving clonal dominance and the reorganization of the HSPC compartment towards a leukemic stem cell (LSC) compartment. Woll et al. (2014) identified that MDS-LSCs are located within the lineage− CD34+ CD38− CD90+ CD45RA− compartment and these LSC give rise to MEPs and GMPs therefore establishing their hierarchical relationship. In line with these findings, we could show that mutations present in bulk BM of our MDS patients were always detected on the HSC level and with a high VAF (n=3, **Table S2**). We assume, when sorting lineage- CD45dim CD34+ CD38- CD45RA- CD90+ HSCs, we also purify LSC in case of MDS and pre-leukemic stem cells in case of CHIP. Our results showing deviating hierarchical structures for most MDS patients and a median of 3 deregulated rates per patient demonstrating the complex reorganization of the hematopoietic tree, potentially driven by specific characteristics of LSCs such as LSC-specific gene expression programs (Velten et al., 2021). Surprisingly, this transformation towards a disorderly hematopoiesis can also be seen in CHIP, but at a lower frequency and a lower manifestation.

Although we found no pattern of kinetic alterations to reappear in the 10 MDS samples and no correlation between specific mutations and specific altered rates, we noted that the vast

majority of MDS samples showed alterations located on the HSC level. This was different in CHIP, only 2 out of 7 samples showed altered HSC rates. Of the total 13 altered HSC rates, 10 rates were differentiation rates from the HSC compartment towards the MEP or mature compartment, which are both transitions not described by the classical model of hematopoiesis. On the technical side, this differentiation path skipping several HSPC subcompartments could also be an artefact caused by rapid differentiation through these HSPC subcompartments.

For achieving clonal dominance, HSCs need to have a growth advantage or increased fitness level (Watson et al., 2020). The quality of alterations we found in CHIP and MDS samples do not serve as an explanation for clonal dominance. However, our approach is based on 7-day measurements, whereas clonal dominance is achieved over years or as proven for myeloproliferative neoplasms over the lifespan of an individual (Watson *et al.*, 2020; Williams et al., 2020). In cell culture, HSCs are supported to divide and differentiate which is limited, whereas HSCs do engraft and build a stable system *in vivo*. Furthermore, our HSC culture approach is focused on cell intrinsic driven alterations, whereas the normal and diseased hematopoietic system is influenced by the microenvironment *in vivo*. Future studies should therefore include additional analyses of extrinsic effects, such as stem and progenitor trafficking (Hoggatt et al., 2013), regulation of quiescence through interaction with the BM niche (Goncalves et al., 2016), or the block of BM to blood egress, which would contribute to the observed MDS cytopenia in the presence of hypercellular BM.

In bulk analysis, results are dominated by the biggest cell clones grown in culture, whereas clones with a few cells get lost in the shuffle. In contrast, single cell assays allow assessment of smaller clones by monitoring cell growth in each well starting with one HSC. Whereas the averaged cellular yield could not show differences between MDS and age-matched healthy controls (**Figure 14C**), the assessment of individual clones revealed differences between the groups: MDS HSCs divided earlier than the healthy controls and whereas single HSCs from healthy individuals mostly yielded 1 to 3 cells, HSCs from MDS patients mostly yielded 4 to 15 cells after 7-day culture (**Figure 15**). A faster first cell division represents a higher activity of MDS HSCs, which is in line with previous studies showing an expansion of phenotypic defined HSCs in MDS (Shastri et al., 2017). However, cell division does not automatically mean self-renewal and it is also associated with differentiation, which are both controlled by a symmetric versus asymmetric cell division mode of HSCs (Florian and Geiger, 2010; Giebel, 2008;

Schroeder, 2007; Wu et al., 2007). In fact, our bulk analyses showed an unusual differentiation pattern in 6 out of 10 MDS cases with a direct or rapid differentiation of HSCs towards the MEP or mature cell compartment (**Figure 13E**).

When analyzing the average clone size after 7 days in the single cell experiment, it is not clear which kind of cells contribute to each clone. During aging and disease, HSCs were shown to have a diverse lineage potential and to be biased towards a specific lineage. A different mix of biased HSCs producing either myeloid (granulocytic and/or monocytic) or erythroid colonies might be a reason for different clone sizes originating from MDS HSCs compared to the healthy control as shown in **Figure 15C** and **D**. Indeed, MDS HSCs do show a different CFU capacity, with a lower number of erythroid colonies compared to age-matched healthy samples (**Figure 11**).

Analyzing the proliferative potential of single-HSCs in time-lapse experiments provides detailed data on cell cycle length of each tracked cell. For this analysis, an MDS sample with mutations in *ASXL1*, *SF3B1*, *TET2*, and *WT1* was chosen. MDS354 showed more asynchronous cell divisions of sister cells compared to the healthy controls (**Figure 16C** and **D**). The cell cycle length might be linked to a specific cell type and could indicate a preceding asymmetric cell division. Alternating cell cycle lengths could also indicate cell cycle disruptions provoked by impaired function of ASXL1 or SF3B1 since wild type ASXL1 was shown to interact with the cohesion complex maintaining chromatid separation in normal hematopoiesis (Li et al., 2017), and disruption of SF3B1 leads to cell cycle arrest in hematopoietic cells (Dolatshad et al., 2015).

5.2 A failed MDS mouse model for investigating properties of mesenchymal stem cells

Although *ASXL1* is expressed in various hematopoietic cell types (Fisher et al., 2010), our *Vav-cre+ ASXL1*$^{fl/fl}$ mice only show very small effects on the hematopoietic phenotype and we were not able to recapitulate the previously reported results by Abdel-Wahab et al (2013). They observed a phenotype with progressive, multilineage cytopenia and dysplasia, as well as increased numbers of HSPCs. Abdel-Wahab *et al.* (2013) either utilized *Vav-cre+ ASXL1*$^{fl/fl}$ mice with a cre recombinase regulated by the hematopoietic expressed *vav*-promotor or they utilized the *Mx1-cre+ ASXL1* $^{fl/fl}$ mice with an interferon inducible cre recombinase. Whereas in their study decreased BM cellularity was shown for *Vav-cre+ ASXL1*$^{fl/fl}$ mice and data was

not shown for *Mx1-cre+ ASXL1* $^{fl/fl}$ mice, the progressive peripheral leukopenia and anemia was only depicted for *Mx1-cre+ ASXL1*$^{fl/fl}$ mice. Furthermore, dysplasia was shown for *Mx1-cre+ ASXL1*$^{fl/fl}$ mice and not for *Vav-cre+ ASXL1*$^{fl/fl}$ mice and increased numbers of HSCs were only shown for *Vav-cre+ ASXL1*$^{fl/fl}$ mice. Thus, most important criteria for an MDS-like phenotype were investigated in *Mx1-cre+ ASXL1*$^{fl/fl}$ mice and might not be as clear in *Vav-cre+ ASXL1*$^{fl/fl}$ mice. However, phenotypic differences in mice with the same genotype could also be based on differences in genetic background or environmental factors including stress triggered by regularly blood sampling that was performed in their studies. Furthermore, to detect subtle phenotypes, a relatively high number of mice is needed.

In addition to the aforementioned study, several studies investigated the hematopoietic compartment in mice with a constitutive knockout of *ASXL1*, though with conflicting results. While Wang et al. (2014) clearly see an MDS-like phenotype in mice with *ASXL1* deletion, Fisher *et al.* (2010) detected a mild phenotype with no clear MDS-like disease.

Considering studies showing cytopenia and dysplasia in *ASXL1*-deficient mice and also with the knowledge that *ASXL1* is one of the most common mutated genes in MDS (Bejar *et al.*, 2011), *ASXL1* seemed to be a very promising candidate for an MDS mouse model. However, adverse results question the idea of an MDS mouse model triggered by *ASXL1* loss-of-function-mutation. Indeed, most human *ASXL1* mutations occur in exon 12 (Schnittger *et al.*, 2013) and a truncated protein resulting from such a mutation could be detected at low levels in cell lines (Inoue et al., 2016). Mouse models expressing a truncated form of ASXL1 within the hematopoietic system were generated in recent studies and these mice developed myeloid malignancies including AML, MPN, MDS, and MDS/MPN (Uni et al., 2019; Yang et al., 2018). However, the gain of function mouse model also shows an inconclusive phenotype since not all studies could detect a strong phenotype sufficient to match criteria for a myeloid disease (Hsu et al., 2017). It is also important to emphasize that somatic mutations in *ASXL1* do not only occur in humans with myeloid malignancies but also in healthy individuals with CHIP while only a few of these individuals will develop myeloid malignancies (Jaiswal *et al.*, 2014; Steensma *et al.*, 2015).

The original goal of establishing this mouse model was to serve as a tool to investigate alterations within the BM niche occurring during MDS development. Since our *Vav-cre+ ASXL1*$^{fl/fl}$ mice failed to show a clear MDS-like phenotype, we did not expect distinct alterations

in the BM niche. This was confirmed by our investigations on the BM niche cell distribution and MSC expansion and differentiation capacity.

6 Supplements

6.1 Supplementary Figures

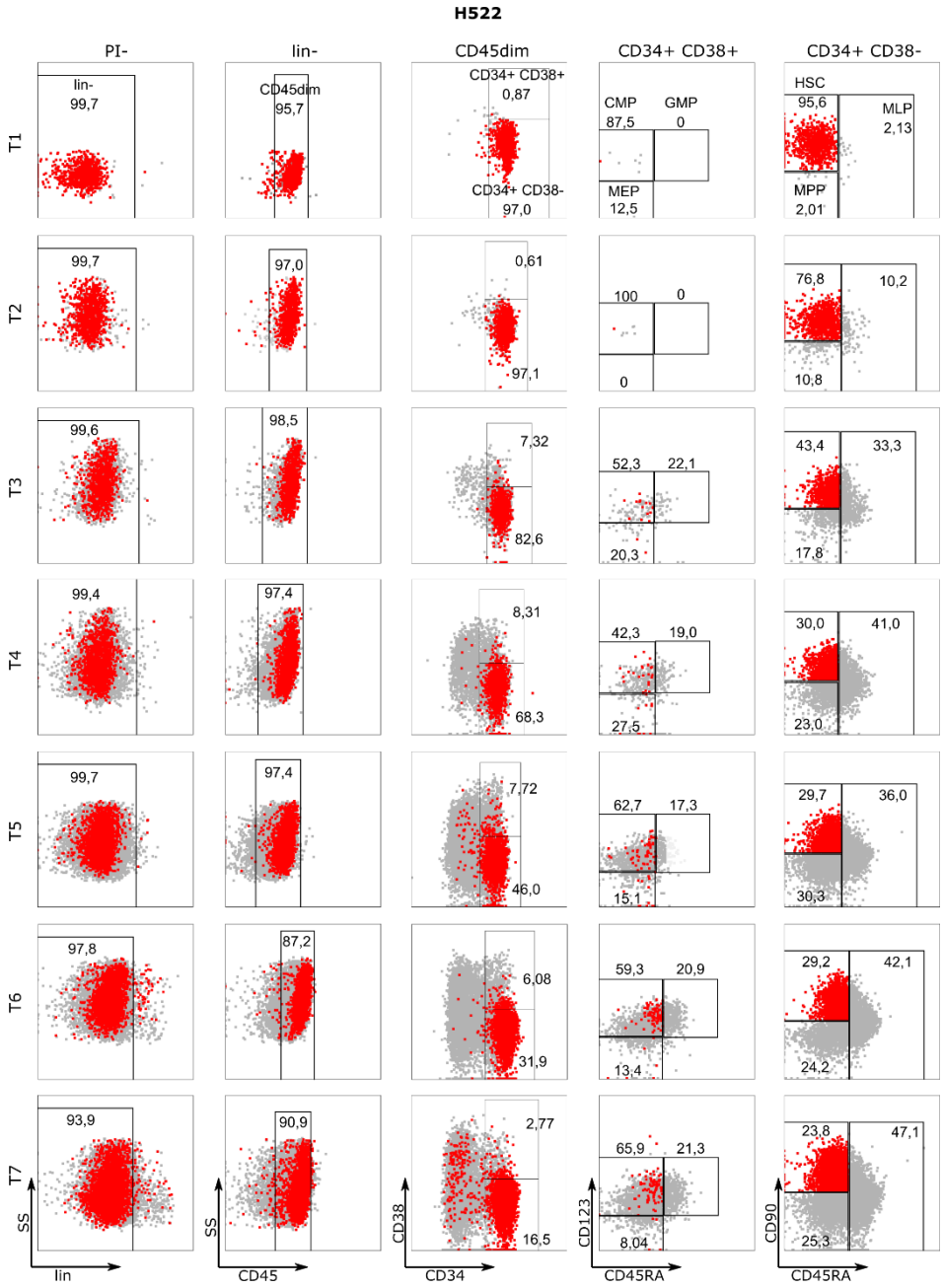

Figure S1: Investigation of HSCs, MPPs, MLPs, CMPs, GMPs, and MEPs in HSC cultures from a healthy young individual. Cultures were analyzed at day 1 to day 7 (T1 – T7). To better identify the HSC population, all cells being CD90+, CD45RA- were highlighted in red.

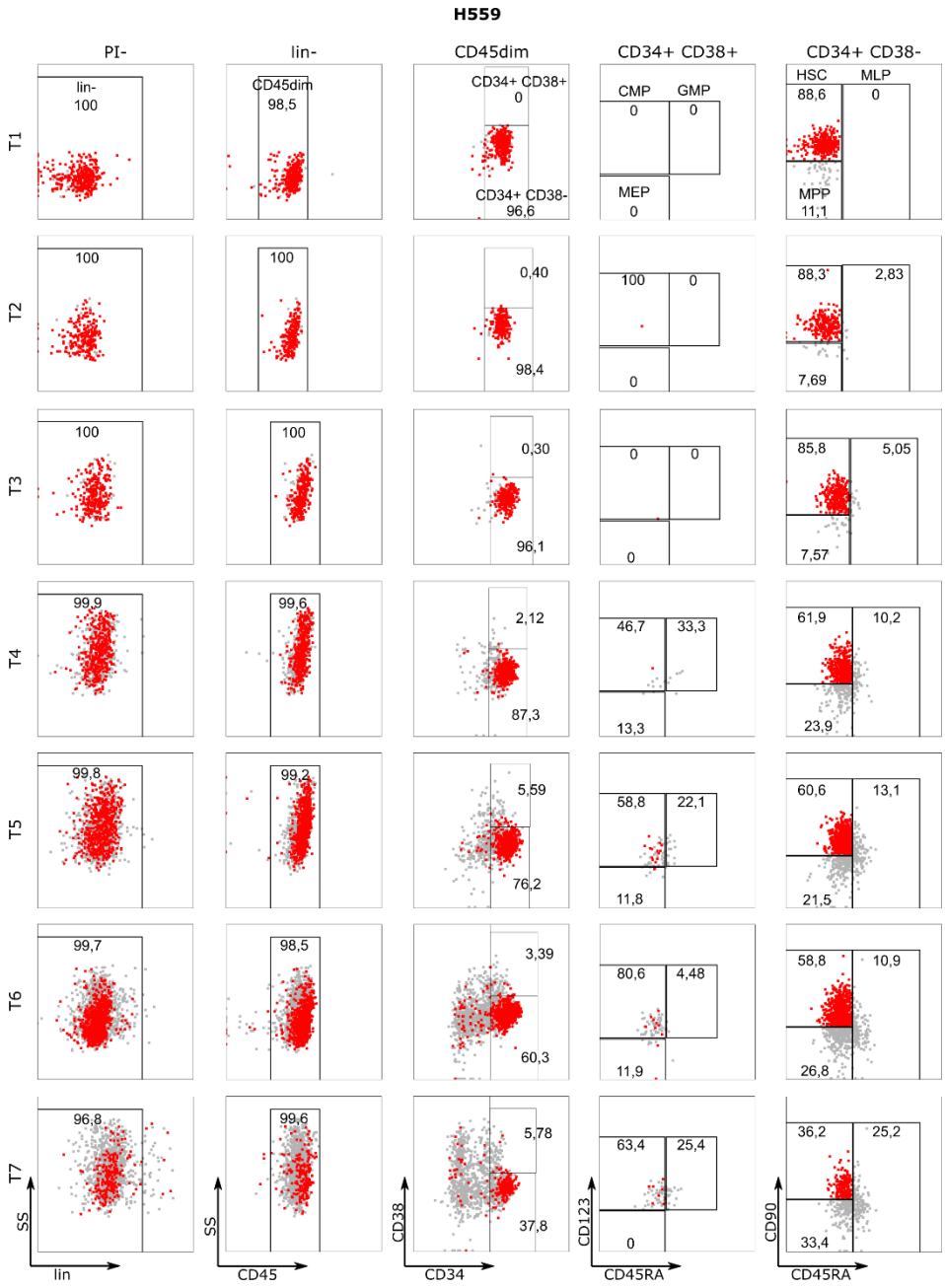

Figure S2: Investigation of HSCs, MPPs, MLPs, CMPs, GMPs, and MEPs in HSC cultures from a healthy aged individual. Cultures were analyzed at day 1 to day 7 (T1 – T7). To better identify the HSC population, all cells being CD90+, CD45RA- were highlighted in red.

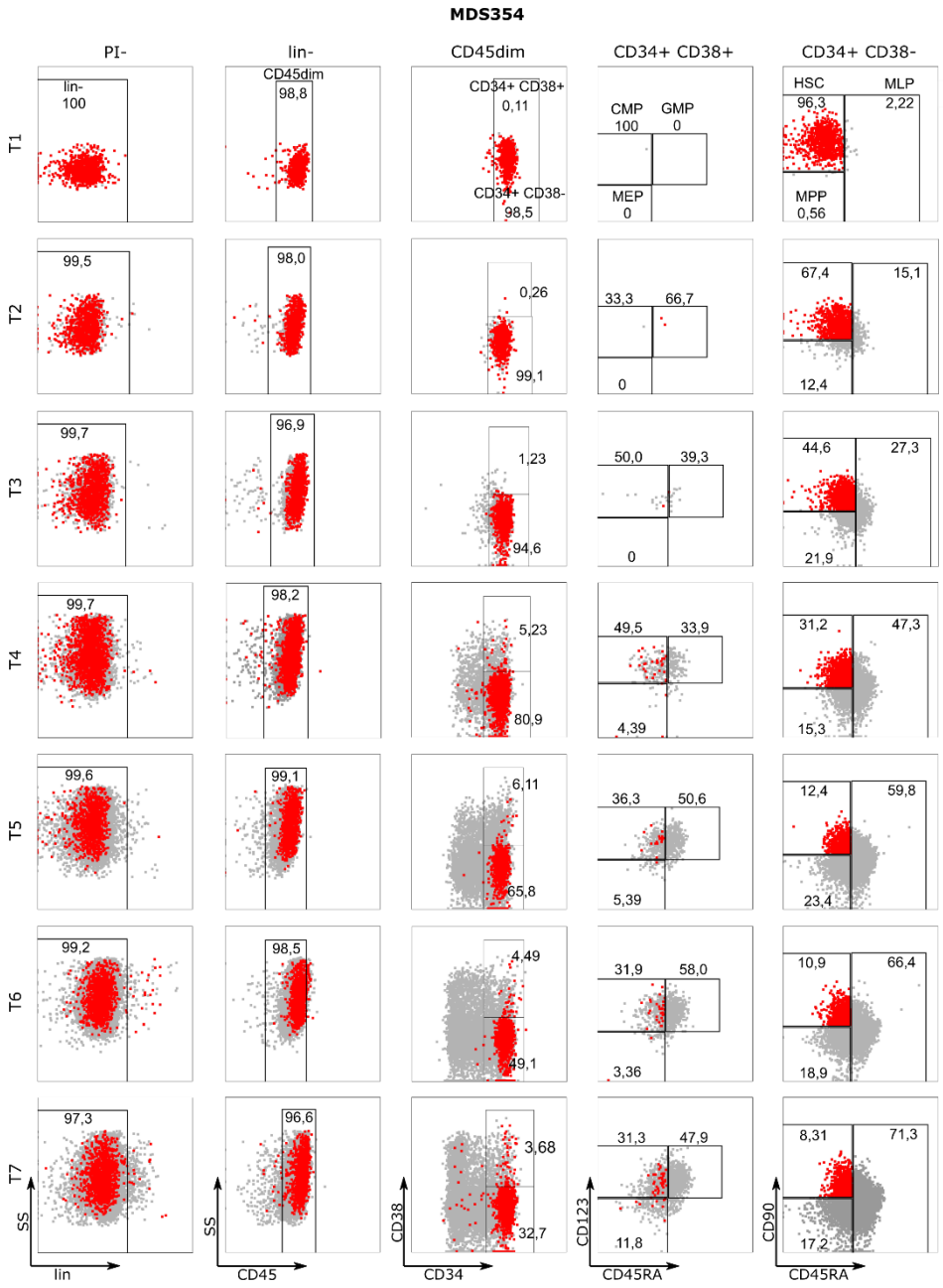

Figure S3: Investigation of HSCs, MPPs, MLPs, CMPs, GMPs, and MEPs in HSC cultures from a patient with MDS. Cultures were analyzed at day 1 to day 7 (T1 – T7). To better identify the HSC population, all cells being CD90+, CD45RA- were highlighted in red.

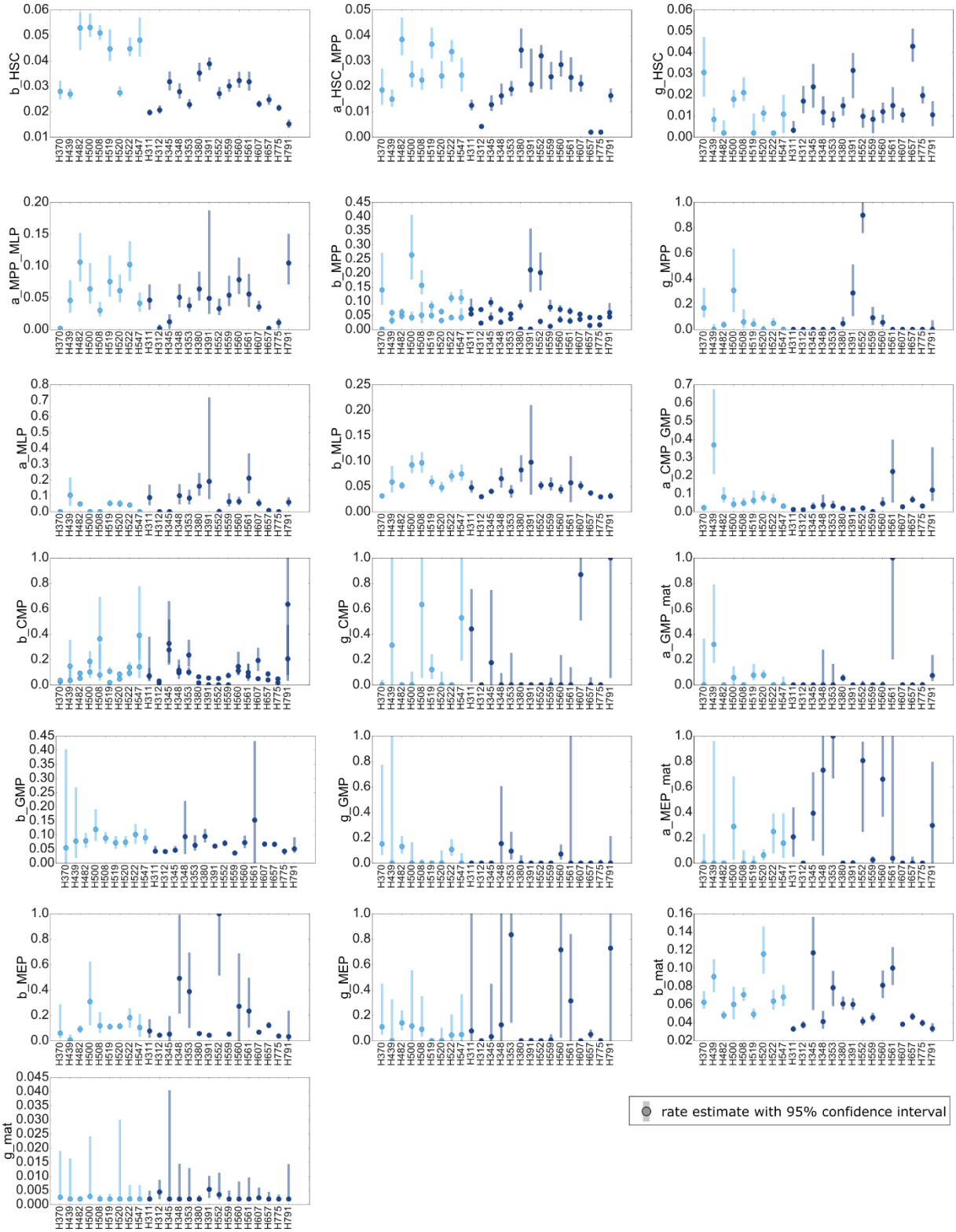

Figure S4: Rate estimates to identify proliferation (b), differentiation (a), and cell death (g) of HSCs, MPPs, MLPs, CMPs, GMPs, MEPs, and CD34- cells (mat) in healthy young (light blue) and aged (dark blue) individuals. Bars indicate the 95% confidence interval for each rate estimate.

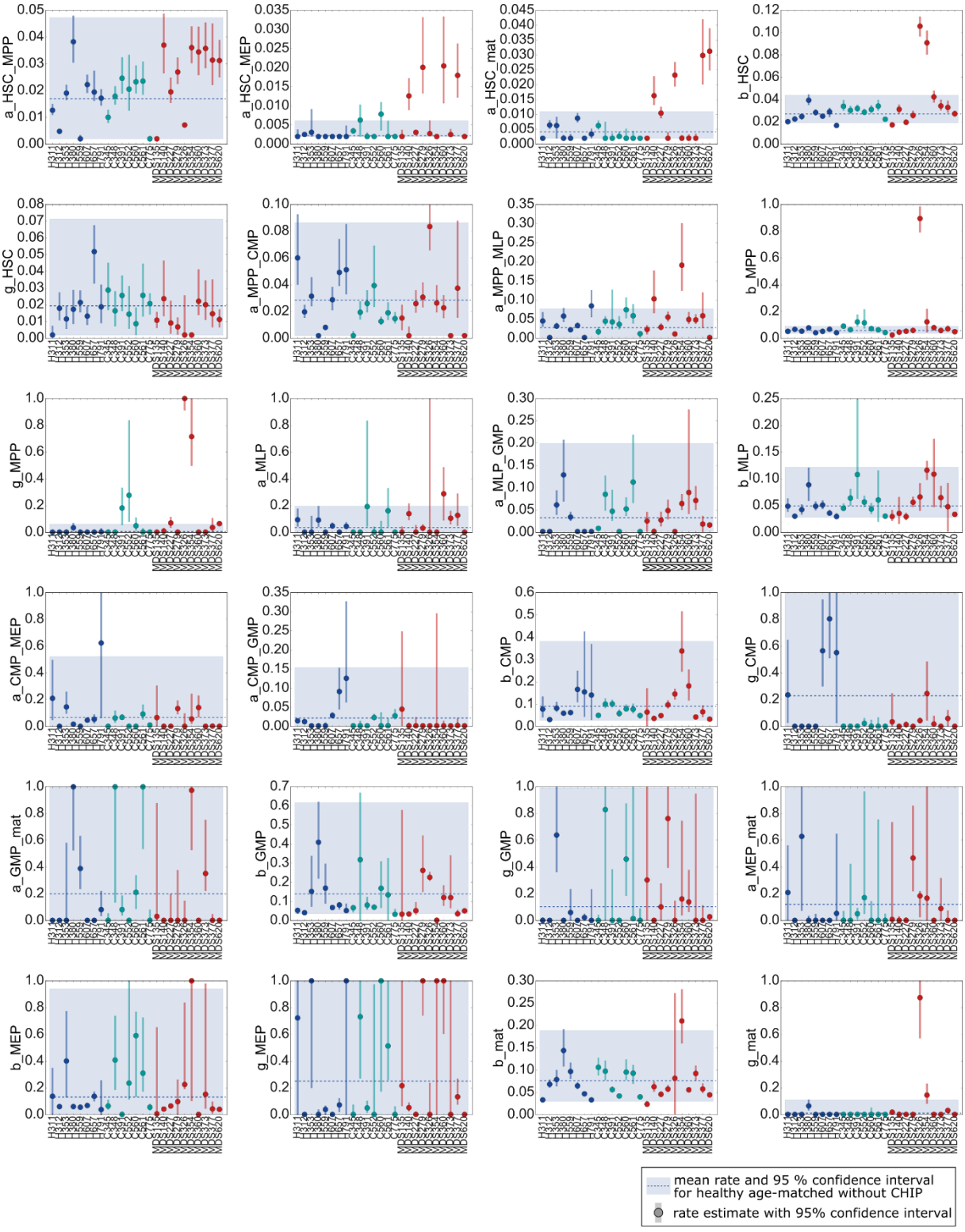

Figure S5: Rate estimates identifying proliferation (b), differentiation (a), and cell death (g) of HSCs, MPPs, MLPs, CMPs, GMPs, MEPs, and CD34- cells (mat) in healthy aged (dark blue), CHIP (green), and MDS (red) samples. Bars indicate the 95% confidence interval for each rate estimate. Shaded in blue is the 90% confidence interval (CI) based on parameter estimates and uncertainties of age-matched healthy samples to identify accelerated and decelerated rates in CHIP and MDS samples.

6.2 Supplementary Tables

Table S1: Sample characteristics for investigating age-related differences in the hematopoietic system. Age cut off for distinguishing young and aged individuals is 55 years.

young		
ID	**Age**	**Gender**
H450	20	f
H439	24	m
H547	26	m
H482	29	m
H520	37	f
H508	43	m
H522	44	m
H519	46	m
H370	51	m
H500	52	f

aged		
ID	**Age**	**Gender**
H353	57	m
H345	58	f
H657	62	f
H311	63	m
H380	63	m
H791	63	f
H391	65	f
H607	68	f
H552	68	f
H312	70	m
H560	70	f
H775	72	f
H559	76	f
H561	76	m
H348	79	f

Table S2: Detailed mutational characteristics including DNA variant, protein variant, and information if mutation was analyzed in bulk or on sorted HSCs. VAF: variant allele frequency.

ID	Gene	Variant_DNA	Variant_Prot	Analyzed in	VAF Bulk (%)	VAF HSC (%)
C345	**DNMT3A**	c.2393T>A	p.Leu798His	Bulk	**4**	
C391	**DNMT3A**	c.2401A>G	p.Met801Val	Bulk	**12**	
C552	**SF3B1**	c.1873C>T	p.Arg625Cys	Bulk	**15**	
C560	**DNMT3A**	c.1015-2A>G	p=? splice-site Variante	Bulk	**5**	
C775	**KRAS**	c.40G>A	p.Val14Ile	Bulk	**2.43**	
C561	**TP53**	c.536A>G	p.His179Arg	Bulk	**4,5**	
	DNMT3A	c.1949T>G	p.Leu650Arg	Bulk	**1,3**	
C348	**DNMT3A**	c.2644C>T	p.Arg882Cys	Bulk	**27**	
	NFE2	c.578_581del	p.Asn193Ilefs*12	Bulk	**25**	
MDS360	**SF3B1**	c.1866G>T	p.Glu622Asp	Bulk/HSC	**50**	**41**
	SRSF2	c.283C>A	p.Pro95Leu	HSC		**42**
MDS373	**SF3B1**	c.2098A>G	p.Lys700Glu	Bulk/HSC	**33**	**49**
	DNMT3A	c.1906G>A	p.Val636Met	HSC		**61**
	TET2	c.978delA	p.Lys326Asnfs*21	HSC		**45**
	TET2	c.1630C>T	p.Arg544*	HSC		**15**
MDS377	**ASXL1**	c.1934dup	p.Gly646Trpfs*12	Bulk	**12**	
	DNMT3A	c.939G>A	p.Trp313*	Bulk	**32**	
	SETBP1	c.2608G>A	p.Gly870Ser	Bulk	**11**	
MDS227	**SF3B1**	c.2098A>G	p.Lys700Glu	Bulk/HSC	**50**	**50**
	TET2	c.5620G>A	p.Glu1874Lys	Bulk/HSC	**50**	**39**
MDS279	**ASXL1**	c.1900_1922del	p.Glu635Argfs*15	Bulk	**18**	
	KRAS	c.34G>A	p.Gly12Ser	Bulk	**8**	
MDS620	**ASXL1**	unknown	unknown	Bulk		
MDS140	**ASXL1**	c.1772dupA	p.Tyr591*	Bulk	**50**	
	RUNX1	c.1014dupC	plle339Hisfs*234	Bulk	**40**	
	SRSF2	c.284C>A	p.Pro95His	Bulk	**45**	
	TET2	c.3300delT	plLeu1101Serfs*5	Bulk	**50**	
MDS326	**TET2**	c.2562del	p.Phe854Leufs*19	Bulk	**3.53**	
MDS135	**ASXL1**	c.1900A>T	p.Arg634*	Bulk	**43**	
	SF3B1	c.2098A>G	p.Lys700Glu	Bulk	**45**	
	TET2	c.3986T>G	p.Leu1329Arg	Bulk	**45**	
		c.4210C>T	p.Arg1404*	Bulk	**49**	
	WT1	c.1048T>C	p.Cys350Arg	Bulk	**51**	
MDS354	**ASXL1**	c.1900A>T	p.Arg634*	Bulk	**43**	
	SF3B1	c.2098A>G	p.Lys700Glu	Bulk	**45**	
	TET2	c.3986T>G	p.Leu1329Arg	Bulk	**43**	
		c.4210C>T	p.Arg1404*	Bulk	**50**	
	WT1	c.1048T>C	p.Cys350Arg	Bulk	**51**	

Table S3: Summary of statistical analysis performed by GraphPad Prism. If multiple parameters were analyzed at one time, p-values were Bonferroni corrected according to the number of analyzed parameters.

Snapshot analysis, healthy young vs aged			
	Mann-Whitney	Bonferroni correction	Significant
HSPC	0,0176	-	**yes**
HSC	0,0396	0,2376	no
MPP	0,0503	0,3018	no
MLP	0,1275	0,765	no
CMP	0,0307	0,1842	no
GMP	0,3138	1,8828	no
MEP	0,1393	0,8358	no

Snapshot analysis normalized to assumed cellularity			
	Mann-Whitney	Bonferroni correction	Significant
HSC	0,4781	-	no
HSPC	0,3937	-	no

% of cells in 7-day HSC culture, healthy young vs aged			
	Mann-Whitney	Bonferroni correction	Significant
HSPC	0,1058	-	no
HSC	0,0784	0,4704	no
MPP	0,3529	2,1174	no
MLP	0,1681	1,0086	no
CMP	0,2587	1,5522	no
GMP	0,2458	1,4748	no
MEP	0,4675	2,805	no

Cells per input HSCs, healthy young vs aged			
	Mann-Whitney	Bonferroni correction	Significant
HSPC	0,0074	-	**yes**
CD34-	0,0106	-	**yes**
HSC	0,1188	-	no

Rate estimates, healthy young vs aged			
	Mann-Whitney	Bonferroni correction	Significant
a_HSC_MPP	0,0202	0,4242	no
b_HSC	0,0022	0,0462	**yes**
g_HSC	0,1585	3,3285	no
a_MPP_MLP	0,1445	3,0345	no
a_MPP_CMP	0,0418	0,8778	no
b_MPP	0,0477	1,0017	no
g_MPP	0,137	2,877	no
a_MLP	0,0486	1,0206	no
b_MLP	0,0366	0,7686	no
a_CMP_GMP	0,0204	0,4284	no
a_CMP_MEP	0,3359	7,0539	no
b_CMP	0,0774	1,6254	no
g_CMP	0,2845	5,9745	no
a_GMP_mat	0,1475	3,0975	no
b_GMP	0,0126	0,2646	no
g_GMP	0,2123	4,4583	no
a_MEP_mat	0,1377	2,8917	no
b_MEP	0,3602	7,5642	no
g_MEP	0,437	9,177	no

b_mat	0,0318	0,6678	no
g_mat	0,3353	7,0413	no

Snapshot analysis, healthy age-matched vs CHIP vs MDS

	Kruskal Wallis test	Bonferroni correction	Significant	Dunn's multiple comparison		
				H vs C	H vs M	C vs M
HSPC	0,0441	-	**yes**	0,4625	**0,0382**	> 0,9999
HSC	0,1827	1,0962	no	-	-	-
MPP	0,2722	1,6332	no	-	-	-
MLP	0,771	4,626	no	-	-	-
CMP	0,0025	0,015	**yes**	> 0,9999	**0,0031**	0,0505
GMP	0,0027	0,0162	**yes**	> 0,9999	**0,0074**	**0,0167**
MEP	0,2246	1,3476	no	-	-	-

CFU-capacity, healthy age-matched vs CHIP vs MDS

	Kruskal Wallis test	Bonferroni correction	Significant	Dunn's multiple comparison		
				H vs C	H vs M	C vs M
CFU-GEMM	0,0585	0,2925	no	-	-	-
CFU-GM	0,0163	0,0815	no	-	-	-
CFU-G	0,0211	0,1055	no	-	-	-
CFU-M	0,01	0,05	**yes**	> 0,9999	0,0659	0,0593
BFU-E	< 0,0001	0,0005	**yes**	> 0,9999	**0,0011**	0,071
total	0,0002	-	**yes**	> 0,9999	**0,0055**	0,0512

% of cells in 7-day HSC culture, healthy age-matched vs CHIP vs MDS

	Kruskal Wallis test	Bonferroni correction	Significant	Dunn's multiple comparison		
				H vs C	H vs M	C vs M
HSPC	0,79	-	no	-	-	-
HSC	0,8961	5,3766	no	-	-	-
MPP	0,1512	0,9072	no	-	-	-
MLP	0,3504	2,1024	no	-	-	-
CMP	0,171	1,026	no	-	-	-
GMP	0,1986	1,1916	no	-	-	-
MEP	0,8428	5,0568	no	-	-	-

Cells per input HSCs, healthy age-matched vs CHIP vs MDS

	Kruskal Wallis test	Bonferroni correction	Significant	Dunn's multiple comparison		
				H vs C	H vs M	C vs M
HSPC	0,615	-	no	-	-	-
CD34-	0,8224	-	no	-	-	-
HSC	0,5159	-	no	-	-	-

Wells filled with wells, healthy age-matched vs CHIP vs MDS

	Kruskal Wallis test	Bonferroni correction	Significant	Dunn's multiple comparison		
				H vs C	H vs M	C vs M
	0,4065	-	no	-	-	-

Cells at day 7 per input cells, healthy age-matched vs CHIP vs MDS

	Kruskal Wallis test	Bonferroni correction	Significant	Dunn's multiple comparison		
				H vs C	H vs M	C vs M
	0,207	-	no	-	-	-

Bloodvalues 6-10 months old mice

	Mann-Whitney	Bonferroni correction	Significant
Hb	0,7283	-	no
WBC	0,0163	-	**yes**
plateletts	0,2777	-	no

Bloodvalues 15-25 months old mice

	Kruskal Wallis test	Bonferroni correction	Significant	Dunn's multiple comparison		
				Δ/Δ vs Δ/wt	Δ/Δ vs fl/fl	Δ/wt vs fl/fl
Hb	0,0364	-	**yes**	**0,0339**	0,3374	> 0,9999
WBC	0,0225	-	**yes**	0,1715	> 0,9999	**0,0262**
plateletts	0,8263	-	no	-	-	-

Analysis of mature blood cells in the BM

	Kruskal Wallis test	Bonferroni correction	Significant	Dunn's multiple comparison		
				Δ/Δ vs Δ/wt	Δ/Δ vs fl/fl	Δ/wt vs fl/fl
T-lymphocytes	0,2518	-	no	-	-	-
B-lymphocytes	0,5101	-	no	-	-	-
Granulocytes	0,0627	-	no	-	-	-
Monocytes	0,0966	-	no	-	-	-

Analysis of stem and progenitor cells within the BM

	Kruskal Wallis test	Bonferroni correction	Significant	Dunn's multiple comparison		
				Δ/Δ vs Δ/wt	Δ/Δ vs fl/fl	Δ/wt vs fl/fl
MP	0,0627	-	no	-	-	-
LSK	0,0545	-	no	-	-	-
LT-HSC	0,03	-	**yes**	> 0,9999	0,0931	0,0725
ST-HSC	0,436	-	no	-	-	-

Analysis of colony forming units (CFU) assessed after culturing BM cells in methylcellulose-based medium

	Kruskal Wallis test	Bonferroni correction	Significant	Dunn's multiple comparison		
				Δ/Δ vs Δ/wt	Δ/Δ vs fl/fl	Δ/wt vs fl/fl
total	0,2821	-	no	-	-	-
CFU-GM	0,5071	-	no	-	-	-
CFU-GM	0,25	-	no	-	-	-
CFU-M	0,225	-	no	-	-	-
CFU-E	0,6786	-	no	-	-	-

Analysis of niche composition

	Kruskal Wallis test	Bonferroni correction	Significant	Dunn's multiple comparison		
				Δ/Δ vs Δ/wt	Δ/Δ vs fl/fl	Δ/wt vs fl/fl
EC	0,8786	-	no	-	-	-
OBC	0,9929	-	no	-	-	-
MSC	0,8286	-	no	-	-	-

CFU-F per 100 input-MSCs

	Kruskal Wallis test	Bonferroni correction	Significant	Dunn's multiple comparison		
				Δ/Δ vs Δ/wt	Δ/Δ vs fl/fl	Δ/wt vs fl/fl
CFU-F	0,7081	-	no	-	-	-

Investigation of spontanious differentiation of MSCs by early osteogenic and adipogenic marker

	Kruskal Wallis test	Bonferroni correction	Significant	Dunn's multiple comparison		
				Δ/Δ vs Δ/wt	Δ/Δ vs fl/fl	Δ/wt vs fl/fl

RUNX1	0,6643	-	no	-	-	-
PPARG	0,8786	-	no	-	-	-

7 References

Abdel-Wahab, O., Adli, M., LaFave, L.M., Gao, J., Hricik, T., Shih, A.H., Pandey, S., Patel, J.P., Chung, Y.R., Koche, R., Perna, F., Zhao, X., Taylor, J.E., Park, C.Y., Carroll, M., Melnick, A., Nimer, S.D., Jaffe, J.D., Aifantis, I., Bernstein, B.E., and Levine, R.L. (2012). ASXL1 mutations promote myeloid transformation through loss of PRC2-mediated gene repression. Cancer Cell *22*, 180-193. 10.1016/j.ccr.2012.06.032.

Abdel-Wahab, O., Gao, J., Adli, M., Dey, A., Trimarchi, T., Chung, Y.R., Kuscu, C., Hricik, T., Ndiaye-Lobry, D., Lafave, L.M., Koche, R., Shih, A.H., Guryanova, O.A., Kim, E., Li, S., Pandey, S., Shin, J.Y., Telis, L., Liu, J., Bhatt, P.K., Monette, S., Zhao, X., Mason, C.E., Park, C.Y., Bernstein, B.E., Aifantis, I., and Levine, R.L. (2013). Deletion of Asxl1 results in myelodysplasia and severe developmental defects in vivo. J Exp Med *210*, 2641-2659. 10.1084/jem.20131141.

Adolfsson, J., Månsson, R., Buza-Vidas, N., Hultquist, A., Liuba, K., Jensen, C.T., Bryder, D., Yang, L., Borge, O.J., Thoren, L.A., Anderson, K., Sitnicka, E., Sasaki, Y., Sigvardsson, M., and Jacobsen, S.E. (2005). Identification of Flt3+ lympho-myeloid stem cells lacking erythro-megakaryocytic potential a revised road map for adult blood lineage commitment. Cell *121*, 295-306. 10.1016/j.cell.2005.02.013.

Agency, E.M. (1995). ICH Q2 (R1) Validation of analytical procedures: text and methodology.

Akashi, K., Traver, D., Miyamoto, T., and Weissman, I.L. (2000). A clonogenic common myeloid progenitor that gives rise to all myeloid lineages. Nature *404*, 193-197. 10.1038/35004599.

Arber, D.A., Orazi, A., Hasserjian, R., Thiele, J., Borowitz, M.J., Le Beau, M.M., Bloomfield, C.D., Cazzola, M., and Vardiman, J.W. (2016). The 2016 revision to the World Health Organization classification of myeloid neoplasms and acute leukemia. Blood *127*, 2391-2405. 10.1182/blood-2016-03-643544.

Asada, N., Takeishi, S., and Frenette, P.S. (2017). Complexity of bone marrow hematopoietic stem cell niche. Int J Hematol *106*, 45-54. 10.1007/s12185-017-2262-9.

Asada, S., Goyama, S., Inoue, D., Shikata, S., Takeda, R., Fukushima, T., Yonezawa, T., Fujino, T., Hayashi, Y., Kawabata, K.C., Fukuyama, T., Tanaka, Y., Yokoyama, A., Yamazaki, S., Kozuka-Hata, H., Oyama, M., Kojima, S., Kawazu, M., Mano, H., and Kitamura, T. (2018). Mutant ASXL1 cooperates with BAP1 to promote myeloid leukaemogenesis. Nat Commun *9*, 2733. 10.1038/s41467-018-05085-9.

Bast, L., Buck, M.C., Hecker, J.S., Oostendorp, R.A.J., Götze, K.S., and Marr, C. (2021). Computational modeling of stem and progenitor cell kinetics identifies plausible hematopoietic lineage hierarchies. iScience *24*, 102120. 10.1016/j.isci.2021.102120.

Beerman, I., Bhattacharya, D., Zandi, S., Sigvardsson, M., Weissman, I.L., Bryder, D., and Rossi, D.J. (2010). Functionally distinct hematopoietic stem cells modulate hematopoietic lineage

potential during aging by a mechanism of clonal expansion. Proc Natl Acad Sci U S A *107*, 5465-5470. 10.1073/pnas.1000834107.

Bejar, R., Stevenson, K., Abdel-Wahab, O., Galili, N., Nilsson, B., Garcia-Manero, G., Kantarjian, H., Raza, A., Levine, R.L., Neuberg, D., and Ebert, B.L. (2011). Clinical effect of point mutations in myelodysplastic syndromes. N Engl J Med *364*, 2496-2506. 10.1056/NEJMoa1013343.

Birbrair, A., and Frenette, P.S. (2016). Niche heterogeneity in the bone marrow. Ann N Y Acad Sci *1370*, 82-96. 10.1111/nyas.13016.

Bonnet, D. (2002). Haematopoietic stem cells. J Pathol *197*, 430-440. 10.1002/path.1153.

Carbuccia, N., Murati, A., Trouplin, V., Brecqueville, M., Adélaïde, J., Rey, J., Vainchenker, W., Bernard, O.A., Chaffanet, M., Vey, N., Birnbaum, D., and Mozziconacci, M.J. (2009). Mutations of ASXL1 gene in myeloproliferative neoplasms. Leukemia *23*, 2183-2186. 10.1038/leu.2009.141.

Challen, G.A., Boles, N.C., Chambers, S.M., and Goodell, M.A. (2010). Distinct hematopoietic stem cell subtypes are differentially regulated by TGF-beta1. Cell Stem Cell *6*, 265-278. 10.1016/j.stem.2010.02.002.

Chen, J., Kao, Y.R., Sun, D., Todorova, T.I., Reynolds, D., Narayanagari, S.R., Montagna, C., Will, B., Verma, A., and Steidl, U. (2019). Myelodysplastic syndrome progression to acute myeloid leukemia at the stem cell level. Nat Med *25*, 103-110. 10.1038/s41591-018-0267-4.

Cordeiro-Spinetti, E., Taichman, R.S., and Balduino, A. (2015). The bone marrow endosteal niche: how far from the surface? J Cell Biochem *116*, 6-11. 10.1002/jcb.24952.

de Haan, G., and Van Zant, G. (1999). Dynamic changes in mouse hematopoietic stem cell numbers during aging. Blood *93*, 3294-3301.

Dolatshad, H., Pellagatti, A., Fernandez-Mercado, M., Yip, B.H., Malcovati, L., Attwood, M., Przychodzen, B., Sahgal, N., Kanapin, A.A., Lockstone, H., Scifo, L., Vandenberghe, P., Papaemmanuil, E., Smith, C.W., Campbell, P.J., Ogawa, S., Maciejewski, J.P., Cazzola, M., Savage, K.I., and Boultwood, J. (2015). Disruption of SF3B1 results in deregulated expression and splicing of key genes and pathways in myelodysplastic syndrome hematopoietic stem and progenitor cells. Leukemia *29*, 1092-1103. 10.1038/leu.2014.331.

Dongle, T.D. (2016). How to Use FlowJo's Script Editor with Index Sorted Data. https://flowjo.typepad.com/the_daily_dongle/2016/12/how-to-use-flowjos-script-editor-with-index-sorted-data.html

Doulatov, S., Notta, F., Eppert, K., Nguyen, L.T., Ohashi, P.S., and Dick, J.E. (2010). Revised map of the human progenitor hierarchy shows the origin of macrophages and dendritic cells in early lymphoid development. Nat Immunol *11*, 585-593. 10.1038/ni.1889.

Doulatov, S., Notta, F., Laurenti, E., and Dick, J.E. (2012). Hematopoiesis: a human perspective. Cell Stem Cell *10*, 120-136. 10.1016/j.stem.2012.01.006.

Dykstra, B., Olthof, S., Schreuder, J., Ritsema, M., and de Haan, G. (2011). Clonal analysis reveals multiple functional defects of aged murine hematopoietic stem cells. J Exp Med *208*, 2691-2703. 10.1084/jem.20111490.

Ergen, A.V., Boles, N.C., and Goodell, M.A. (2012). Rantes/Ccl5 influences hematopoietic stem cell subtypes and causes myeloid skewing. Blood *119*, 2500-2509. 10.1182/blood-2011-11-391730.

Fischbach, N.A., Rozenfeld, S., Shen, W., Fong, S., Chrobak, D., Ginzinger, D., Kogan, S.C., Radhakrishnan, A., Le Beau, M.M., Largman, C., and Lawrence, H.J. (2005). HOXB6 overexpression in murine bone marrow immortalizes a myelomonocytic precursor in vitro and causes hematopoietic stem cell expansion and acute myeloid leukemia in vivo. Blood *105*, 1456-1466. 10.1182/blood-2004-04-1583.

Fisher, C.L., Pineault, N., Brookes, C., Helgason, C.D., Ohta, H., Bodner, C., Hess, J.L., Humphries, R.K., and Brock, H.W. (2010). Loss-of-function Additional sex combs like 1 mutations disrupt hematopoiesis but do not cause severe myelodysplasia or leukemia. Blood *115*, 38-46. 10.1182/blood-2009-07-230698.

Florian, M.C., Dörr, K., Niebel, A., Daria, D., Schrezenmeier, H., Rojewski, M., Filippi, M.D., Hasenberg, A., Gunzer, M., Scharffetter-Kochanek, K., Zheng, Y., and Geiger, H. (2012). CDC42 ACTIVITY REGULATES HEMATOPOIETIC STEM CELL AGING AND REJUVENATION. Cell Stem Cell *10*, 520-530. 10.1016/j.stem.2012.04.007.

Florian, M.C., and Geiger, H. (2010). Concise review: polarity in stem cells, disease, and aging. Stem Cells *28*, 1623-1629. 10.1002/stem.481.

Florian, M.C., Klose, M., Sacma, M., Jablanovic, J., Knudson, L., Nattamai, K.J., Marka, G., Vollmer, A., Soller, K., Sakk, V., Cabezas-Wallscheid, N., Zheng, Y., Mulaw, M.A., Glauche, I., and Geiger, H. (2018). Aging alters the epigenetic asymmetry of HSC division. PLoS Biol *16*, e2003389. 10.1371/journal.pbio.2003389.

Forsberg, E.C., Serwold, T., Kogan, S., Weissman, I.L., and Passegué, E. (2006). New evidence supporting megakaryocyte-erythrocyte potential of flk2/flt3+ multipotent hematopoietic progenitors. Cell *126*, 415-426. 10.1016/j.cell.2006.06.037.

Frelin, C., Herrington, R., Janmohamed, S., Barbara, M., Tran, G., Paige, C.J., Benveniste, P., Zuniga-Pflucker, J.C., Souabni, A., Busslinger, M., and Iscove, N.N. (2013). GATA-3 regulates the self-renewal of long-term hematopoietic stem cells. Nat Immunol *14*, 1037-1044. 10.1038/ni.2692.

Geiger, H., de Haan, G., and Florian, M.C. (2013). The ageing haematopoietic stem cell compartment. Nat Rev Immunol *13*, 376-389. 10.1038/nri3433.

Germing, U., Kobbe, G., Haas, R., and Gattermann, N. (2013). Myelodysplastic syndromes: diagnosis, prognosis, and treatment. Dtsch Arztebl Int *110*, 783-790. 10.3238/arztebl.2013.0783.

Geyh, S., Oz, S., Cadeddu, R.P., Fröbel, J., Brückner, B., Kündgen, A., Fenk, R., Bruns, I., Zilkens, C., Hermsen, D., Gattermann, N., Kobbe, G., Germing, U., Lyko, F., Haas, R., and Schroeder, T. (2013). Insufficient stromal support in MDS results from molecular and functional deficits of mesenchymal stromal cells. Leukemia *27*, 1841-1851. 10.1038/leu.2013.193.

Giebel, B. (2008). Cell polarity and asymmetric cell division within human hematopoietic stem and progenitor cells. Cells Tissues Organs *188*, 116-126. 10.1159/000112842.

Giebel, B., and Bruns, I. (2008). Self-renewal versus differentiation in hematopoietic stem and progenitor cells: a focus on asymmetric cell divisions. Curr Stem Cell Res Ther *3*, 9-16. 10.2174/157488808783489444.

Golas, M.M., Sander, B., Will, C.L., Lührmann, R., and Stark, H. (2003). Molecular architecture of the multiprotein splicing factor SF3b. Science *300*, 980-984. 10.1126/science.1084155.

Goncalves, K.A., Silberstein, L., Li, S., Severe, N., Hu, M.G., Yang, H., Scadden, D.T., and Hu, G.F. (2016). Angiogenin Promotes Hematopoietic Regeneration by Dichotomously Regulating Quiescence of Stem and Progenitor Cells. Cell *166*, 894-906. 10.1016/j.cell.2016.06.042.

Gondek, L.P., Zheng, G., Ghiaur, G., DeZern, A.E., Matsui, W., Yegnasubramanian, S., Lin, M.T., Levis, M., Eshleman, J.R., Varadhan, R., Tucker, N., Jones, R., and Gocke, C.D. (2016). Donor cell leukemia arising from clonal hematopoiesis after bone marrow transplantation. Leukemia *30*, 1916-1920. 10.1038/leu.2016.63.

Greenberg, P.L., Tuechler, H., Schanz, J., Sanz, G., Garcia-Manero, G., Solé, F., Bennett, J.M., Bowen, D., Fenaux, P., Dreyfus, F., Kantarjian, H., Kuendgen, A., Levis, A., Malcovati, L., Cazzola, M., Cermak, J., Fonatsch, C., Le Beau, M.M., Slovak, M.L., Krieger, O., Luebbert, M., Maciejewski, J., Magalhaes, S.M., Miyazaki, Y., Pfeilstöcker, M., Sekeres, M., Sperr, W.R., Stauder, R., Tauro, S., Valent, P., Vallespi, T., van de Loosdrecht, A.A., Germing, U., and Haase, D. (2012). Revised international prognostic scoring system for myelodysplastic syndromes. Blood *120*, 2454-2465. 10.1182/blood-2012-03-420489.

Guidi, N., Sacma, M., Ständker, L., Soller, K., Marka, G., Eiwen, K., Weiss, J.M., Kirchhoff, F., Weil, T., Cancelas, J.A., Florian, M.C., and Geiger, H. (2017). Osteopontin attenuates aging-associated phenotypes of hematopoietic stem cells. Embo j *36*, 1463. 10.15252/embj.201796968.

Haas, S., Trumpp, A., and Milsom, M.D. (2018). Causes and Consequences of Hematopoietic Stem Cell Heterogeneity. Cell Stem Cell *22*, 627-638. 10.1016/j.stem.2018.04.003.

Haferlach, T., Nagata, Y., Grossmann, V., Okuno, Y., Bacher, U., Nagae, G., Schnittger, S., Sanada, M., Kon, A., Alpermann, T., Yoshida, K., Roller, A., Nadarajah, N., Shiraishi, Y.,

Shiozawa, Y., Chiba, K., Tanaka, H., Koeffler, H.P., Klein, H.U., Dugas, M., Aburatani, H., Kohlmann, A., Miyano, S., Haferlach, C., Kern, W., and Ogawa, S. (2014). Landscape of genetic lesions in 944 patients with myelodysplastic syndromes. Leukemia *28*, 241-247. 10.1038/leu.2013.336.

Hartsock, R.J., Smith, E.B., and Petty, C.S. (1965). NORMAL VARIATIONS WITH AGING OF THE AMOUNT OF HEMATOPOIETIC TISSUE IN BONE MARROW FROM THE ANTERIOR ILIAC CREST. A STUDY MADE FROM 177 CASES OF SUDDEN DEATH EXAMINED BY NECROPSY. Am J Clin Pathol *43*, 326-331. 10.1093/ajcp/43.4.326.

Hecker, J.S., Hartmann, L., Rivière, J., Buck, M.C., van der Garde, M., Rothenberg-Thurley, M., Fischer, L., Winter, S., Ksienzyk, B., Ziemann, F., Solovey, M., Rauner, M., Tsourdi, E., Sockel, K., Schneider, M., Kubasch, A.S., Nolde, M., Hausmann, D., Paulus, A.C., Lützner, J., Roth, A., Bassermann, F., Spiekermann, K., Marr, C., Hofbauer, L.C., Platzbecker, U., Metzeler, K.H., and Götze, K.S. (2021). CHIP & HIPs: Clonal Hematopoiesis is Common in Hip Arthroplasty Patients and Associates with Autoimmune Disease. Blood. 10.1182/blood.2020010163.

Hoggatt, J., Mohammad, K.S., Singh, P., Hoggatt, A.F., Chitteti, B.R., Speth, J.M., Hu, P., Poteat, B.A., Stilger, K.N., Ferraro, F., Silberstein, L., Wong, F.K., Farag, S.S., Czader, M., Milne, G.L., Breyer, R.M., Serezani, C.H., Scadden, D.T., Guise, T.A., Srour, E.F., and Pelus, L.M. (2013). Differential stem- and progenitor-cell trafficking by prostaglandin E2. Nature *495*, 365-369. 10.1038/nature11929.

Hsu, Y.C., Chiu, Y.C., Lin, C.C., Kuo, Y.Y., Hou, H.A., Tzeng, Y.S., Kao, C.J., Chuang, P.H., Tseng, M.H., Hsiao, T.H., Chou, W.C., and Tien, H.F. (2017). The distinct biological implications of Asxl1 mutation and its roles in leukemogenesis revealed by a knock-in mouse model. J Hematol Oncol *10*, 139. 10.1186/s13045-017-0508-x.

Ikonomi, N., Kühlwein, S.D., Schwab, J.D., and Kestler, H.A. (2020). Awakening the HSC: Dynamic Modeling of HSC Maintenance Unravels Regulation of the TP53 Pathway and Quiescence. Front Physiol *11*, 848. 10.3389/fphys.2020.00848.

Inoue, D., Matsumoto, M., Nagase, R., Saika, M., Fujino, T., Nakayama, K.I., and Kitamura, T. (2016). Truncation mutants of ASXL1 observed in myeloid malignancies are expressed at detectable protein levels. Exp Hematol *44*, 172-176.e171. 10.1016/j.exphem.2015.11.011.

Ito, K., and Suda, T. (2014). Metabolic requirements for the maintenance of self-renewing stem cells. Nat Rev Mol Cell Biol *15*, 243-256. 10.1038/nrm3772.

Jaiswal, S., Fontanillas, P., Flannick, J., Manning, A., Grauman, P.V., Mar, B.G., Lindsley, R.C., Mermel, C.H., Burtt, N., Chavez, A., Higgins, J.M., Moltchanov, V., Kuo, F.C., Kluk, M.J., Henderson, B., Kinnunen, L., Koistinen, H.A., Ladenvall, C., Getz, G., Correa, A., Banahan, B.F., Gabriel, S., Kathiresan, S., Stringham, H.M., McCarthy, M.I., Boehnke, M., Tuomilehto, J., Haiman, C., Groop, L., Atzmon, G., Wilson, J.G., Neuberg, D., Altshuler, D., and Ebert, B.L. (2014). Age-related clonal hematopoiesis associated with adverse outcomes. N Engl J Med *371*, 2488-2498. 10.1056/NEJMoa1408617.

Kataoka, K., Sato, T., Yoshimi, A., Goyama, S., Tsuruta, T., Kobayashi, H., Shimabe, M., Arai, S., Nakagawa, M., Imai, Y., Kumano, K., Kumagai, K., Kubota, N., Kadowaki, T., and Kurokawa, M. (2011). Evi1 is essential for hematopoietic stem cell self-renewal, and its expression marks hematopoietic cells with long-term multilineage repopulating activity. J Exp Med *208*, 2403-2416. 10.1084/jem.20110447.

Kiel, M.J., Yilmaz, O.H., Iwashita, T., Yilmaz, O.H., Terhorst, C., and Morrison, S.J. (2005). SLAM family receptors distinguish hematopoietic stem and progenitor cells and reveal endothelial niches for stem cells. Cell *121*, 1109-1121. 10.1016/j.cell.2005.05.026.

Kode, A., Manavalan, J.S., Mosialou, I., Bhagat, G., Rathinam, C.V., Luo, N., Khiabanian, H., Lee, A., Murty, V.V., Friedman, R., Brum, A., Park, D., Galili, N., Mukherjee, S., Teruya-Feldstein, J., Raza, A., Rabadan, R., Berman, E., and Kousteni, S. (2014). Leukaemogenesis induced by an activating β-catenin mutation in osteoblasts. Nature *506*, 240-244. 10.1038/nature12883.

Kuranda, K., Vargaftig, J., de la Rochere, P., Dosquet, C., Charron, D., Bardin, F., Tonnelle, C., Bonnet, D., and Goodhardt, M. (2011). Age-related changes in human hematopoietic stem/progenitor cells. Aging Cell *10*, 542-546. 10.1111/j.1474-9726.2011.00675.x.

Laurenti, E., and Göttgens, B. (2018). From haematopoietic stem cells to complex differentiation landscapes. Nature *553*, 418-426. 10.1038/nature25022.

Li, Z., Zhang, P., Yan, A., Guo, Z., Ban, Y., Li, J., Chen, S., Yang, H., He, Y., Li, J., Guo, Y., Zhang, W., Hajiramezanali, E., An, H., Fajardo, D., Harbour, J.W., Ruan, Y., Nimer, S.D., Yu, P., Chen, X., Xu, M., and Yang, F.C. (2017). ASXL1 interacts with the cohesin complex to maintain chromatid separation and gene expression for normal hematopoiesis. Sci Adv *3*, e1601602. 10.1126/sciadv.1601602.

Majeti, R., Park, C.Y., and Weissman, I.L. (2007). Identification of a hierarchy of multipotent hematopoietic progenitors in human cord blood. Cell Stem Cell *1*, 635-645. 10.1016/j.stem.2007.10.001.

Månsson, R., Hultquist, A., Luc, S., Yang, L., Anderson, K., Kharazi, S., Al-Hashmi, S., Liuba, K., Thorén, L., Adolfsson, J., Buza-Vidas, N., Qian, H., Soneji, S., Enver, T., Sigvardsson, M., and Jacobsen, S.E. (2007). Molecular evidence for hierarchical transcriptional lineage priming in fetal and adult stem cells and multipotent progenitors. Immunity *26*, 407-419. 10.1016/j.immuni.2007.02.013.

Manz, M.G., Miyamoto, T., Akashi, K., and Weissman, I.L. (2002). Prospective isolation of human clonogenic common myeloid progenitors. Proc Natl Acad Sci U S A *99*, 11872-11877. 10.1073/pnas.172384399.

Maryanovich, M., Zahalka, A.H., Pierce, H., Pinho, S., Nakahara, F., Asada, N., Wei, Q., Wang, X., Ciero, P., Xu, J., Leftin, A., and Frenette, P.S. (2018). Adrenergic nerve degeneration in bone marrow drives aging of the hematopoietic stem cell niche. Nat Med *24*, 782-791. 10.1038/s41591-018-0030-x.

Morita, Y., Ema, H., and Nakauchi, H. (2010). Heterogeneity and hierarchy within the most primitive hematopoietic stem cell compartment. J Exp Med *207*, 1173-1182. 10.1084/jem.20091318.

Mossner, M., Jann, J.C., Wittig, J., Nolte, F., Fey, S., Nowak, V., Obländer, J., Pressler, J., Palme, I., Xanthopoulos, C., Boch, T., Metzgeroth, G., Röhl, H., Witt, S.H., Dukal, H., Klein, C., Schmitt, S., Gelß, P., Platzbecker, U., Balaian, E., Fabarius, A., Blum, H., Schulze, T.J., Meggendorfer, M., Haferlach, C., Trumpp, A., Hofmann, W.K., Medyouf, H., and Nowak, D. (2016). Mutational hierarchies in myelodysplastic syndromes dynamically adapt and evolve upon therapy response and failure. Blood *128*, 1246-1259. 10.1182/blood-2015-11-679167.

Muller-Sieburg, C.E., and Sieburg, H.B. (2006). Clonal diversity of the stem cell compartment. Curr Opin Hematol *13*, 243-248. 10.1097/01.moh.0000231421.00407.65.

Nimmo, R.A., May, G.E., and Enver, T. (2015). Primed and ready: understanding lineage commitment through single cell analysis. Trends Cell Biol *25*, 459-467. 10.1016/j.tcb.2015.04.004.

Notta, F., Zandi, S., Takayama, N., Dobson, S., Gan, O.I., Wilson, G., Kaufmann, K.B., McLeod, J., Laurenti, E., Dunant, C.F., McPherson, J.D., Stein, L.D., Dror, Y., and Dick, J.E. (2016). Distinct routes of lineage development reshape the human blood hierarchy across ontogeny. Science *351*, aab2116. 10.1126/science.aab2116.

Ogawa, S. (2019). Genetics of MDS. Blood *133*, 1049-1059. 10.1182/blood-2018-10-844621.

Ostendorf, B.N., Flenner, E., Florcken, A., and Westermann, J. (2018). Phenotypic characterization of aberrant stem and progenitor cell populations in myelodysplastic syndromes. PLoS One *13*, e0197823. 10.1371/journal.pone.0197823.

Pang, W.W., Pluvinage, J.V., Price, E.A., Sridhar, K., Arber, D.A., Greenberg, P.L., Schrier, S.L., Park, C.Y., and Weissman, I.L. (2013). Hematopoietic stem cell and progenitor cell mechanisms in myelodysplastic syndromes. Proc Natl Acad Sci U S A *110*, 3011-3016. 10.1073/pnas.1222861110.

Pang, W.W., Price, E.A., Sahoo, D., Beerman, I., Maloney, W.J., Rossi, D.J., Schrier, S.L., and Weissman, I.L. (2011). Human bone marrow hematopoietic stem cells are increased in frequency and myeloid-biased with age. Proc Natl Acad Sci U S A *108*, 20012-20017. 10.1073/pnas.1116110108.

Papaemmanuil, E., Cazzola, M., Boultwood, J., Malcovati, L., Vyas, P., Bowen, D., Pellagatti, A., Wainscoat, J.S., Hellstrom-Lindberg, E., Gambacorti-Passerini, C., Godfrey, A.L., Rapado, I., Cvejic, A., Rance, R., McGee, C., Ellis, P., Mudie, L.J., Stephens, P.J., McLaren, S., Massie, C.E., Tarpey, P.S., Varela, I., Nik-Zainal, S., Davies, H.R., Shlien, A., Jones, D., Raine, K., Hinton, J., Butler, A.P., Teague, J.W., Baxter, E.J., Score, J., Galli, A., Della Porta, M.G., Travaglino, E., Groves, M., Tauro, S., Munshi, N.C., Anderson, K.C., El-Naggar, A., Fischer, A., Mustonen, V., Warren, A.J., Cross, N.C., Green, A.R., Futreal, P.A., Stratton, M.R., and Campbell, P.J. (2011).

Somatic SF3B1 mutation in myelodysplasia with ring sideroblasts. N Engl J Med *365*, 1384-1395. 10.1056/NEJMoa1103283.

Papaemmanuil, E., Gerstung, M., Malcovati, L., Tauro, S., Gundem, G., Van Loo, P., Yoon, C.J., Ellis, P., Wedge, D.C., Pellagatti, A., Shlien, A., Groves, M.J., Forbes, S.A., Raine, K., Hinton, J., Mudie, L.J., McLaren, S., Hardy, C., Latimer, C., Della Porta, M.G., O'Meara, S., Ambaglio, I., Galli, A., Butler, A.P., Walldin, G., Teague, J.W., Quek, L., Sternberg, A., Gambacorti-Passerini, C., Cross, N.C., Green, A.R., Boultwood, J., Vyas, P., Hellstrom-Lindberg, E., Bowen, D., Cazzola, M., Stratton, M.R., and Campbell, P.J. (2013). Clinical and biological implications of driver mutations in myelodysplastic syndromes. Blood *122*, 3616-3627; quiz 3699. 10.1182/blood-2013-08-518886.

Passegué, E., Wagers, A.J., Giuriato, S., Anderson, W.C., and Weissman, I.L. (2005). Global analysis of proliferation and cell cycle gene expression in the regulation of hematopoietic stem and progenitor cell fates. J Exp Med *202*, 1599-1611. 10.1084/jem.20050967.

Pellin, D., Loperfido, M., Baricordi, C., Wolock, S.L., Montepeloso, A., Weinberg, O.K., Biffi, A., Klein, A.M., and Biasco, L. (2019). A comprehensive single cell transcriptional landscape of human hematopoietic progenitors. Nat Commun *10*, 2395. 10.1038/s41467-019-10291-0.

Pleyer, L., Valent, P., and Greil, R. (2016). Mesenchymal Stem and Progenitor Cells in Normal and Dysplastic Hematopoiesis-Masters of Survival and Clonality? Int J Mol Sci *17*. 10.3390/ijms17071009.

Povsic, T.J., Zhou, J., Adams, S.D., Bolognesi, M.P., Attarian, D.E., and Peterson, E.D. (2010). Aging is not associated with bone marrow-resident progenitor cell depletion. J Gerontol A Biol Sci Med Sci *65*, 1042-1050. 10.1093/gerona/glq110.

Raaijmakers, M.H., Mukherjee, S., Guo, S., Zhang, S., Kobayashi, T., Schoonmaker, J.A., Ebert, B.L., Al-Shahrour, F., Hasserjian, R.P., Scadden, E.O., Aung, Z., Matza, M., Merkenschlager, M., Lin, C., Rommens, J.M., and Scadden, D.T. (2010). Bone progenitor dysfunction induces myelodysplasia and secondary leukaemia. Nature *464*, 852-857. 10.1038/nature08851.

Rojek, K., Nickels, E., Neistadt, B., Marquez, R., Wickrema, A., Artz, A., van Besien, K., Larson, R.A., Lee, M.K., Segal, J.P., King, M.C., Walsh, T., Shimamura, A., Keel, S.B., Churpek, J.E., and Godley, L.A. (2016). Identifying Inherited and Acquired Genetic Factors Involved in Poor Stem Cell Mobilization and Donor-Derived Malignancy. Biol Blood Marrow Transplant *22*, 2100-2103. 10.1016/j.bbmt.2016.08.002.

Rossi, D.J., Bryder, D., Zahn, J.M., Ahlenius, H., Sonu, R., Wagers, A.J., and Weissman, I.L. (2005). Cell intrinsic alterations underlie hematopoietic stem cell aging. Proc Natl Acad Sci U S A *102*, 9194-9199. 10.1073/pnas.0503280102.

Rothenberg-Thurley, M., Amler, S., Goerlich, D., Kohnke, T., Konstandin, N.P., Schneider, S., Sauerland, M.C., Herold, T., Hubmann, M., Ksienzyk, B., Zellmeier, E., Bohlander, S.K., Subklewe, M., Faldum, A., Hiddemann, W., Braess, J., Spiekermann, K., and Metzeler, K.H.

(2017). Persistence of pre-leukemic clones during first remission and risk of relapse in acute myeloid leukemia. Leukemia. 10.1038/leu.2017.350.

Rundberg Nilsson, A., Soneji, S., Adolfsson, S., Bryder, D., and Pronk, C.J. (2016). Human and Murine Hematopoietic Stem Cell Aging Is Associated with Functional Impairments and Intrinsic Megakaryocytic/Erythroid Bias. PLoS One *11*, e0158369. 10.1371/journal.pone.0158369.

Sanjuan-Pla, A., Macaulay, I.C., Jensen, C.T., Woll, P.S., Luis, T.C., Mead, A., Moore, S., Carella, C., Matsuoka, S., Bouriez Jones, T., Chowdhury, O., Stenson, L., Lutteropp, M., Green, J.C., Facchini, R., Boukarabila, H., Grover, A., Gambardella, A., Thongjuea, S., Carrelha, J., Tarrant, P., Atkinson, D., Clark, S.A., Nerlov, C., and Jacobsen, S.E. (2013). Platelet-biased stem cells reside at the apex of the haematopoietic stem-cell hierarchy. Nature *502*, 232-236. 10.1038/nature12495.

Schemenau, J., Baldus, S., Anlauf, M., Reinecke, P., Braunstein, S., Blum, S., Nachtkamp, K., Neukirchen, J., Strup, C., Aul, C., Haas, R., Gattermann, N., and Germing, U. (2015). Cellularity, characteristics of hematopoietic parameters and prognosis in myelodysplastic syndromes. Eur J Haematol *95*, 181-189. 10.1111/ejh.12512.

Schnittger, S., Eder, C., Jeromin, S., Alpermann, T., Fasan, A., Grossmann, V., Kohlmann, A., Illig, T., Klopp, N., Wichmann, H.E., Kreuzer, K.A., Schmid, C., Staib, P., Peceny, R., Schmitz, N., Kern, W., Haferlach, C., and Haferlach, T. (2013). ASXL1 exon 12 mutations are frequent in AML with intermediate risk karyotype and are independently associated with an adverse outcome. Leukemia *27*, 82-91. 10.1038/leu.2012.262.

Schroeder, T. (2007). Asymmetric cell division in normal and malignant hematopoietic precursor cells. Cell Stem Cell *1*, 479-481. 10.1016/j.stem.2007.10.016.

Shastri, A., Will, B., Steidl, U., and Verma, A. (2017). Stem and progenitor cell alterations in myelodysplastic syndromes. Blood *129*, 1586-1594. 10.1182/blood-2016-10-696062.

Shojaei, F., Trowbridge, J., Gallacher, L., Yuefei, L., Goodale, D., Karanu, F., Levac, K., and Bhatia, M. (2005). Hierarchical and ontogenic positions serve to define the molecular basis of human hematopoietic stem cell behavior. Dev Cell *8*, 651-663. 10.1016/j.devcel.2005.03.004.

Silver, A.J., and Jaiswal, S. (2019). Clonal hematopoiesis: Pre-cancer PLUS. Adv Cancer Res *141*, 85-128. 10.1016/bs.acr.2018.12.003.

Steensma, D.P., Bejar, R., Jaiswal, S., Lindsley, R.C., Sekeres, M.A., Hasserjian, R.P., and Ebert, B.L. (2015). Clonal hematopoiesis of indeterminate potential and its distinction from myelodysplastic syndromes. Blood *126*, 9-16. 10.1182/blood-2015-03-631747.

Takano, H., Ema, H., Sudo, K., and Nakauchi, H. (2004). Asymmetric division and lineage commitment at the level of hematopoietic stem cells: inference from differentiation in daughter cell and granddaughter cell pairs. J Exp Med *199*, 295-302. 10.1084/jem.20030929.

Taraldsrud, E., Grogaard, H.K., Solheim, S., Lunde, K., Floisand, Y., Arnesen, H., Seljeflot, I., and Egeland, T. (2009). Age and stress related phenotypical changes in bone marrow CD34+ cells. Scand J Clin Lab Invest *69*, 79-84. 10.1080/00365510802419447.

Thomas, W., Haedrich, J., Alexander, S., Piotr, R., and Joerg, S. (2016). Guidance Document on the Estimation of LOD and LOQ for Measurements in the Field of Contaminants in Feed and Food. Publications Office of the European Union. 10.2787/8931.

Uni, M., Masamoto, Y., Sato, T., Kamikubo, Y., Arai, S., Hara, E., and Kurokawa, M. (2019). Modeling ASXL1 mutation revealed impaired hematopoiesis caused by derepression of p16Ink4a through aberrant PRC1-mediated histone modification. Leukemia *33*, 191-204. 10.1038/s41375-018-0198-6.

Velten, L., Haas, S.F., Raffel, S., Blaszkiewicz, S., Islam, S., Hennig, B.P., Hirche, C., Lutz, C., Buss, E.C., Nowak, D., Boch, T., Hofmann, W.K., Ho, A.D., Huber, W., Trumpp, A., Essers, M.A., and Steinmetz, L.M. (2017). Human haematopoietic stem cell lineage commitment is a continuous process. Nat Cell Biol *19*, 271-281. 10.1038/ncb3493.

Velten, L., Story, B.A., Hernández-Malmierca, P., Raffel, S., Leonce, D.R., Milbank, J., Paulsen, M., Demir, A., Szu-Tu, C., Frömel, R., Lutz, C., Nowak, D., Jann, J.C., Pabst, C., Boch, T., Hofmann, W.K., Müller-Tidow, C., Trumpp, A., Haas, S., and Steinmetz, L.M. (2021). Identification of leukemic and pre-leukemic stem cells by clonal tracking from single-cell transcriptomics. Nat Commun *12*, 1366. 10.1038/s41467-021-21650-1.

Walter, D., Lier, A., Geiselhart, A., Thalheimer, F.B., Huntscha, S., Sobotta, M.C., Moehrle, B., Brocks, D., Bayindir, I., Kaschutnig, P., Muedder, K., Klein, C., Jauch, A., Schroeder, T., Geiger, H., Dick, T.P., Holland-Letz, T., Schmezer, P., Lane, S.W., Rieger, M.A., Essers, M.A., Williams, D.A., Trumpp, A., and Milsom, M.D. (2015). Exit from dormancy provokes DNA-damage-induced attrition in haematopoietic stem cells. Nature *520*, 549-552. 10.1038/nature14131.

Walter, M.J., Shen, D., Ding, L., Shao, J., Koboldt, D.C., Chen, K., Larson, D.E., McLellan, M.D., Dooling, D., Abbott, R., Fulton, R., Magrini, V., Schmidt, H., Kalicki-Veizer, J., O'Laughlin, M., Fan, X., Grillot, M., Witowski, S., Heath, S., Frater, J.L., Eades, W., Tomasson, M., Westervelt, P., DiPersio, J.F., Link, D.C., Mardis, E.R., Ley, T.J., Wilson, R.K., and Graubert, T.A. (2012). Clonal architecture of secondary acute myeloid leukemia. N Engl J Med *366*, 1090-1098. 10.1056/NEJMoa1106968.

Wang, J., Li, Z., He, Y., Pan, F., Chen, S., Rhodes, S., Nguyen, L., Yuan, J., Jiang, L., Yang, X., Weeks, O., Liu, Z., Zhou, J., Ni, H., Cai, C.L., Xu, M., and Yang, F.C. (2014). Loss of Asxl1 leads to myelodysplastic syndrome-like disease in mice. Blood *123*, 541-553. 10.1182/blood-2013-05-500272.

Watson, C.J., Papula, A.L., Poon, G.Y.P., Wong, W.H., Young, A.L., Druley, T.E., Fisher, D.S., and Blundell, J.R. (2020). The evolutionary dynamics and fitness landscape of clonal hematopoiesis. Science *367*, 1449-1454. 10.1126/science.aay9333.

Weickert, M.T., Hecker, J.S., Buck, M.C., Schreck, C., Rivière, J., Schiemann, M., Schallmoser, K., Bassermann, F., Strunk, D., Oostendorp, R.A.J., and Götze, K.S. (2021). Bone marrow stromal cells from MDS and AML patients show increased adipogenic potential with reduced Delta-like-1 expression. Sci Rep *11*, 5944. 10.1038/s41598-021-85122-8.

Will, B., Zhou, L., Vogler, T.O., Ben-Neriah, S., Schinke, C., Tamari, R., Yu, Y., Bhagat, T.D., Bhattacharyya, S., Barreyro, L., Heuck, C., Mo, Y., Parekh, S., McMahon, C., Pellagatti, A., Boultwood, J., Montagna, C., Silverman, L., Maciejewski, J., Greally, J.M., Ye, B.H., List, A.F., Steidl, C., Steidl, U., and Verma, A. (2012). Stem and progenitor cells in myelodysplastic syndromes show aberrant stage-specific expansion and harbor genetic and epigenetic alterations. Blood *120*, 2076-2086. 10.1182/blood-2011-12-399683.

Williams, N., Lee, J., Moore, L., Baxter, E.J., Hewinson, J., Dawson, K.J., Menzies, A., Godfrey, A.L., Green, A.R., Campbell, P.J., and Nangalia, J. (2020). Phylogenetic reconstruction of myeloproliferative neoplasm reveals very early origins and lifelong evolution. bioRxiv, 2020.2011.2009.374710. 10.1101/2020.11.09.374710.

Wiseman, D.H. (2011). Donor cell leukemia: a review. Biol Blood Marrow Transplant *17*, 771-789. 10.1016/j.bbmt.2010.10.010.

Woll, P.S., Kjällquist, U., Chowdhury, O., Doolittle, H., Wedge, D.C., Thongjuea, S., Erlandsson, R., Ngara, M., Anderson, K., Deng, Q., Mead, A.J., Stenson, L., Giustacchini, A., Duarte, S., Giannoulatou, E., Taylor, S., Karimi, M., Scharenberg, C., Mortera-Blanco, T., Macaulay, I.C., Clark, S.A., Dybedal, I., Josefsen, D., Fenaux, P., Hokland, P., Holm, M.S., Cazzola, M., Malcovati, L., Tauro, S., Bowen, D., Boultwood, J., Pellagatti, A., Pimanda, J.E., Unnikrishnan, A., Vyas, P., Göhring, G., Schlegelberger, B., Tobiasson, M., Kvalheim, G., Constantinescu, S.N., Nerlov, C., Nilsson, L., Campbell, P.J., Sandberg, R., Papaemmanuil, E., Hellström-Lindberg, E., Linnarsson, S., and Jacobsen, S.E. (2014). Myelodysplastic syndromes are propagated by rare and distinct human cancer stem cells in vivo. Cancer Cell *25*, 794-808. 10.1016/j.ccr.2014.03.036.

Wu, M., Kwon, H.Y., Rattis, F., Blum, J., Zhao, C., Ashkenazi, R., Jackson, T.L., Gaiano, N., Oliver, T., and Reya, T. (2007). Imaging hematopoietic precursor division in real time. Cell Stem Cell *1*, 541-554. 10.1016/j.stem.2007.08.009.

Xiao, P., Dolinska, M., Sandhow, L., Kondo, M., Johansson, A.S., Bouderlique, T., Zhao, Y., Li, X., Dimitriou, M., Rassidakis, G.Z., Hellström-Lindberg, E., Minato, N., Walfridsson, J., Scadden, D.T., Sigvardsson, M., and Qian, H. (2018). Sipa1 deficiency-induced bone marrow niche alterations lead to the initiation of myeloproliferative neoplasm. Blood Adv *2*, 534-548. 10.1182/bloodadvances.2017013599.

Yang, H., Kurtenbach, S., Guo, Y., Lohse, I., Durante, M.A., Li, J., Li, Z., Al-Ali, H., Li, L., Chen, Z., Field, M.G., Zhang, P., Chen, S., Yamamoto, S., Li, Z., Zhou, Y., Nimer, S.D., Harbour, J.W., Wahlestedt, C., Xu, M., and Yang, F.C. (2018). Gain of function of ASXL1 truncating protein in the pathogenesis of myeloid malignancies. Blood *131*, 328-341. 10.1182/blood-2017-06-789669.

Zakrzewski, W., Dobrzyński, M., Szymonowicz, M., and Rybak, Z. (2019). Stem cells: past, present, and future. Stem Cell Res Ther *10*, 68. 10.1186/s13287-019-1165-5.

Zhou, Z., Gong, Q., Wang, Y., Li, M., Wang, L., Ding, H., and Li, P. (2020). The biological function and clinical significance of SF3B1 mutations in cancer. Biomark Res *8*, 38. 10.1186/s40364-020-00220-5.

8 List of own Publications

Bast*, L., **Buck*, M.C.**, Hecker, J.S., Oostendorp, R.A.J., Götze*, K.S., and Marr*, C. (2021). Computational modeling of stem and progenitor cell kinetics identifies plausible hematopoietic lineage hierarchies. iScience 24, 102120. 10.1016/j.isci.2021.102120. *shared authorship

Hecker, J.S., Hartmann, L., Rivière, J., **Buck, M.C.**, van der Garde, M., Rothenberg-Thurley, M., Fischer, L., Winter, S., Ksienzyk, B., Ziemann, F., Solovey, M., Rauner, M., Tsourdi, E., Sockel, K., Schneider, M., Kubasch, A.S., Nolde, M., Hausmann, D., Paulus, A.C., Lützner, J., Roth, A., Bassermann, F., Spiekermann, K., Marr, C., Hofbauer, L.C., Platzbecker, U., Metzeler, K.H., and Götze, K.S. (2021). CHIP & HIPs: Clonal Hematopoiesis is Common in Hip Arthroplasty Patients and Associates with Autoimmune Disease. Blood. 10.1182/blood.2020010163.

Kyncl, M., Bast, L., Henkel, L., Theis, F., Oostendorp, R.A.J., Marr, C., and Götze, K.S. (2018). Data Driven Computational Modeling of Hematopoiesis in Myelodysplastic Syndromes Unveils Differences in Hematopoietic Stem Cell Kinetics Compared to Age-Matched Healthy Controls. Blood 132, 4354-4354. 10.1182/blood-2018-99-115942.

Hartmann, S., Zheng, F., **Kyncl, M.C.**, Karch, S., Voelkl, K., Zott, B., D'Avanzo, C., Lomoio, S., Tesco, G., Kim, D.Y., Alzheimer, C., and Huth, T. (2018). β-Secretase BACE1 Promotes Surface Expression and Function of Kv3.4 at Hippocampal Mossy Fiber Synapses. J Neurosci 38, 3480-3494. 10.1523/jneurosci.2643-17.2018.

Landspersky, T., Saçma, M., Rivière, J., Hecker, J.S., Hettler, F., Hameister, E., Brandstetter, K., Istvanffy, R., Romero Marquez, S., Ludwig, R., Götz, M., **Buck, M.C.**, Wolf, M., Schiemann, M., Ruland, J., Strunk, D., Shimamura, A., Myers, K.C., Yamaguchi, T.P., Kieslinger, M., Leonhardt, H., Bassermann, F., Götze, K.S., Geiger, H., Schreck, C., and Oostendorp, R.A.J. (2021). Autophagy In Mesenchymal Progenitors Protects Mice Against Bone Marrow Failure After Severe Intermittent Stress. Blood. 10.1182/blood.2021011775.

Schouten, J.P.E., Matek, C., Jacobs, L.F.P., **Buck, M.C.**, Bošnački, D., and Marr, C. (2021). Tens of images can suffice to train neural networks for malignant leukocyte detection. Sci Rep 11, 7995. 10.1038/s41598-021-86995-5.

Tirado-Gonzalez, I., Descot, A., Soetopo, D., Nevmerzhitskaya, A., Schäffer, A., Kur, I.M., Czlonka, E., Wachtel, C., Tsoukala, I., Müller, L., Schäfer, A.L., Weitmann, M., Dinse, P., Alberto, E., **Buck, M.C.**, Landry, J.J., Baying, B., Slotta-Huspenina, J., Roesler, J., Harter, P.N., Kubasch, A.S., Meinel, J., Elwakeel, E., Strack, E., Quang, C.T., Abdel-Wahab, O., Schmitz, M., Weigert, A., Schmid, T., Platzbecker, U., Benes, V., Ghysdael, J., Bonig, H., Götze, K.S., Rothlin, C.V., Ghosh, S., and Medyouf, H. (2021). AXL Inhibition in Macrophages Stimulates Host-versus-Leukemia Immunity and Eradicates Naïve and Treatment-Resistant Leukemia. Cancer Discov 11, 2924-2943. 10.1158/2159-8290.Cd-20-1378.

Weickert, M.T., Hecker, J.S., **Buck, M.C.**, Schreck, C., Rivière, J., Schiemann, M., Schallmoser, K., Bassermann, F., Strunk, D., Oostendorp, R.A.J., and Götze, K.S. (2021). Bone marrow stromal cells from MDS and AML patients show increased adipogenic potential with reduced Delta-like-1 expression. Sci Rep 11, 5944. 10.1038/s41598-021-85122-8.

Wenk, C., Garz, A.K., Grath, S., Huberle, C., Witham, D., Weickert, M., Malinverni, R., Niggemeyer, J., **Kyncl, M.**, Hecker, J., Pagel, C., Mulholland, C.B., Müller-Thomas, C., Leonhardt, H., Bassermann, F., Oostendorp, R.A.J., Metzeler, K.H., Buschbeck, M., and Götze, K.S. (2018). Direct modulation of the bone marrow mesenchymal stromal cell compartment by azacitidine enhances healthy hematopoiesis. Blood Adv 2, 3447-3461. 10.1182/bloodadvances.2018022053.

9 Acknowledgements

First and foremost, I would like to thank my supervisor Prof. Dr. Katharina Götze for her guidance, advice, and continuous support during my PhD study. She encouraged my personal development and broadened my knowledge in the hemato-oncology field. I also thank my second supervisor Dr. Bernhard Küster and my mentor Prof. Dr. Marc Schmidt-Supprian for their input and support.

I would like to offer my special thanks to all my cooperation partners, especially Dr. Carsten Marr, Prof. Dr. Robert Oostendorp, Dr. Lisa Bast, Prof. Dr. Joachim Rädler, Dr. Alexandra Murschhauser, Lea Schuh, and Moritz Thomas for great discussions and a successful partnership.

My appreciation also goes to my colleagues, lab mates, and friends – Theresa Landspersky, Judith Hecker, Jennifer Rivière, Luisa Vogel, Mark van der Garde, Marie-Theresa Weickert, Christina Schreck, and Franziska Hettler for their help and support that have made my study a wonderful time.

Finally, I would like to say a special thank you to Maximilian and to my family, for their love and support over the last years.